

**NANOSORPTION-MEMBRANE FILTRATION FOR
HEAVY METAL REMOVAL**

BY

WANIDA CHOOAKSORN

**A DISSERTATION SUBMITTED IN PARTIAL FULFILLMENT OF
THE REQUIREMENTS FOR THE DEGREE OF DOCTOR OF
PHILOSOPHY (ENGINEERING AND TECHNOLOGY)
SIRINDHORN INTERNATIONAL INSTITUTE OF TECHNOLOGY
THAMMASAT UNIVERSITY
ACADEMIC YEAR 2016**

**NANOSORPTION-MEMBRANE FILTRATION FOR
HEAVY METAL REMOVAL**

BY

WANIDA CHOOAKSORN

**A DISSERTATION SUBMITTED IN PARTIAL FULFILLMENT OF
THE REQUIREMENTS FOR THE DEGREE OF DOCTOR OF
PHILOSOPHY (ENGINEERING AND TECHNOLOGY)
SIRINDHORN INTERNATIONAL INSTITUTE OF TECHNOLOGY
THAMMASAT UNIVERSITY
ACADEMIC YEAR 2016**



NANOSORPTION-MEMBRANE FILTRATION FOR HEAVY METAL
REMOVAL

A Dissertation presented

By

WANIDA CHOOAKSORN


Submitted to

Sirindhorn International Institute of Technology

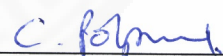
Thammasat University

In partial fulfillment of the requirements for the degree of
DOCTOR OF PHILOSOPHY (ENGINEERING AND TECHNOLOGY)

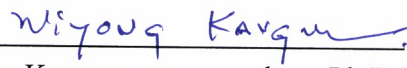
Approved as to style and content by

Advisor and Chairperson of Thesis Committee 
(Assoc.Prof. Rachnarin Nitisoravut, Ph.D.)

Co-Advisor 
(Kritapas Laohhasurayotin, Ph.D.)

Committee Member and
Chairperson of Examination Committee 
(Prof. Chongrak Polprasert, Ph.D.)

Committee Member 
(Assoc.Prof. Sandhya Babel, Ph.D.)

Committee Member 
(Wiyong Kangwansupamonkon, Ph.D.)

External Examiner: Prof. Saravanamuth Vigneswaran, Ph.D.

JANUARY 2017

Acknowledgements

I would like to express my sincere gratitude to my advisor, Assoc. Prof. Dr. Rachnarin Nitisoravut, for his persistent advice, valuable guidance and effective approach to encourage me throughout my study.

I also would like to extend my gratitude to my committee members, Dr. Kritapas Laohhasurayotin, Prof. Dr. Chongrak Polprasert, Assoc. Prof. Dr. Sandhya Babel and Dr. Wiyong Kangwansupamonkon, for their kind suggestions and guidance for this research.

I gratefully acknowledge the support of the Higher Education Research Promotion and National Research University Project of Thailand, Office of the Higher Education Commission and Sirindhorn International Institute of Technology graduate scholarship program, Thammasat University, Thailand for funding this study.

Finally, I am very much appreciate to my parents and my friends who make my life more cheerful during the hard period of experiments.

Abstract

NANOSORPTION-MEMBRANE FILTRATION FOR HEAVY METAL REMOVAL

by

WANIDA CHOOAKSORN

B.Sc.in Health Science, Faculty of Science and Technology,
Thammasat University, 2001

M.Sc. in Environmental Science, Faculty of Science and Technology,
Thammasat University, 2004

A novel technique has been developed for heavy metal removal. This allows a simultaneous filtration and adsorption by coating modified adsorbent onto supporting materials which lead to shorten treatment process and improve the adsorption capacity for heavy metal removal. New biosorbent in nanoscale was prepared and investigated for its efficiency for heavy metal removal. Chitosan nanoparticles (CN) was prepared by using ionic gelation method. The adsorbent was introduced onto the supporting material using a dip coating method. Moreover, CN were modified using glutaraldehyde (GLA), and polyethylene glycol (PEG) in order to increase the stability and binding properties. The size and morphology of adsorbents and supporting materials were characterized by using an atomic force microscope (AFM) and scanning electron microscope (SEM). The element and chemical analysis was examined by energy dispersive spectrometer (EDS). Interaction between components of adsorbent and supporting material were also characterized by Fourier transform infrared spectrometer (FTIR). The experiments were performed under batch and continuous system at room temperature. The mechanism of adsorption was studied using

adsorption isotherms and adsorption kinetics. The efficiency of removal was tested by three different heavy metals which are Cr(VI), Cu(II), and Ni(II).

The dry sizes of CN were in the range of 23-26 nm based on AFM examination. SEM images showed significant changes on the surface morphology from a coarse to a smooth uniform surface of film-like morphology. The film became thicker and smoother as the CN loading increased. FTIR spectra showed no interaction between the CN and the supporting material. The EDS composition before and after heavy metal adsorption provided direct evidence for heavy metal adsorption by the adsorbent.

In batch experiments, bituminous activated carbon (AC) and ceramic balls (CB) were used as supporting material for Cr(VI) and Cu(II) removal. The experiments were carried out to investigate the influences of several operational parameters such as contact time, adsorbent dose, agitation rate, pH, and initial concentration. The CN-coated AC demonstrated an increase in Cr(VI) removal efficiency and also in adsorption capacity. The adsorption capacity of the CN-coated AC (77.52 mg/g) was more than twice that of the uncoated AC (36.36 mg/g) or pure chitosan (32.57 mg/g) at pH 5. CN-coated CB showed difference adsorption capacity between Cr(VI) and Cu(II). The adsorption capacity for Cu(II) was more than three times as compared to the Cr(VI) adsorption. The adsorption isotherms were well described using the Freundlich and Langmuir models. Adsorption kinetics followed that of the pseudo-second-order kinetics, suggesting chemisorption as a rate limiting step.

For the continuous system, the experiments were performed to study the effect of adsorbent dosage, pH, initial concentration, and flow rate. CB and tubular microfiltration ceramic membrane (CM) were used as supporting materials for Cu(II) and Ni(II) removals.

The performance of CN-coated CB for Cu(II) removal through a fixed-bed column was evaluated. The adsorption capacity increased with increasing the initial concentrations, but decreased with increasing flow rate and CN loading (187.4 mg/g). The Thomas and Yoon-Nelson models were shown to have excellent fit for the breakthrough curves, indicating that CN-coated CB is suitable for a columnar design.

The efficiency for Cr(VI) removal was low. Thus, only Cu(II) and Ni(II) were investigated in the continuous system. The CN was introduced onto the CM surface (CN-coated CM) for Cu(II) and Ni(II) removal through a continuous system of

simultaneous filtration and adsorption method. CN crosslinked with GLA provided the highest adsorption capacity of 240.3 mg/g at flow rate 2.5 mL/min. It is over 30% improvement of adsorption capacity as compared to native CN. However, the reduction of percentage and adsorption capacity can be attributed to a short contact time insufficient for Cu(II) diffusion into the inner pores of adsorbent.

For Ni(II) removal, the adsorption capacity was 123.0 mg/g. The amount of Ni(II) removed increased with an increase in flow rate due to larger flow, but decreased with an increase in the amount of CN loading, indicating that the adsorption takes place mainly on the surface of CN film which, in turn, is controlled by surface area of the membrane. The adsorption kinetics were well described using the Thomas model for both Cu(II) and Ni(II). The permeate flux of all conditions slightly decreased and then the plateau with time. The permeate flux decreases because of the thicker CN layer on the membrane surface and the concentration polarization. This tendency showed that interaction between the CM and CN led to the formation of the CN layer on the surface of CM and induced a reduction of the membrane pore size. The simultaneously filtration and adsorption experiments exhibited a high adsorption capacity for Cu(II) removal by using CN crosslinked with GLA (CMCN-GLA) coated membrane at pH 5 and the flowrate 2.5 mL/min.

The results are useful for further applications of tertiary wastewater treatment system design at low concentration of heavy metals from industrial effluents prior to their discharge. The advantage of this method is that heavy metals can be simultaneously treated by filtration of particulate matters whose size is greater than the membrane pore size together with simultaneous adsorption of heavy metals onto the coating surface of the membrane.

Keywords: Adsorption, Batch experiment, Continuous experiment, Heavy metal, Membrane filtration

Table of Contents

Chapter	Title	Page
	Signature Page	i
	Acknowledgements	ii
	Abstract	iii
	Table of Contents	vi
	List of Figures	xii
	List of Tables	xvi
	List of Abbreviations	xviii
1	Introduction	1
	1.1 Rationale statement	1
	1.2 Objectives of the study	3
	1.3 Scope of the study	3
2	Literature Reviews	5
	2.1 Heavy metals contamination	5
	2.2 Methods used for heavy metals removal	6
	2.2.1 Chemical precipitation	6
	2.2.2 Ion exchange	7
	2.2.3 Solvent extraction	7
	2.2.4 Electrochemical treatment	8
	2.2.5 Flotation process	8
	2.2.6 Adsorption process	9
	2.2.7 Membrane filtration process	9
	2.3 Application of adsorption process for heavy metal removal	11
	2.3.1 Chitosan biosorbent	12

Chapter	Title	Page
	2.3.1.1 Adsorption mechanism onto chitosan	13
	2.3.1.2 Parameters affecting heavy metal adsorption by chitosan	14
	(1) Deacetylated units fraction	14
	(2) Influence of pH	15
	(3) Influence of dose	15
	(4) Influence of contact time	15
	2.3.1.3 Nanochitosan application for heavy metal removal	16
	2.3.1.4 Comparison of adsorption capacity by chitosan adsorbents	17
	2.3.2 Common isotherms for heavy metal adsorption	18
	2.3.2.1 Langmuir isotherm	19
	2.3.2.2 Freundlich isotherm	19
	2.3.2.2 Sips isotherm	20
	2.3.3 Kinetics model for heavy metal adsorption	21
	2.3.3.1 Lagergren pseudo-first order	21
	2.3.3.2 Pseudo-second order	22
	2.3.3.3 Elovich equation	23
	2.3.3.4 Intraparticle diffusion	23
	2.3.4 Adsorption process operation	23
	2.3.4.1 Batch process	24
	2.3.4.2 Continuous process	24
	(1) Thomas model	24
	(2) Yoon-Nelson model	25
	2.4 Application of membrane filtration process for heavy metal Removal	25
	2.4.1 Membrane filtration operation	27
	2.4.2 Parameters affecting membrane performances	27
	2.4.2.1 Fouling and compaction	27
	2.4.2.2 Applied pressure or feed pressure	28

Chapter	Title	Page
	2.5 Application of adsorption-filtration technique for heavy metal removal	28
3	Materials and Methods	30
	3.1 Chemicals and materials	30
	3.1.1 Adsorbent	30
	3.1.2 Supporting materials	30
	3.1.3 Synthetic wastewater	30
	3.2 Experimental procedures	31
	3.2.1 Preparation of chitosan nanoparticles	31
	3.2.2 Preparation of cross-linked chitosan nanoparticles	31
	3.2.2.1 Chitosan nanoparticles-glutaraldehyde	31
	3.2.2.2 Chitosan nanoparticles-polyethylene glycol	31
	3.2.3 Surface coating of supporting material	33
	3.2.3.1 Dip coating method	33
	3.2.3.1 Wet impregnation coating method	33
	3.2.4 Heavy metal removal operations	34
	3.2.4.1 Batch adsorption experiment	34
	(1) Application of adsorption isotherms	34
	(2) Application of adsorption kinetics	35
	3.2.4.2 Fixed-bed column experiment	36
	3.2.4.3 Adsorption-microfiltration experiment	38
	3.2.4.4 Desorption experiment	39
	3.2.5 Analytical methods	39
	3.2.5.1 Chitosan nanoparticles analysis	39
	3.2.5.2 Surface analysis of supporting material	41
	3.2.5.3 Heavy metals analysis	41

Chapter	Title	Page
4	Results and Discussion	42
	4.1 Characterization of chitosan nanoparticles	42
	4.1.1 Formation of chitosan nanoparticles	42
	4.1.2 Size of chitosan nanoparticles	43
	4.1.3 Summary	45
	4.2 Characterization of adsorbent coated on supporting material	45
	4.2.1 By wet impregnation coating method	45
	4.2.2 By dip coating method	46
	4.2.2.1 Characterization of adsorbent coated on alumina ceramic balls	47
	4.2.2.2 Characterization of adsorbent coated on ceramic membrane	49
	4.2.3 Summary	52
	4.3 Cr(VI) removal using nanochitosan coated on bituminous activated carbon	52
	4.3.1 Properties of adsorption	53
	4.3.2 Adsorption isotherms	54
	4.3.3 Adsorption kinetics	55
	4.3.4 Summary	59
	4.4 Cr(VI) removal using nanochitosan coated on alumina ceramic balls	60
	4.4.1 Elemental analysis of adsorbent	60
	4.4.2 Batch adsorption experiment	60
	4.4.2.1 Adsorption isotherms	60
	4.4.2.2 Adsorption kinetics	62
	4.4.3 Fixed-bed column adsorption experiment	63
	4.4.3.1 Influence of initial concentration on the breakthrough curve	67

Chapter	Title	Page
	4.4.3.2 Influence of flow rate on the breakthrough curve	68
	4.4.3.3 Application of model	69
	4.4.4 Summary	71
	4.5 Cu(II) removal from aqueous solutions by nanochitosan coated alumina balls in fixed-bed column	72
	4.5.1 Parameters affecting the column performance	72
	4.5.1.1 Effect of initial concentration on breakthrough curve	72
	4.5.1.2 Effect of flow rate on breakthrough curve	74
	4.5.1.3 Effect of nanochitosan loading on breakthrough curve	75
	4.5.1.4 Application of Thomas and Yoon-Nelson model	77
	4.5.2 Summary	79
	4.6 Ni(II) removal from aqueous solutions by chitosan coated ceramic membrane in adsorption-filtration membrane	80
	4.6.1 Ni(II) removal	80
	4.6.2 Permeate flux	81
	4.6.3 Adsorption kinetics and breakthrough curves	81
	4.6.4 Summary	86
	4.7 Cu(II) removal by modified nanochitosan coated ceramic membrane in adsorption-filtration membrane	86
	4.7.1 Cu(II) removal	87
	4.7.2 Permeate flux	89
	4.7.3 Breakthrough curves	91
	4.7.4 Kinetics models	91
	4.7.5 Simulation of adsorption-filtration membrane for Cu(II) removal	94
	4.7.6 Summary	96
5	Conclusions and Recommendations	97

Chapter	Title	Page
	5.1 Conclusions	97
	5.2 Recommendations	99
	References	100
	Appendix	120



List of Figures

Figures	Page
1.1 Overall experimentations of this study	4
2.1 Basic terms of adsorption process	12
2.2 The structure of chitosan	13
2.3 Schematic of principle membrane process	26
2.4 The types of membrane filtration	27
3.1 The experimental strategies	32
3.2 Experimental setup used for column adsorption experiments	36
3.3 Flow diagram of the bench-scale membrane test unit	40
3.4 Picture of the bench-scale membrane test unit including: (a) feed tank, (b) permeate container, (c) membrane modules, (d) feed pump, (e) feed pressure gauge, (f) permeate flow meter, (g) pH and conductivity monitor, (h) control panel, and (i) retentate container	40
4.1 Influence of chitosan and TPP concentrations on the particle size: (a) at TPP concentration of 1 mg/mL and (b) at chitosan concentration of 1 mg/mL	43
4.2 AFM images show the topographic and three-dimensional image of chitosan nanoparticles	44
4.3 SEM images of bituminous activated carbon surface show morphology of chitosan nanoparticles: (a) non-dialyzed CN-AC and (b) dialyzed CN-AC	46
4.4 SEM images of bituminous activated carbon surface show morphology of chitosan nanoparticles: (a) non-dialyzed CN-AC (b) dialyzed CN-AC	47
4.5 SEM images of alumina ceramic balls prepared at different amount of nanochitosan loadings: (a) 0 mg, (b) 15 mg, (c) 25 mg, and (d) 35 mg	48
4.6 SEM images of membrane prepared at different amounts of chitosan loadings: (a) 0 mg, (b) 10 mg, (c) 15 mg, and (d) 20 mg	50

Figures	Page
4.7 SEM images of membrane prepared at different adsorbents: (a) CM, (b) CMCN, (c) CMCN-GLA, and (d) CMCN-PEG	51
4.8 Thickness of adsorbent on ceramic membrane	52
4.9 Relationship between C_e and % Cr (VI) removal for various adsorbents (at pH5, adsorbent dose 1 g/L, contact time 3 h, agitation speed 100 rpm, and room temperature)	54
4.10 Relationship between C_e and adsorption capacities for various adsorbents (at pH5, adsorbent dose 1 g/L, contact time 3 h, agitation speed 100 rpm, and room temperature)	55
4.11 Adsorption capacity of CN-AC/DC for Cr (VI) (at Cr (VI) initial concentration 10 mg/L, pH 5, adsorbent dose 1 g/L, agitation speed 100 rpm, and room temperature)	57
4.12 Adsorption capacity of CN-AC/WI for Cr (VI) (at Cr (VI) initial concentration 10 mg/L, pH 5, adsorbent dose 1 g/L, agitation speed 100 rpm, and room temperature)	57
4.13 The SEM images of alumina ceramic balls coated chitosan at 5,000x and the corresponding EDS: (a) bare alumina ceramic balls, (b) CN-CB before Cr(VI) adsorption, and (c) CN-CB after Cr(VI) adsorption	61
4.14 Adsorption capacity and removal efficiency of Cr(VI) on CN-CB (at pH 5, adsorbent dose 1.0 g/L, agitation speed 100 rpm, and room temperature)	62
4.15 Adsorption of the Cr(VI) on CN-CB at various concentrations: (a) time course of Cr(VI) removal efficiency, (b) adsorption capacity of Cr(VI) as a function of initial concentration of Cr(VI), and (c) Time course of the cumulative Cr(VI) mass removed (at pH 5, flow rate 2.5 mL/min, and room temperature)	64

Figures	Page
4.16 Adsorption of the Cr(VI) on CN-CB at various flow rates: (a) removal efficiency of Cr(VI) removal efficiency, (b) adsorption capacity of Cr(VI), and (c) cumulative of Cr(VI) mass (at Cr (VI) initial concentration 10 mg/L, pH 5, and room temperature)	66
4.17 The breakthrough curve of Cr(VI) adsorption on CN-CB with different initial concentrations (at pH 5, flow rate 2.5 mL/min, and room temperature)	67
4.18 The breakthrough curve of Cr(VI) adsorption on CN-CB with different flow rates (at Cr (VI) initial concentration 10 mg/L, pH 5, and room temperature)	68
4.19 Breakthrough curve of Cu(II) at different initial concentrations (at pH 5, flow rate 2.5 mL/min, CN-CB dose 25 mg, and room temperature)	73
4.20 Adsorption capacity and % removal efficiency of Cu(II) at different initial concentrations (at pH 5, flow rate 2.5 mL/min, CN-CB dose 25 mg, and room temperature)	73
4.21 Breakthrough curve of Cu(II) at different flow rates (at Cu (II) initial concentration 10 mg/L, pH 5, CN-CB dose 25 mg, and room temperature)	75
4.22 Adsorption capacity total adsorption capacity and % Removal efficiency of Cu(II) at different flow rates (at Cu(II) initial concentration 10 mg/L, pH 5, CN-CB dose 25 mg, and room temperature)	75
4.23 Breakthrough curve of Cu(II) at different nanochitosan loadings (at Cu(II) initial concentration 10 mg/L, flow rate 2.5 mL/min, pH 5, and room temperature)	76
4.24 Adsorption capacity total adsorption capacity and % removal efficiency of Cu(II) at different nanochitosan loadings (at Cu(II) initial concentration 10 mg/L, flow rate 2.5 mL/min, pH 5, and room temperature)	76

Figures	Page
4.25 Adsorption of the Ni(II) on CN-coated ceramic membrane at various chitosan loadings and flow rate: (a) time course of Ni(II) removal efficiency, (b) adsorption capacity of Ni(II), and (c) time course of the cumulative Ni(II) mass (at Ni(II) initial concentration 10 mg/L, pH 5, and room temperature)	82
4.26 Flux decline profiles of Ni(II) concentration with different chitosan loadings and flow rates (at Ni(II) initial concentration 10 mg/L, pH 5, and room temperature)	83
4.27 Influence of chitosan loadings on the breakthrough curve of Ni(II) adsorption on CN-coated ceramic membrane (a) flow rate of 2.5 mL/min and (b) flow rate of 5.0 mL/min (at Ni(II) initial concentration 10 mg/L, pH 5, and room temperature)	84
4.28 Adsorption of the Cu(II) by various adsorbents coated on ceramic membrane for difference flow rates: (a) Time course of Cu(II) removal efficiency, (b) adsorption capacity of Cu(II), and (c) Time course of the cumulative Cu(II) mass (at Cu (II) initial concentration 50 mg/L, adsorbent dose 20 mg, pH 5, and room temperature)	88
4.29 SEM images of ceramic membrane surface coated with chitosan at 15,000X and EDS analysis: (a) bare ceramic membrane, (b) before Cu(II) adsorption; and (c) after Cu(II) adsorption	90
4.30 The permeate flux of various adsorbents at (a) 2.5 mL/min and (b) 5.0 mL/min (at Cu(II) initial concentration 50 mg/L, adsorbent dose 20 mg, pH 5, and room temperature)	92
4.31 The breakthrough curves for various adsorbents at (a) 2.5 mL/min and (b) 5.0 mL/min (at Cu(II) initial concentration 50 mg/L, adsorbent dose 20 mg, pH 5, and room temperature)	93
4.32 Schematic of adsorption-filtration membrane unit	94

List of Tables

Tables	Page
2.1 Effect and MCLs of some heavy metals on mammals	5
2.2 Advantages and disadvantages of various heavy metals removal methods	10
2.3 Comparison of adsorption capacity of chitosan adsorbents for heavy metals	17
2.4 Adsorption isotherms for water treatment	20
2.5 Mathematical equations in heavy metals adsorption kinetics	22
4.1 Formation of the chitosan particles with addition of TPP	42
4.2 Equilibrium adsorption analysis for the adsorption of Cr(VI) on various adsorbents	56
4.3 Kinetic parameters for the adsorption of Cr(VI) by CN-AC/DC and CN-AC/WI	58
4.4 Adsorption capacity of modification activated carbon for Cr(VI) removal in batch mode	59
4.5 Equilibrium adsorption analysis for the adsorption of Cr(VI) on adsorbents	63
4.6 The kinetic parameters for the adsorption of Cr(VI) by CN-CB	65
4.7 Characteristic parameters of Thomas model for Cr(VI) adsorption onto CN-CB	70
4.8 Comparative adsorption capacity results from literature and experimental data of Cr(VI) onto batch and fixed-bed column experiments	71
4.9 Adsorption capacity of chitosan-coated on various supporting materials for Cu(II) removal	78
4.10 Thomas and Yoon-Nelson model parameters at different flow rates, initial concentrations and doses for Cu(II)adsorption onto CN-CB	79
4.11 Characteristic parameters of kinetic model for the adsorption of Ni(II) onto CN-coated ceramic membrane	85

Tables	Page
4.12 Characteristic parameters of Thomas model for the adsorption of Cu(II) onto several adsorbents	94
4.13 The estimated amount of mass adsorbent at various scenarios based on experimental data	96



List of Abbreviations

AC	Bituminous activated carbon
AFM	Atomic force microscopy
CB	Ceramic balls
C_e	Equilibrium concentrations of heavy metal
C_0	Initial concentration of heavy metal
C_t	Concentration of heavy metal at time
CM	Ceramic membrane
CN	Chitosan nanoparticles/nanochitosan
CN-AC/DC	Chitosan nanoparticles coated on bituminous activated carbon by dip coating method
CN-AC/WI	Chitosan nanoparticles coated on bituminous activated carbon by wet impregnation method
CN-CB	Chitosan nanoparticle coated alumina ceramic balls
CN-GLA	Chitosan nanoparticles cross linked with glutaraldehyde
CN-PEG	Chitosan nanoparticles mixed with polyethylene glycol
CTS	Chitosan flake
Cu_{ads}	Amount of Cu(II) adsorbed
Cu_{des}	Amount of Cu(II) desorbed
EDS	Energy dispersive spectrometer
FTIR	Fourier transform infrared spectrometer
J	Permeate flux
K_F	Freundlich constant
K_L	Langmuir constant
k_{Th}	Thomas model adsorption rate constant
k_{YN}	Yoon Nelson model adsorption rate constant
q_e	Adsorption capacity at equilibrium
q_m	Maximum adsorption capacity
q_t	Adsorption capacity at time
Q_0	Influent volume
Q_1	Effluent volume

R_L	Equilibrium parameter
SEM	Scanning electron microscope
SSE	Sum of squared error
TPP	Sodium tripolyphosphate



Chapter 1

Introduction

1.1 Rationale statement

Wastewater from industrial remains a major problem in the environment. A discharge of heavy metals in wastewater is one of the most significant environmental problems due to its hazards for human and ecological systems [1-4]. The most common sources of heavy metals are from mining operations, electroplating, tanning, textile dyeing, batteries manufacturing, paper pulping, petroleum refining, and metal finishing processes [5-10]. There are many existing methods for removal of heavy metals from wastewater include physical and chemical process such as electrochemical treatment, chemical precipitation/filtration, coagulation and flocculation, chelation/complexation, solvent extraction, ion- exchange, reverse osmosis, adsorption, and membrane processing [5, 11-15]. From these methods, adsorption is a commonly used method that is highly effective, inexpensive, flexible in design and easy to operate to separate heavy metals from wastewater [16-20]. The use of biosorbents is of industrial interest because of the cost advantage. Moreover, it has been proposed as an alternative, as this has been proven effective at low concentration [21].

Many adsorbents have been reported for heavy metals removal such as clarified sludge, bark, oak sawdust, fly ash, olive cake, peanut husk, pine needles, almond shells, cactus leaves, coconut shell charcoal, commercial activated carbon, activated alumina, chitosan, lignin, modified wool, and seaweeds [22-24]. Chitosan is one of the outstanding adsorbent because it has several required properties like hydrophilicity, biodegradability, anti-bacterial property, and non-toxicity [25-27]. Chitosan has been reported to show the very efficient for removing heavy metals through chelation mechanisms involving amine groups [18, 28, 29]. It was used as an adsorbent for wastewater treatment [30]. Chitosan can be modified by many chemicals to improve its properties and extend its applications such as cross-linking using epichlorohydrin, formaldehyde or glutaraldehyde and graft-copolymerization with polyethylene glycol (PEG), vinyl acetate, acrylonitrile or polystyrene [31-33].

Today, nanotechnology is considered as effective technology in solving problems of wastewater from industry. Nanomaterials have more performance due to their large specific efficient surface area [34, 35]. The possible use of chitosan has attracted high attention for the advance of its particles of nano-scale. Several studies have also used nanochitosan in the development of drug delivery. However, there are small numbers of research reported on the application nanoparticles of chitosan coated with supporting materials for heavy metal removal.

Membrane filtration is one technique used in wastewater treatment and it is in practice for solid-liquid separation. The principle of the different separation systems basically depends on the pore size of the membrane and the size of the particle that is to be separated. The membrane classification is based on size and molecular weight of particles that can be separated from the entering streams. Membrane systems such as microfiltration (MF), ultrafiltration (UF), nanofiltration (NF) and reverse osmosis (RO) are now being used alone or with other treatment technologies in implementing pollution prevention [36]. Membrane technologies such as UF, NF, and RO are methods for removing divalent ions of heavy metals, but economic studies have shown it to be the most costly. Membrane filtration shows high heavy metal removal, high permeate fluxes, convenient operation and space saving. It can be continuously processed and can simply be integrated with other methods [7, 10, 37].

Basically, the adsorption process regularly needs an additional step to separate adsorbent from treated wastewater. Membrane filtration is appropriate technology to separate solid from liquid. Therefore, the combination of adsorption process and membrane filtration is of interest. In this study, different supporting materials, adsorbents, and system of operations were investigated for enhancement of heavy metal adsorption.

An alternative method for heavy metal removal was developed to overcome the mass transfer limitations by coating nanochitosan on the surface of supporting materials such as bituminous activated carbon, alumina ball and microfiltration ceramic membrane. A novel method of simultaneous adsorption and filtration of heavy metal using nanochitosan-coated ceramic membrane is developed in order to shorten the treatment process and to improve the adsorption capacity for heavy metals removal. The efficiency of heavy metals uptake onto nanochitosan coated with supporting

material was explored in batch and continuous systems. This research brought about a new approach for wastewater treatment, particularly for metal removal. Wastewater can be simultaneously treated by filtration of particulate matters with the size that is greater than the membrane pore size and the adsorption of heavy metals onto the coating surface of the membrane.

1.2 Objectives of the study

This study developed a novel method for heavy metals removal from industrial wastewater in order to protect the environment and human health from heavy metals. The objectives of this study are as follows:

1.2.1 To investigate the adsorption capacity of chitosan nanoparticles coated onto supporting materials.

1.2.2 To investigate the use of microfiltration ceramic membrane as supporting material for heavy metal adsorption.

1.2.3 To study a novel method for the removal of heavy metals by combining adsorption and membrane filtration under the batch and the continuous operation.

1.2.4 To investigate efficiency of simultaneous adsorption and filtration for heavy metal removal.

1.3 Scope of the study

In order to accomplish the objectives of this study, the scope was set as follows:

1.3.1 Synthesis wastewater was used spiking heavy metals including nickel (Ni), chromium (Cr), and copper (Cu).

1.3.2 The heavy metals removal was conducted in batch and continuous processes.

1.3.3 Membrane in this study is tubular microfiltration ceramic membrane.

1.3.4 The membrane filtration experiments were conducted in the bench-scale unit.

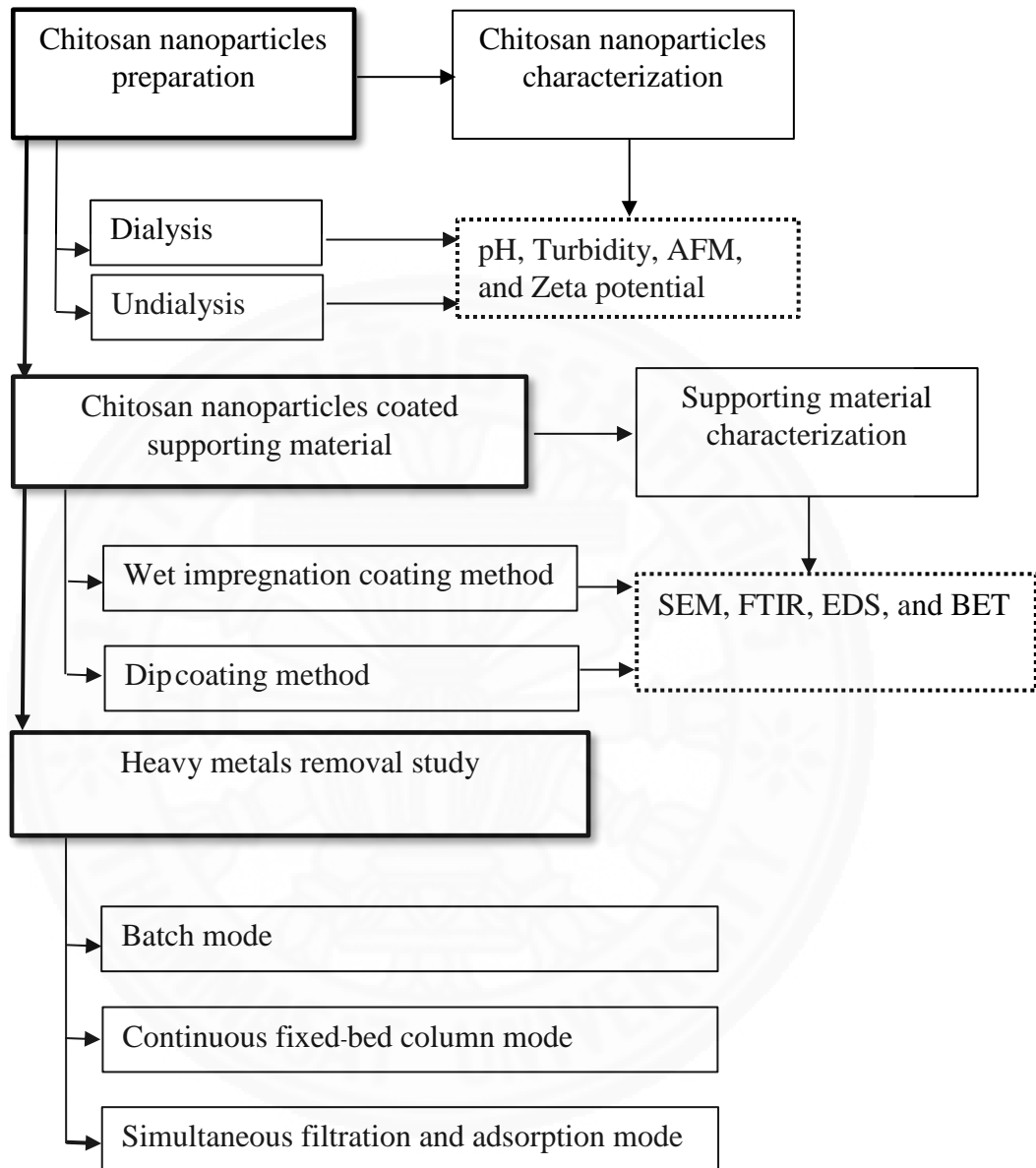


Figure 1.1 Overall experimentations of this study

Chapter 2

Literature Reviews

2.1 Heavy metals contamination

Many industries generate a large portion of wastewater containing heavy metals resulted in an increasing and accumulation of heavy metals in environment. Contamination of heavy metal in environment is becoming a severe problem because of their toxic effects to health of human and ecological system even at very low concentrations. Heavy metals in wastewater are discharged by chemical industries including cadmium, chromium, mercury, nickel, copper, and lead. The toxicity of heavy metals compounds has been of global concern because of their probable role in promoting cancer of the bladder, lung, skin, and prostate in humans. The United State Environmental Protection Agency (USEPA) established the wastewater regulations in order to reduce human and environmental exposure to the toxicity of heavy metals [38]. The effect and maximum concentration levels (MCLs) for drinking water of some heavy metals, established by USEPA are shown in Table 2.1.

Table 2.1 Effect and MCLs of some heavy metals on mammals

Heavy metals	Effects	MCLs (mg/L)	References
Copper	Causing cancer, liver damage, wilson disease, anemia, growth inhibition and insomnia	1.3	[16]
Chromium	Allergic dermatitis, headache, diarrhea, nausea, vomiting, and carcinogenic	0.1	[39]
Nickel	Neurological deficits, dermatitis, nausea, chronic asthma, cardiovascular disease, coughing, human carcinogen, and high blood pressure	0.1	[38]

Table 2.1 (cont)

Heavy metals	Effects	MCLs (mg/L)	References
Cadmium	Carcinogen and teratogen impacting lungs, kidneys, liver damage dysfunction, hypertension, hepatic injury and reproductive organs	0.005	[40]
Mercury	Kidney damage, nausea, vomiting, encephalopathy (headache, seizures, ataxia, obtundation)	0.002	[41]
Lead	Diseases of the kidneys, anemia, headache, damage the fetal brain and nervous system	0.015	[42]

2.2 Methods used for heavy metals removal

There are several methods used for heavy metals removal consist of physical and chemical processes such as chemical precipitation, ion-exchange, solvent extraction, electrochemical treatment, flotation, membrane filtration, adsorption, and. They have their advantages and disadvantages in application. Moreover, they are also relatively high in operational, incomplete removal, maintenance costs, and production of large quantities of wastes [18, 43]. The summary advantages and disadvantages of these approaches will be presented in the following paragraphs and Table 2.2.

2.2.1 Chemical precipitation

Chemical precipitation is the creation of a solid from a solution which usually used methods for many heavy metals removal in the industry because of simple and inexpensive to operate. There are a lot of studies in this method, but this method needs a large quantity of chemicals to form insoluble precipitates and separated solid from the water by sedimentation or filtration [10, 44]. Cu(II), Cr(VI), Zn(II), Ni(II), and Fe(II) were removed 85- 100% under the types of precipitant, pH, and initial concentrations [45, 46]. Chemical precipitation by coagulation-flocculation is applied

to remove heavy metal by sedimentation and filtration. Coagulation is used to increase the particle size of the unstable particles into bulky flocs [47]. The pH adjustment and addition of coagulant such as ferric/alum salts are necessary to overcome the repulsive forces between particles for this method [48]. The mechanism of chemical precipitation method for heavy metal removal is demonstrated in Equation (2.1). Chemical precipitation requires further treatment for excessive sludge production [49].



where M^{2+} and OH^- are the dissolved metal ions and the precipitant, respectively, while $M(OH)_2$ is the insoluble metal hydroxide. The adjustment of pH in chemical precipitation process is the main parameter to improve the heavy metal removal [38]. Chemical precipitation are unfavorable particularly when dealing with great volumes of matter which contains in low concentration of heavy metals [50].

2.2.2 Ion exchange

Ion exchange process have been usually used to remove heavy metals from water and wastewater because of their several advantages, such as high removal efficiency, fast kinetics, and high treatment capacity [51]. Ion exchange can be removed Pb(II), Hg(II), Cd(II), Ni(II), Cr(III,VI), Cu(II) and Zn(II) from a solution or substances [50]. The capacity of this method depends on the concentration forms and types of ion exchangers in the system [50]. However, ion exchange also noted that it is cannot handle at matrix of concentrated metal solution as becomes simply fouled by organics and other solids in the wastewater. Moreover, ion exchange process is very sensitive to the pH and is nonselective of the solution [52].

2.2.3 Solvent extraction

Solvent extraction is usually used to processes of heavy metal ions removal, ranging from aqueous solutions in hydrometallurgical treatment to environmental applications. Solvent extraction process is suggested as appropriate method to remove heavy metals from the wastewaters of the electronic and chemical industries [53]. Cadmium and zinc were successfully removed from rinse waters by using

triisooctylamine and organophosphoric acid DEHPA (bis (2-ethylhexyl) phosphoric acid), respectively [53]. Moreover, it is used a suitable method in order to increase the concentration of the heavy metals, commonly considered in the separation processes [54, 55].

2.2.4 Electrochemical treatment

Electrochemical treatment can recover metals in the elemental metal state. It is used to remove heavy metals in the plating- out on a cathode surface. Electrochemical treatment involves the production of coagulants in situ by dissolving electrically either iron or aluminum ions from electrodes of iron or aluminum. Tran et al [56] found that the removal efficiency of heavy metal ions was 22.5% by using electrochemical treatment. However, this method involve the expensive electricity supply and relatively large capital investment [57]. The great majority of metallic ions can be electrodeposited in a metallic form on a cathode, electrochemistry offers a way of treating almost all of these types of wastewater. However, when treating effluents, it is normal to work with low concentrations of heavy metals in solution (less that 1000 mg/L). When two-dimensional electrodes are used as cathodes, the low concentration originates transport problems of these ions to the cathode at high current densities [58].

2.2.5 Flotation process

Flotation process is usually used in wastewater treatment and employed in order to separate heavy metal from solution using bubble attachment. Flotation by dissolved air are the main flotation processes for the removal of metal ions [10]. The potential of flotation process was implemented to remove Cd(II), Pb(II) and Cu(II). The removal efficiency of Pb(II), Cu(II) and Cd(II) display 89.95%, 81.13% and 71.17%, respectively [59]. Moreover, Polat and Erdogan (2007) [60] found that the removal of Cu(II), Zn(II), Cr(III) and Ag(I) reached about 74% under low pH. The flotation process is depended on imparting the pH and ionic metal species in hydrophobic of wastewaters by using the surfactants and subsequent removal of the hydrophobic species by air bubbles [60, 61].

2.2.6 Adsorption process

Adsorption process has considered significance as an effective method to separate metal ions from wastewater because it is easy operation, highly effective, and inexpensive among the physical and chemical treatment processes. The capacity of adsorbent was investigated to remove many types of heavy metal such as Pb(II), Cd(II), Zn(II), Cr(VI), Ni(II), Ag(I) and Cu(II). The use of biosorbents has been proposed as an alternative, as it has been proven effective on low initial concentration. Biosorption is of industrial interest, not only for its ability to remove metals from wastewaters, but also for the possibility of recovering metals. The adsorption capacities of biosorbents (crosslinked chitosan) for Cu(II) and Cd(II) removal were 164 and 150 mg/g, respectively [62]. Many industries always use biosorption on a large scale such as acid mine drainage, metal plating and metal processing. The natural mineral sources accelerating reduce, there is a necessity of metals recycling in use. Moreover, the prices for some metals have increased over recent years, which also makes recycling interesting from a profitable aspect. The adsorption process can be treated and adsorbed metal recycled [63].

2.2.7 Membrane filtration process

The membrane filtration process constitutes one of the possibilities for a method for heavy metal removal. There are many types of membrane used for heavy metals removal such as ultrafiltration, nanofiltration, reverse osmosis and electrodialysis. The micellar enhanced ultrafiltration was used to remove Cd(II), Cu(II), Ni(II), Pb(II) and Zn(II) from wastewater. The results showed the rejection coefficients up to 99% [64]. From the literature, the Cu(II) removal efficiency can reject 70.0-99.5% by using reverse osmosis with different initial concentration and operation pressure [65, 66]. For nanofiltration method, The removal efficiency of Cu(II) shows rejection 47-98% from synthetic wastewater [67]. Cifuentes et al. (2009) [68] studied the removal efficiency of electrodialysis for Cu(II) separation. The result showed that the removal of electrodialysis very high for Cu(II) separation. The membrane filtration process is gained considerable for heavy metal removal because of their advantages such as high efficiency, easy operation, and space saving [10].

Table 2.2 Advantages and disadvantages of various heavy metals removal methods

Methods	Advantages	Disadvantages
Chemical precipitation	-Simple and inexpensive operation -Non-metal selective	-Needs a great amount of chemicals for metals reduction -Large production of sludge -High cost of disposal sludge
Ion exchange	-Energy efficient -Metal selective -High regeneration of materials -Low maintenance	-Solution concentration must be monitored -High initial capital and maintenance cost -Solution heating encouraged to maximize efficiency
Solvent extraction	-Selective heavy metal removal -Continuous concentrate metal solution recovery	-Capital costs -Toxic solvent discharges
Electrochemical treatment	-Metal selective -Potential treat effluent > 2,000 mg/L	-High initial capital cost
Flotation process	-Simplicity and rapidity -Economy and good separation yields	-Less selective for heavy metals
Adsorption process	-Low-cost -Easy operating settings -Having wide-ranging of pH -High binding capacities of metal	-Low selectivity -Forming of waste products

Table 2.2 (cont)

Methods	Advantages	Disadvantages
Membrane filtration	-High chemical stability; high thermal stability -Less production of solid waste -Low chemical consumption -Less space requirement	-High cost; low surface -High initial capital and maintenance cost -Low flow rate -Membrane fouling

2.3 Application of adsorption process for heavy metal removal

There are many approaches for removal of heavy metals from wastewater include chemical precipitation, ion exchange, solvent extraction, ion-exchange, electrochemical treatment, flotation, membrane filtration and adsorption [5, 12, 13, 69, 70]. Among these approaches, adsorption process is nowadays accepted as an economic, its flexibility in design and effective method to remove heavy metal from wastewater treatment [10]. Adsorption is also a widely used method that can have quite low cost depending mainly on the sorbent cost and is found to be more environmentally friendly. The use of biosorbents has been proposed as an alternative, as it has proven effective on low concentration flows. Adsorption process is a phase transfer or mass transfer process which transferring of substance occurs from the liquid phase to the surface of a solid and bonding follows by physical and/or chemical interaction. Therefore, adsorption process can be categorized by way of physical adsorption and chemical adsorption process. The process of physical adsorption is mainly because of van der Waals forces. This process is a reversible phenomenon. The substance will be adsorbed onto the adsorbent surface, when the forces of attraction between substance and the solvent are lower than the molecular forces of attraction between the substance and interface. For the chemical adsorption process, a chemical reaction takes place between the solids and the absorbed solute. This reaction is commonly irreversible [71].

The step of basic terms of adsorption combines both mass transfer (diffusion) and addition terms which is displayed in Figure 2.1 and as follow: [72]

- The adsorbate from the bulk liquid phase transfers to the boundary layer of adsorbent particle

- The film diffusion or external diffusion, adsorbate from the boundary layer of adsorbent particle transfers to the external surface of the adsorbent

- The intraparticle diffusion or internal diffusion process occurs in this step. The adsorbate at external surface of the adsorbent transfers into the inner of the adsorbent particle by diffusion in the pore liquid (pore diffusion) and/or by diffusion in the adsorbed state along the internal surface (surface diffusion)

- The energetic interaction between the molecules of adsorbate and the final adsorption places

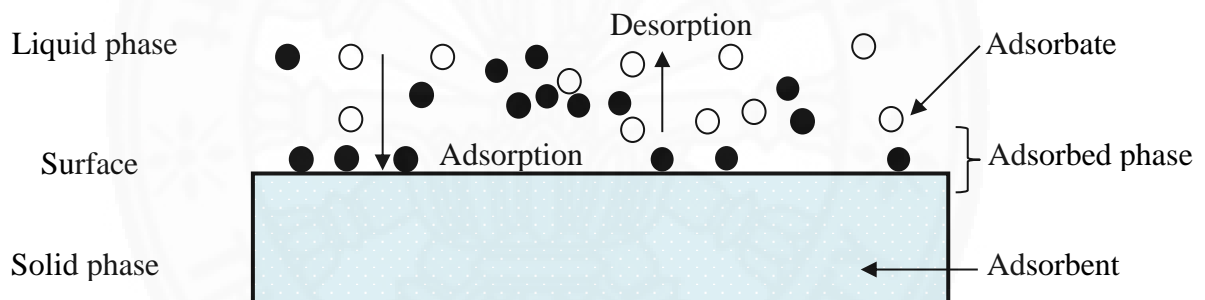


Figure 2.1 Basic terms of adsorption process

2.3.1 Chitosan biosorbent

Adsorption process is of industrial interest, not only for its ability to remove metals from wastewaters, but also for the possibility of recovering metals. In recent years, adsorption is the alternative process to remove heavy metals, numerous adsorbents have been developed because of the wide number of natural materials or agricultural wastes gathering in abundance from environment [73]. There are many adsorbents including activated carbon, sludge, bark, oak saw dust, fly ash, olive cake, peanut husk, pine needles, almond shells, cactus leaves, coconut shell charcoal, commercial activated carbon, activated alumina, chitin, lignin, modified wool, carbon nanotubes and seaweeds [22-24, 74-76].

Among these materials, chitosan has proven to be a promising adsorbent [77]. Chitosan has many properties that have biodegradable, inexpensive, nontoxic nature, biocompatible, and made of natural polymers. It has been revealed to be an effective sorbent for heavy metal removal from aqueous solutions [18, 28, 29]. Moreover, the advantage of using chitosan is simply that the sorbent is a waste product that can be recycled [28, 29, 78]. Chitosan have two properties that are of interest for water treatment: firstly, they are important chelation agents and secondly, they are heavy metal traps [79].

Chitosan is a polysaccharide containing mainly of unbranched chains of β -(1 \rightarrow 4)-2-acetoamido-2-deoxy-d-glucose. It is a type of natural polyaminosaccharide, which can be formed by deacetylation of chitin (Figure 2.2). Chitosan is outstanding adsorbent of adsorption process which interacts very efficiently with transition metal ions and a great chelating agent, even at low concentrations [21] because its amino groups can serve as chelation sites [18, 80]. Moreover, chitosan was used as an adsorbent to remove heavy metal due to the attribute to (1) flexible of structure in polymer chain (2) existence a plenty of functional groups (acetamido, primary amino and/or hydroxyl groups) (3) high reactivity of chemical in these groups and (4) high hydrophilicity because of great amount of hydroxyl groups. The hydroxyl groups (OH) and amino groups (NH₂) can serve as the active sites [81]. In the acidic media, NH₂ groups can be cationized and they adsorb anionic ion powerfully by electrostatic attraction [25].

The reactive of amine group will be selectively binds to practically all group of III transition metal ions. Moreover, the protonation of amine groups leads to adsorption of metal anions because of its cationic behavior in acidic media [71, 82].

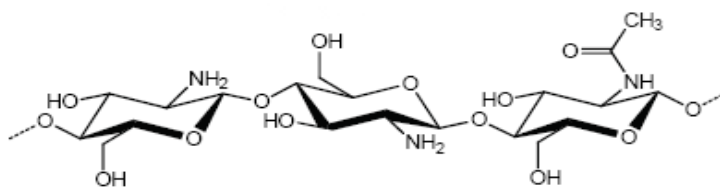


Figure 2.2 The structure of chitosan [63]

2.3.1.1 Adsorption mechanism onto chitosan

The removal mechanisms of heavy metals on chitosan as adsorbent combines to heavy metals is certainly limited as it is reliant on cationic of chitosan. The

amino groups of chitosan composites can form to protonated amine which it can adsorb metal ions molecules through chelation and electrostatic attractions mechanisms [83]. The crosslinking by poly functional reagents allows the use of chitosan for heavy metals adsorption solution. The crosslinking agents comprise other functional groups and can be of varying length than those contained in cross linking [84]. Normally, the decreasing of adsorption capacity depends on the amount of crosslinking agent as it reduces the reactive sites on the chitosan polymer [85] however, the adsorption capacity of can expand, depending on the crosslinking agent of the functional groups [86]. Jin and Bai (2002) [87] studied the mechanisms of lead adsorption on chitosan/PVA (polyvinyl alcohol) hydrogel beads found that the only adsorption sites for lead are at the nitrogen atoms of the amino groups in chitosan and the oxygen atoms of the hydroxyl groups in both chitosan and PVA.

2.3.1.2 Parameters affecting heavy metal adsorption by chitosan

The adsorption efficiency depends on physical and chemical properties such as particle size, porosity, and surface area of adsorbents. There are various parameters influence the adsorption capacity of potential chitosan during the adsorption process. In the context of this study, parameter affecting on adsorption capacity was emphasized on deacetylated fraction of chitosan, pH, dose, and contact time.

(1) Deacetylated units fraction

The good chitosan polymer needs to have a high degree of deacetylation, on the other hand a low fraction of acetylated units [71, 88]. The content of glucosamine will be controlled by deacetylation degree which the fraction of free amine groups available for metal binding. The available number of free amine groups is significant to take into the available number of the heavy metal ions. The amine sites of chitosan are occasionally complicated in the inter- and intra-molecular bonds to the metal ions [71]. The available chitosan has deacetylated ranging 66% to 95% [89]. The study of Mohanasrinivasan et al. found that efficiency adsorption capacity of Cu(II) was 99% with 75% deacetylated [90].

(2) Influence of pH

The influence of pH is main factor for adsorption of heavy metal ions because pH affects the solubility of the metal ions, ionization degree of the adsorbate during reaction and counter ions concentration on the functional groups of the adsorbent. The pH of heavy metal solution is very important because it not only influence the surface charge of adsorption, but also the ionization degree and adsorbate speciation during reaction. The present process is strongly pH-dependent due to the competition of proton and metal ions, a more cautious manner for data presentation and a generalized model are required to describe the sorption equilibria of metal ions. This is especially the case in binary metal systems [18]. As found by many literatures, the optimum pH range for Cr(VI) adsorption by chitosan is a narrow range of 3.0 to 5 [91]. For Cu(II) and Ni(II), the optimum pH range 4-5 [92] [93] and 4.5-5.5 [92] respectively. The study of Kalyani et al. [94] found that pH 5.0 was the best condition for Cu(II) and Ni(II) removal. However, under acidic conditions (at pH below 3) the chitosan adsorbent undertakes dissolution [95].

(3) Influence of dose

The dose of adsorbent be able to influence the extent of heavy metal uptake from aqueous solution [94], when the amount of chitosan increase resulting in the removal percentage increases [19]. This is estimated because of the fact that the availability of exchangeable sites for the ions increased when the dose increased of adsorbents [91]. The adsorption capacity of Cr(VI), Ni(II), and Cu(II) on chitosan dose was studied by many researchers. Nomanbhay et al. [91] showed that 28-30 g/L was the optimum dose with 20 mg/L of Cr(VI) solution. The study of Swayampakula et al. [94] found that 40 g/L of chitosan adsorbent was a suitable amount for Ni(II) and Cu(II) solution with 100 mg/L.

(4) Influence of contact time

The contact time for adsorption process is important parameter for heavy metal removal efficiency. The nanochitosan require an optimum of contact time because of the availability of several functional groups on the surface of chitosan which were required the time for interaction with anions and cations of heavy metal [94]

which the optimum contact time related to the impact of agitation time on the capacity of adsorption of metals at different concentrations. As found by numerous researchers, the optimum contact time range for Cr(VI), Ni(II), and Cu(II) adsorption by chitosan is a narrow range of 150-240 min [91, 93, 94]. The optimum contact time for Cr(VI) removal showed 180 min [91]. Vijayalakshmi et al. [93] found that the optimum contact time for Cu(II) removal was 240 min. While the optimum contact time for Ni(II) and Cu(II) solutions were found to be 150 min by the study of Swayampakula et al. [94].

2.3.1.3 Nanochitosan application for heavy metal removal

The present advances in nanotechnology pointed out that nanomaterial can be useful in solving the problems pollution from heavy metal. Chitosan in nanoscale, nanochitosan, have much higher surface areas than bulk materials and show different properties because of their small size. The properties of nanochitosan or nanoadsorbents is being taken advantage for increasing more effective sorbents and improving the existing ones to remove heavy metal ions and to recover from effluents. The surface reactivity and high surface area compared with granular forms allow the nanoparticles to generate a lower the hazardous by products and remediate more material at a higher rate [96]. The surface sorption method by various adsorbents has the edge over other methods due to low operating and waste treatment costs, lower volume and easier-to-remove sludge formation, less consumption of reagents and their relatively easy transportation and storage [97]. Nanoadsorbents could be worked most effectively both in a very low and high concentration range of pollution (1-1,000 mg/L), where other methods are ineffective, or time-consuming. Moreover, nanoadsorbents are greatly transportable in porous of media because they are much smaller than the relevant pore spaces, so they can be transported well by the flow in porous of media [98]. Therefore, the nanoadsorbents can be operated in situ, within the polluted zone where treatment is needed. In situ, involves treatment of contaminants in place, in comparison to ex situ where treatment occur after transferring the contaminated material to a more convenient location [99], adding more cost and environmental impact to the process (e.g. pumping, transportation, instrumentations and treatment of contaminants). However, the disadvantage of nanoadsorbent is difficult to separate.

The novel sorbent nanochitosan is the good alternative for removal heavy metals because advantage of nanotechnology will enhance efficiency of chitosan. Govindarajan et al. [100] studied the removal of cadmium and chromium ions from aqueous solutions using nanochitosan(NC)/carboxymethyl cellulose (CMC) blend. The results indicate that under the optimum conditions, the NC/CMC blend was found as an effective adsorbent for cadmium.

2.3.1.4 Comparison of adsorption capacity by chitosan adsorbents

There many parameters affect to the adsorption capacity of chitosan such as the source of the polysaccharide, preparation conditions, the degree of acetylation, molecular weight, crystallinity, and hydrophilicity [101]. The binding of chitosan onto substance nanoparticles will probably yield another novel nano-adsorbent for the efficient removal of heavy metal ions [102]. Table 2.3 displays the comparison of adsorption capacity (mg/g) of chitosan onto substance for many types of heavy metal and adsorbents.

Table 2.3 Comparison of adsorption capacity of chitosan as adsorbents to remove heavy metals

Adsorbents	Adsorption capacity (mg/g)						Refs.	
	Cd	Cr	Hg	Cu	Pb	Ni		Co
Chitosan				59.0				[103]
Chitosan				16.8		2.4		[104]
Chitosan				50.0				[16]
Chitosan				33.4				[83]
Chitosan				1.6			1.3	[105]
Chitosan-bound Fe ₃ O ₄ magnetic				21.5				[102]
Coating Fe ₃ O ₄ Magnetic with Humic Acid	50.4		97.7	46.3	92.4			[106]
Chitosan-coated magnetic with α -ketoglutaric acid				81.3				[107]
Magnetic nanoparticles coated by chitosan carrying of α -ketoglutaric acid				96.2				[20]

Table 2.3 (cont)

Adsorbents	Adsorption capacity (mg/g)							Refs.
	Cd	Cr	Hg	Cu	Pb	Ni	Co	
Magnetic chitosan a simple one-step				35.5				[4]
Chitosan-GLA beads				59.7				[108]
Chitosan-ECH beads				62.5				[108]
Chitosan-EGDE beads				45.9				[108]
Chitosan coated perlite				196.1		114.9		[95]
chitosan-coated perlite beads				147.1				[95]
Chitosan-bound silica	18.3				57.7			[109]
Chitosan-coated PVC beads				87.9				[19]
chitosan-coated cotton fibers	15.7		104.3	24.8	101.5	7.63		[110]
Chitosan coated acid treated oil palm shell charcoal		60.3						[91]
Chitosan coated oil palm shell charcoal		52.7						[91]
Acid treated oil palm shell Charcoal		44.7						[91]
EDTA–Chitosan						123.3		[111]
DTPA–Chitosan						117.4		[112]
Chitosan/PVA				47.9				[83]
Amino-functionalized		11.24		12.4				[113]
Amino-functionalized magnetic nanosorbent				25.8				[114]
amino-functionalized Fe ₃ O ₄ @SiO ₂ magnetic	93.1				148.1			[115]
Non-cross linked chitosan				80				[16]
Chitosan acetate crown ether				23.9		0.7		[116]
Chitosan diacetate crown ether				31.3		4.1		[116]
Epichlorohydrine cross- linked chitosan				16.8		6.4		[116]

2.3.2 Common isotherms for heavy metal adsorption

The isotherms were used to estimate the adsorption capacity of adsorbent at equilibrium condition. The relation between amount adsorbed and concentration was used to study the isotherm. Many isotherms were used for heavy metal adsorption.

However, there are two widely accepted and easily linearized adsorption isotherm models of chitosan adsorbent proposed by Langmuir and Freundlich. Sips isotherm is a combination of the Langmuir and Freundlich isotherm. They are the mathematical models that used to explain the distribution of the adsorbate species between liquid and solid phases. The models assume the heterogeneity or homogeneity of the solid surface, the type of coverage, and the possibility of interaction between the adsorbate species as assumption of isotherms [117]. The adsorption isotherms are different according to assumption and results from experiment. Qiu (2007) [118] and Ameesha (2006) [119] summarized the Langmuir, Freundlich, and Sips isotherms for adsorption process as exhibited in Table 2.4.

2.3.2.1 Langmuir isotherm

The assumption of Langmuir isotherm shows occurs in a monolayer or that adsorption may only follow at a fixed number of limited sites on the surface with all adsorption sites identical and energetically equivalent. Langmuir equation is based on the assumptions of a structurally homogeneous adsorbent [20, 120]. From the literature, Langmuir isotherm was used to describe the equilibrium between adsorbed heavy metals on chitosan [4, 5, 14, 20, 80, 91, 109, 114, 117, 121-124].

2.3.2.2 Freundlich isotherm

Freundlich isotherm is the most important multisite adsorption isotherm for rough surfaces which an empirical equation employed to describe heterogeneous systems. Moreover, the sorption on an energetically heterogeneous surface on which the adsorbed molecules are interactive and the amount of solute adsorbed increases infinitely with increase in the concentration and is given [20]. The many researchers found that adsorption isotherms are better fitted to the Freundlich isotherm [14, 100, 117] [19, 93, 94, 125]. The models are able to describe many data effectively. Since the parameters of these models do not have a physical interpretation to them, their use is limited [126, 127].

2.3.2.3 Sips isotherm

Sips isotherm is a combination of the Langmuir and Freundlich isotherm expressions expected for describing the heterogeneous adsorption process [128]. The limitation of the rising heavy metal concentration associated with Freundlich isotherm model. Therefore, at low concentrations of heavy metal it effectively reduces to a Freundlich isotherm, while at high heavy metal concentrations it predicts a monolayer adsorption capacity characteristic of the Langmuir isotherm. Moreover, it has the advantage of reducing to the Freundlich isotherm at low pressures and approaches the monolayer capacity at high pressure similar to the Langmuir isotherm. The equation parameters of Sips isotherm are controlled mostly by the operating conditions such as pH, temperature and concentration [129].

Table 2.4 Adsorption isotherms for water treatment

Isotherm Types	Assumption	Description
Langmuir	<ul style="list-style-type: none"> - Single layer - The surface consists of adsorption sites - All adsorbed species interact only with the sites and not with each other - Adsorption is limited to a monolayer 	<ul style="list-style-type: none"> - Homogeneous surface of adsorbent - Equal adsorption affinity and one site does not affect adjacent site - Limit at low range of adsorbate concentration - Monolayer adsorption
	<ul style="list-style-type: none"> - Adsorption energy of all sites is identical and independent of the presence of adsorbed species on the other sites 	
Freundlich	Empirical	<ul style="list-style-type: none"> - Heterogenous surface of adsorbent - Wide range of adsorbate concentration is acceptable

Table 2.4 (cont)

Isotherm Types	Assumption	Description
Sips	-The assumption depend of concentration of heavy metal -Adsorption is limited to a monolayer at high heavy metal concentrations	The combination of the Langmuir and Freundlich isotherm

2.3.3 Kinetics model for heavy metal adsorption

Adsorption kinetics are the main factors to evaluate the performance of sorbent [16]. Kinetics studies was used to determine the time course of metal uptake. The interaction of adsorbate- adsorbent and system condition are the factor of the adsorption kinetics. A rapid uptake would mean shorter contact times needed between adsorbent and heavy metal, and then smaller equipment and reduced costs [114, 126, 130]. Some of the frequently kinetic models mathematical equations in heavy metals adsorption kinetics are present in Table 2.5 [114].

2.3.3.1 Lagergren pseudo-first order

Lagergren pseudo- first order equation was used to describe the adsorption of liquid-solid systems based on solid capacity. It has been used for the adsorption of an adsorbate from an aqueous solution [130]. The rate of Lagergren pseudo-first order depends on initial concentration of heavy metals [131]. The study of Swayampakula et al. [94] found that the composite chitosan-coated biosorbent for Cu (II), Ni(II), and Co(II) removal follows Lagergren first order kinetic model, while adsorption isotherm were fitted to Freundlich and Langmuir models. Moreover, Lagergren pseudo-first order equation has been usually used for the adsorption of heavy metals onto chitosan, such as the adsorption of As(III) and As(V) [132], adsorption of Cu(II) [83, 133], adsorption of Au(III) [134], adsorption of Cr(VI) and Cu(II) [135].

Table 2.5 Mathematical equations in heavy metals adsorption kinetics [114, 131]

Kinetic models	Linear equations	Plot	Calculated coefficients
Lagergren pseudo-first-order	$\ln(q_e - q_t) = \ln q_e - k_1 t$	$\ln(q_e - q_t)$ vs. t	$k_1 = -\text{slope}$, $q_e = e^{\text{intercept}}$
Pseudo-second-order	$\frac{t}{q_t} = \frac{1}{k_2 q_e^2} + \frac{t}{q_e}$	t/q_t vs. t	$k_2 = \text{slope}^2 / \text{intercept}$, $q_e = 1 / \text{Slope}$
Elovich	$q_t = \frac{1}{\beta} \ln(\alpha\beta) + \frac{1}{\beta} \ln(t)$	q_t vs. $\ln(t)$	$A = e$ (intercept/slope- $\ln(\beta)$) $\beta = 1/\text{slope}$
Intraparticle diffusion	$q_t = k_{\text{intra}} t^{1/2} + C$	q_t vs. $t^{1/2}$	$k_{\text{intra}} = \text{slope}$

Where q_e and q_t are the adsorption capacity (mg/g) at equilibrium and at time t (min), k is the rate constant, and h is the initial sorption rate in pseudo-second order model.

2.3.3.2 Pseudo-second order

Pseudo-second order is generally more appropriate than pseudo first order model to represent kinetic data of heavy metal biosorption in batch reactor, it widely used in many adsorption processes. In most system regression coefficient higher than 0.98 were obtained and calculated [136, 137]. There are two processes involved in metal ion adsorption on chitosan. They are play important role namely, diffusion of metal ion through the boundary layer to the surface of the chitosan and chemical reaction by adsorption of metal ion at an active site on the surface of chitosan via chelation (functional group). The adsorption capacity of chitosan is proportional to the active sites and the number of functional groups on its surface. The high adsorption capacity with short equilibrium time indicates a high degree of affinity between the metal and chitosan. Therefore, the kinetics of adsorption depends on the porosity or surface area and the active site of amine group of chitosan. If the amount of chitosan in the reaction increases, its active surface area and function group are changed. Both factors effect to rate and behavior of adsorption between chitosan and metal ion. Hence, this kinetic is second order which can predict the rate of reaction. However, the effect of surface area can be determined by using BET technique but the effect from amine group of chitosan cannot predict the rate of reaction which this mechanism is called pseudo order. Therefore, most of the researchers found that the kinetics of the

interactions between metal ion and chitosan were best described by pseudo-second-order mechanism. The pseudo-second-order reaction rate is dependent on the amount of heavy metal concentration on the surface and the amount heavy metal at equilibrium [138]. Many studies revealed that the kinetic of chitosan as adsorbent correlated well with pseudo-second order, which indicated that chemisorption is the rate-limiting step [14, 19, 93, 110, 139-141].

2.3.3.3 Elovich equation

The Elovich equation has been widely used in adsorption kinetics, which describes chemical adsorption (chemical reaction) mechanism in nature. The approaching equilibrium parameter of Elovich equation was used here to describe the characteristic curves of adsorption kinetics [142]. The Elovich equation is used to interpret the kinetics of sorption and successfully describe the predominantly chemical sorption on highly heterogeneous sorbents [114]. The rate of the Elovich depends on adsorption capacity (decreasing exponentially with increasing of surface coverage) [131].

2.3.3.4 Intraparticle diffusion

In order to examine the internal diffusion mechanism during the adsorption of metal ions onto chitosan, the intraparticle diffusion equation has been applied for the analysis of adsorption kinetics [142, 143]. It is transportation process including movement of species from the bulk of the solution to the solid phase. Intraparticle diffusion equation is usually used to describe the adsorption process occurring on a porous adsorbent which the rate depends on pore diffusion and surface diffusion of compound in porous of adsorbent which controlled by an external film resistance and/or mass transfer is controlled by internal or intraparticle diffusion [131].

2.3.4 Adsorption process operation

The removal techniques for adsorption process could be categorized into two main types namely batch process and continuous process.

2.3.4.1 Batch process

In the batch process, the adsorbents could be utilized up to the maximum capacity which the effects of different parameters such as pH, initial concentration, dose of adsorbent, contact time, agitation rate, and temperature were investigated in order to find the optimum conditions for implementing. However, the industrial wastewater is not suitable for batch process because the industries largely producing and continuously wastewater, it has to storage the wastewater before treatment by big tanks. Large area is needed to place the tanks, consequently batch process a lot times and expensive are required to complete the process. Therefore, the industries generally using the continuous process to treat the wastewater [144].

2.3.4.2 Continuous process

The continuous process is usually used for the industries wastewater treatment. The fixed bed adsorption column is established for industries wastewater treatment. The adsorbents beds are packed in a column for the wastewater to flow through it. But the bed is easier being saturated with the adsorbate particles after operated. Finally, the bed is completely exhausted after certain time of process. The adsorbent has to be replaced when the bed is exhausted. The regeneration for the adsorption bed is needed when the bed is saturated [144].

Continuous adsorption studies are required to collect the experimental data for the design of adsorption column and for subsequent scale-up from pilot plant to industrial scale operation [145]. For the continuous flow adsorption system, the Thomas model and Yoon nelson model can be used to describe the adsorption kinetics and evaluating the maximum solid phase concentration and rate constant.

(1) Thomas model

Thomas model is one of the most common and widely used to calculate the adsorption rate constant of column performance modeling and prediction of breakthrough curve. Thomas model is categorized as a single resistance mass transfer model. It is suitable to estimate the adsorption process, which the external mass transfer was the rate limiting mechanism during the initial adsorption stages, while intraparticle diffusion was dominant in the middle [146]. Thomas model has been usually predicted

well the adsorption capacity for heavy metals onto chitosan in a fixed bed column, such as the adsorption of Ni(II), Cu(II) and Pb(II) ions [147], adsorption of Cr(VI) ions [148], the adsorption Cu(II) [149].

(2) Yoon-Nelson model

Yoon-Nelson model is based on the assumption that the change in the influent and effluent concentration ratio of a column is proportional to the difference in the adsorption and breakthrough rate. Yoon-Nelson model is less useful to achieve process variables and to predict adsorption under variety conditions [150]. Sugashini and Begum found that Yoon-Nelson and Thomas models predicted well the adsorption capacity for Cr(VI) ions in a fixed bed column [151].

For the continuous system, breakthrough curve is the main part of the adsorption at any time takes place in a relatively narrow adsorption. As the solution continues to flow, the mass-transfer zone which is S-shaped, moves down the column. When almost half of the bed is saturated with solute, the outlet concentration is still approximately zero until the mass-transfer zone start to reach the tower outlet. Then the outlet concentration starts to rise which is called the break point. After break point is reached, the concentration rise rapidly which indicates the end of the break through curve and the bed is already ineffective [152].

The performance of continuous system is described through the concept of a breakthrough curve. A breakthrough curve is a plot of the concentration at a fixed point in the bed, usually at or near the outlet, versus time. Alternatively, it can be plotted in the dimensionless form by dividing the effluent concentration by the inlet concentration. The breakthrough appearance time and the shape of the curve are very important characteristics for determining the operation and the dynamic response of the sorption column [153].

2.4 Application of membrane filtration process for heavy metal removal

The membrane filtration process is one method used in the practice of solid-liquid separation. It displays great ability for heavy metal removal. The membrane filtration processes was used to remove heavy metals from the wastewater such as

ultrafiltration, nanofiltration, and reverse osmosis [10] . The membrane filtration processes will create a new dimension in separation and purification techniques for solid-liquid system. This main technique separates impurities from water. Membrane filtration technology has high cost, process complexity, membrane fouling and low permeate flux [10]. However, there are major advantages such as efficiency for heavy metal removal, low energy consumption, small land area requirement, easy up-grading of existing facilities, continuous separation, better effluent quality, avoidance of any chemical addition. Therefore, membrane filtration technique is the preferred method to reach the excellent choice [154].

Membrane filtration techniques composite a pressure vessel and a semi-permeable membrane inside that permits the feed water to penetrate. The principle of membrane separate process is shown in Figure 2.3. Feed, a mixture of two or more components is separated by means of one or more species move through membrane faster than another or other species. Feed, retentate and permeate are usually liquid or gas, the membrane may be nonporous polymeric film, porous polymer, ceramic, or liquid. The membrane must not dissolve and disintegrate. The important factor that indicates the ability of separation is the flow rate of substance that pass through membrane or permeate flux. Unit of flux is volume or weight or mole of permeate per time. In addition, the ability of separation is also considered from separation factor or rejection coefficient [155].

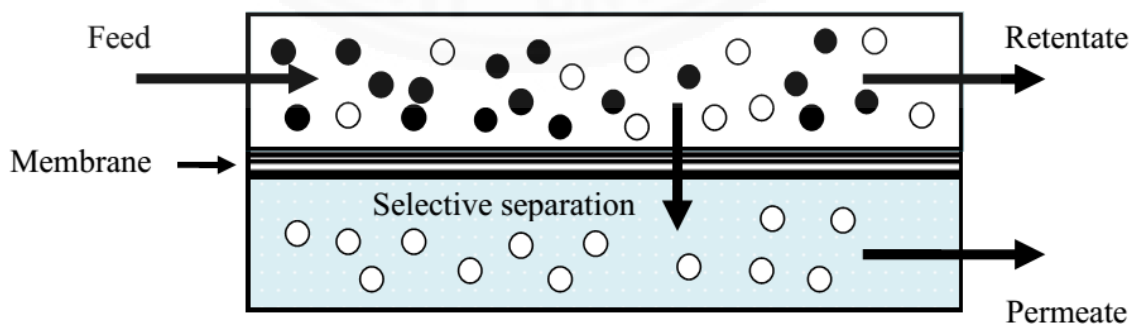


Figure 2.3 Schematic of principle membrane process

2.4.1 Membrane filtration operation

The membrane filtration operation could be divided into two main types namely cross flow and dead-end filtrations. The type depends on module configuration and application. The cross flow filtration operation allows lower fouling and smaller flux decline than the dead-end filtration operation. As the cross flow filtration operation can reduce fouling and cake layer formation on surface of membrane with adjustment of cross flow velocity of feed. While dead end filtration operation, though it creates great membrane fouling, its advantage is high water recovery relative to cross flow type. Schematic figure of the membrane filtration operations are exhibited in Figure 2.4 [131].

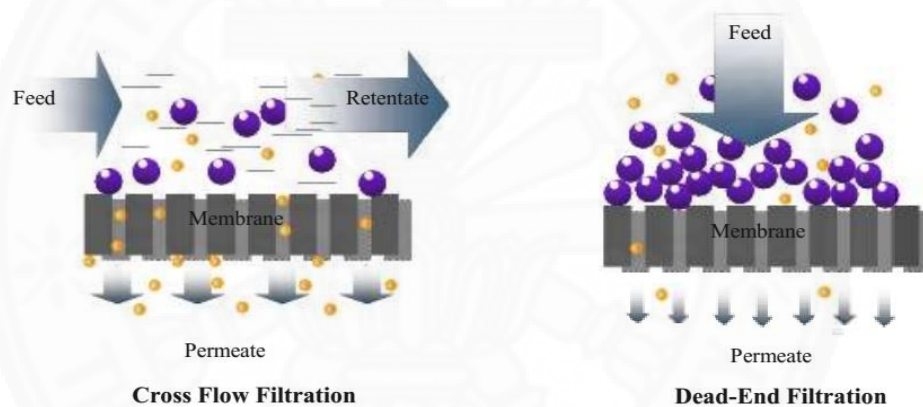


Figure 2.4 The types of membrane filtration operation [131]

2.4.2 Parameters affecting membrane performances

2.4.2.1 Fouling and compaction

The fouling and compaction of membrane are a negative effect on membrane performance. The membrane fouling phenomena is generally indicated as build-up of organic or inorganic matters on the surface of membrane and obstruction of feed channels. At the early steps of membrane fouling, the efficiency changes are like those caused by the compaction phenomena. The fouling development is generally related to a rise in pressure drop. An uncontrolled fouling phenomena of membrane process may result in very strong capacity degradation and through complete damage of membrane elements. The best practical method to control fouling of membrane is to

recognize the source of the fouling phenomena and remove it by the adjusting operating conditions or pretreatment process [156]. From the literature, Wang et al. found that chitosan coated on non-woven fabric composite membranes surface showed high flux, high effluent quality and excellent antifouling property [157]. The modified membranes with chitosan solution exhibited a good anti-fouling properties in reducing the irreversible membrane fouling [158]. However, chemical cleaning can be eliminated the foulant deposits from the surface of membrane. The achievement of the cleaning system depends on proper selection of the cleaning solution and the age of the foulant deposit on membrane surface [156].

The membrane material is exposed to high pressure of the feed water during operation. The exposure of membranes to high pressure may cause a rise in the density of membrane material, which will decline the rate of diffusion of water and dissolved constituents pass through the membrane. As a result of these process, higher pressure has to be used to keep the design permeate flow. The compaction of membrane effects to decline of flux, and has strongest results in during the early operating period [156, 159].

2.4.2.2 Applied pressure or feed pressure

The feed pressure is adjusted to requite for variation of feed water and permeate flux decrease because of fouling or compaction of the membrane. The pump has to be adjusted to run feed pressure parallel to the preliminary membrane capability and to compensate for supposed flux decline. The mechanical strength of the membrane module or element sets the limit of feed flow [160]. However, at the high pressure leads to increase the overall heavy metal removal efficiency and high consumes energy [11]. The performance of membrane also reduces over time, causing the declining permeate flow, rising the pressure requirement and the energy consumption [11, 161, 162].

2.5 Application of adsorption-filtration technique for heavy metal removal

Several studies for heavy metal removal from wastewater have been conduct regarding the adsorption and microfiltration process. The combination of adsorption and membrane filtration is of interest. In order to shorten the treatment process and to enhance the heavy metals removal, adsorbents were coated on the

surface of a membrane, resulting in simultaneous filtration and adsorption on the membrane surface [71]. Many materials were used as supporting of adsorbent. However, the adsorption process regularly requires an additional stage in order to separate adsorbent from treated wastewater. There are only few studies investigating efficiency of treatments applied methods include sorption and membrane filtration. The adsorption through the support and chitosan membrane can be removed almost completely with a membrane capacity of 0.1 g Cu(II)/g chitosan [163]. Zaspalis et al (2007) [164] found that 99% of As(V) ions was eliminated at an initial concentration of 1 mg/L by an adsorption–filtration process using porous ceramic membrane. Chitosan based ceramic membranes using dip coating technique was studied for Hg(II) and As(III) removal. Almost 100% removals Hg(II) and As(III) were observed for both at 0.5 mg/L and 1.0 mg/L of initial concentration, respectively [162].

Chapter 3

Materials and Methods

3.1 Chemicals and materials

3.1.1 Adsorbent

Chitosan flakes with a deacetylation degree of 85 %, size of 1-3 mm, and molecular weight of 50,000 daltons were supplied by Bio 21 Co. Ltd, Thailand. Acetic acid (purity 100 %), sodium tripolyphosphate (TPP, purity 99.9 %) were used for preparation chitosan nanoparticles. The formation of nanoparticles was generated from the interaction between the negative groups of TPP and the positively charged amino groups of chitosan. Glutaraldehyde (GLA, purity 25 %) and polyethylene glycol (PEG 1000) were used graft with chitosan nanoparticles in order to enhance water solubility, chelating, and adsorption capacity. Cellophane (Cellu Sep T4 part#1430-33) was obtained from P. Intertrade Equipment Co., Ltd., Thailand.

3.1.2 Supporting materials

Bituminous activated carbon (TH 12/40 ZY 245) was obtained from Aqua Treatment Co., Ltd., Thailand. Ceramic balls with size 2 mm diameters were purchased from Chemmin Co., Ltd. A cross-flow microfiltration, ZrO₂-ceramic tubular membrane (25 mm length, 6 mm internal diameter, 10 mm external diameter, 0.0047 m² effective area, and 0.4 μm effective pore diameter), were purchased from Tami industries (Germany).

3.1.3 Synthetic wastewater

All the chemicals used in this study were analytical grade and used without any further purification. They comprised copper nitrate hexahydrate (Cu(NO₃)₂·6H₂O, purity 99 %), nickel nitrate hexahydrate (Ni(NO₃)₂·6H₂O, purity 99 %), potassium dichromate (K₂Cr₂O₇, purity 99.9 %). A stock solution of heavy metals was prepared (1,000 mg/L) by dissolving Cu(NO₃)₂·6H₂O, Ni(NO₃)₂·6H₂O, and K₂Cr₂O₇ with deionized water (DI water). Sodium hydroxide (NaOH), sulfuric acid (H₂SO₄) and

hydrochloric acid (HCl) were used for pH adjustment of solution to a pH 4-6. A series of solutions used during the experiments were prepared by diluting the stock solution to the desired concentrations.

3.2 Experimental procedures

This study comprises of three main steps namely: (1) chitosan nanoparticles preparation (2) surface coating of supporting materials and (3) the heavy metal removal process. Figure 3.1 demonstrates the experimental strategy.

3.2.1 Preparation of chitosan nanoparticles

Chitosan nanoparticles (CN) were prepared according to the ionic gelation method with TPP, in which TPP acts as a crosslinking agent. The process is based on the negative groups of the TPP and the positively charged amino groups of chitosan. TPP generates intermolecular crosslinking reactions between the free amino groups of chitosan, which leads to the formation of nanoparticle size colloids [165-167].

Two hundred grams of flake chitosan was added into 200 mL of 1% acetic acid. This mixture was stirred at 400 rpm, room temperature, using a magnetic stirrer until it was completely dissolved. TPP solution (50 mL) was then gradually added to the chitosan solution at a rate of 1.0 mL per minute with a mixing speed of 1,200 rpm. The chitosan solution was neutralized by dialysis with cellophane.

3.2.2 Preparation of cross-linked chitosan nanoparticles

3.2.2.1 Chitosan nanoparticles-glutaraldehyde

The chitosan nanoparticles solution was used in the preparation of chitosan nanoparticles cross linked with glutaraldehyde (CN-GLA). The 0.5 mL of 25% GLA solution was added to the 250 mL of CN solution at an average mixing speed of 1,200 rpm for 2 hr.

3.2.2.2 Chitosan nanoparticles-polyethylene glycol

The chitosan nanoparticles solution was used in the preparation of chitosan nanoparticles mixed with polyethylene glycol (CN-PEG). The 200 mg of PEG

was added to 250 mL of CN solution. The solution was mixed thoroughly and stirred for 2 h at a mixing speed of 1,200 rpm.

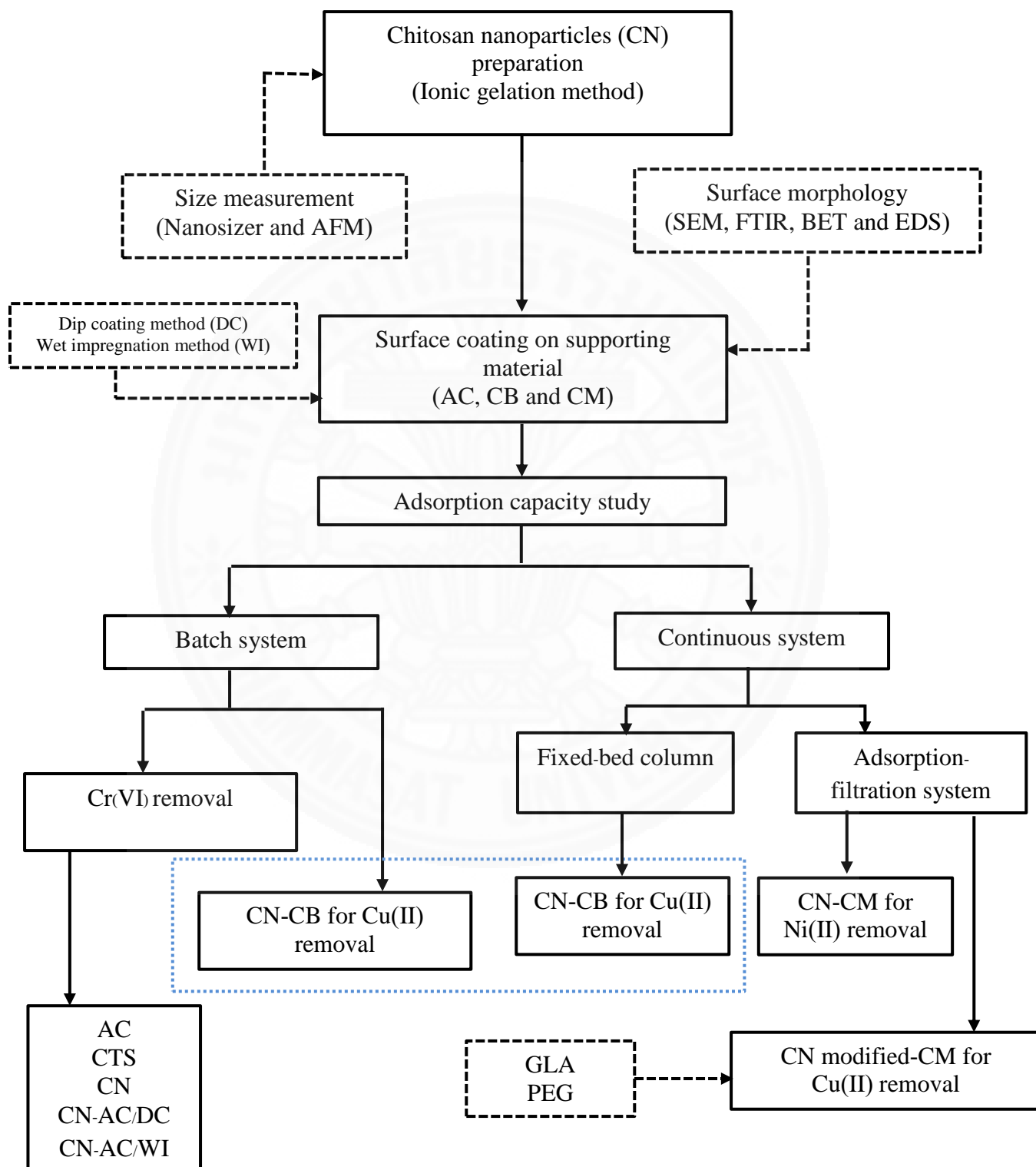


Figure 3.1 The experimental strategies

3.2.3 Surface coating of supporting material

Bituminous activated carbon (AC), alumina ceramic balls (CB) and tubular ceramic membrane (CM) were used as a support for CN. They were washed with deionized water (DI water) to remove impurities and dried at 100°C for 1 hr, after which, it was stored in a desiccator. AC would be subsequently bound to CN via two deposition methods, dip coating and wet impregnation while CB and CM via dip coating method.

3.2.3.1 Dip coating method

The supporting materials were added into CN solution for 2 min. These materials were dried at 60°C in an oven for 15 min. The 2 min coating was selected from the preliminary tests. A coating time beyond 2 min did not result in much increase in the amount of CN coated onto the supporting materials. This step was repeated 10 times to coat a sufficient amount of CN onto the supporting material. Afterward, the CN-coated supporting material were dried at 60°C for 3 h and stored in a desiccator.

3.2.3.2 Wet impregnation coating method

The supporting material was added into the CN solution to obtain a suspension mixture which was subjected to an evaporation afterward. Water was removed from the supporting material for 3 h using an evaporator. The CN-coated supporting material was further dried at 60 °C for 3 h and stored in a desiccator.

The weight percentage of CN coated on supporting materials was calculated by Equation (3.1):

$$\% \text{ CN} = \frac{W_2 - W_1}{W_1} \times 100 \quad \text{Equation (3.1)}$$

where W_1 is the mass of supporting materials, and W_2 is the total mass of supporting materials and CN.

The thickness of membrane coated layer (CMCN, CMCN-GLA, and CMCN-PEG) was evaluated based on Equation (3.2) [37, 168]. Weights of the membrane before and after depositions were determined.

$$L = \frac{m_2 - m_1}{A_p (1 - \varepsilon)} \quad \text{Equation (3.2)}$$

where L is the membrane thickness, m_1 is the mass of membrane support $\text{ZrO}_2\text{-TiO}_2$, m_2 is the total mass of the support and the coated chitosan nanoparticles, A is the membrane area (0.0047 m^2), p is the theoretical density of $\text{ZrO}_2\text{-TiO}_2$ (5.68 g/cm^3), and ε the assumed porosity of the membrane (25%).

3.2.4 Heavy metal removal operations

3.2.4.1 Batch adsorption experiment

The adsorption experiments were carried out using 20 mL of heavy metal solution in a series of 125 mL erlenmeyer flasks. The pH of the heavy metal solution was adjusted in a pH range of 4-6 by using 0.1 M HCl and 0.1 M NaOH solutions prior to the study. For each batch test, 20 mg of adsorbents were put into 20 mL of aqueous solution containing heavy metal for 24 h. The adsorbed amount of heavy metal per unit weight of adsorbent (q_e (mg/g)) was calculated from the mass balance equation (Equation 3.3):

$$q_e = \frac{C_i - C_e}{W} \times V \quad \text{Equation (3.3)}$$

The removal efficiency (E) of heavy metal was measured by Equation (3.4):

$$E (\%) = \frac{C_0 - C_e}{C_0} \times 100 \quad \text{Equation (3.4)}$$

where, C_0 and C_e are the initial and equilibrium concentrations of heavy metal in mg/L, respectively; V is the volume of heavy metal solution, and W is the weight of adsorbent.

(1) Application of adsorption isotherms

Langmuir and Freundlich adsorption isotherms were used to fit the experimental data. The mathematical expressions are presented in Equations (3.5) and (3.6), respectively [20]. The linear regression models were examined by calculating the coefficient of determination (R^2).

$$q_e = \frac{q_m K_L C_e}{1 + K_L C_e} \quad \text{Equation (3.5)}$$

$$q_e = K_F C_e^{\frac{1}{n}} \quad \text{Equation (3.6)}$$

where q_e is the amount of heavy metal adsorbed per unit weight of adsorbents at specified equilibrium (mg/g), C_e is the equilibrium concentration in the solution (mg/L), q_m is the maximum adsorption at monolayer coverage (mg/g), and K_L is the Langmuir constant related to energy of adsorption which quantitatively reflects the affinity of binding sites (L/mg), K_F is a Freundlich constant representing the adsorption capacity (mg/g), and n is a constant depicting the adsorption intensity (dimensionless).

The Langmuir isotherm model can be explained in terms of a dimensionless constant separation factor or equilibrium parameter (R_L), which is defined in Equation (3.7). The R_L values of $R_L > 1$, $0 < R_L < 1$, and $R_L = 0$ suggest that adsorption is unfavorable, favorable and irreversible, respectively [169].

$$R_L = \frac{1}{1 + K_L C_0} \quad \text{Equation (3.7)}$$

where C_0 is initial of heavy metal concentration (mg/L).

(2) Application of adsorption kinetics

The adsorption kinetics was evaluated using pseudo first-order, pseudo second-order equations intraparticle model, and Elovich model.

The equations are described in Equations (3.8), (3.9), (3.10), and (3.11), respectively [70, 170, 171].

$$\log\left(\frac{q_e}{q_e - q_t}\right) = \frac{k_1}{2.303} t \quad \text{Equation (3.8)}$$

$$\frac{1}{q_e - q_t} = \frac{1}{q_e} + k_2 \quad \text{Equation (3.9)}$$

$$q_t = k_i t^{0.5} \quad \text{Equation (3.10)}$$

$$q_t = \beta \ln(\alpha \beta) + \beta \ln t \quad \text{Equation (3.11)}$$

where q_e is the amounts of the sorption capacity at equilibrium (mg/g). q_t is the amounts of the sorption capacity (mg/g) at time t (min). k_1 (1/min) is the rate constant of pseudo-first-order adsorption. k_2 is the second-order rate constant at the equilibrium ((g/mg)/min). k_i is the intraparticle diffusion rate constant ((mg/g)/min^{0.5}). α is the initial heavy metal sorption rate ((mg/g)/min) and β is the desorption constant (g/mg) during any one experiment.

3.2.4.2 Fixed-bed column experiment

The adsorption experiments were conducted on a bench-scale column. The experimental set-up is depicted in Figure 3.2. Cylindrical packed bed column was made of acrylic, 0.8 cm internal diameter and 25 cm length. The column unit was equipped with a flow meter on the outlet exit pipe and a pressure gauge monitoring pressure at both the inlet and the outlet. In order to study the effect of initial concentration on the behavior of the adsorbent column, various concentrations and flow rates were investigated. All experiments were conducted at room temperature in an up flow configuration. The permeate flux and concentration from the column were observed at different time intervals and measured for heavy metal concentration.

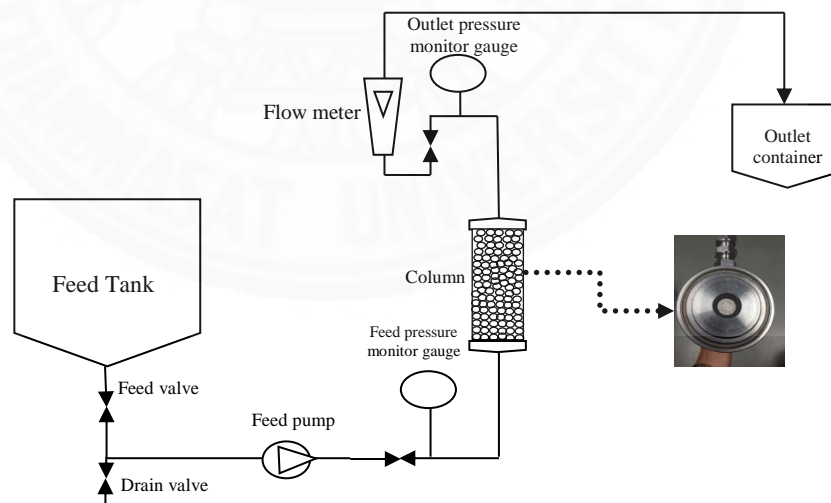


Figure 3.2 Experimental setup used for column adsorption experiments

The uptake capacity (q_e (mg/g)) or the amount of heavy metals bound to adsorbent is given by the equations (3.12) and (3.13) [172, 173].

$$q_{\text{total}} = \frac{Q}{1000} \int_{t=0}^{t=t_{\text{total}}} (C_0 - C_t) dt \quad \text{Equation (3.12)}$$

$$q_{e,\text{max}} = \frac{q_{\text{total}}}{m} \quad \text{Equation (3.13)}$$

where q_{total} is equal to the area under the plot of the adsorbed heavy metal concentration versus time (mg), $q_{e,\text{max}}$ is the maximum adsorption capacity (mg/g), Q is the flow rate (mL/min), C_0 and C_t are concentrations (mg/L) at initial and at set times, respectively, and m is the mass of the adsorbent (mg).

Cumulative mass of Cu(II) adsorbed (mg/g) is the total amount of Cu(II) adsorbed onto the chitosan calculated from the decrease in the Cu(II) concentration in the solution multiplied with the volume of the permeate collected up to that run.

The adsorption rate constant and prediction of the column performance were calculated by using Thomas model and Yoon-Nelson model. They were used to predict a breakthrough curve and adsorption kinetics which the derivation of Thomas model assumes Langmuir kinetics of adsorption-desorption and no axial dispersion so that the driving force for adsorption obeys second-order reversible reaction kinetics. The Yoon-Nelson assumes that the rate of decrease in the probability of adsorption for each adsorbate molecule is proportional to the probability of adsorbate adsorption and the probability of adsorbate breakthrough on the adsorbent. This model is simpler than other models, and also requires no data about the characteristics of the system such as the type of adsorbent and the physical properties of the adsorption bed [173].

The expression using the Thomas model for adsorption column is presented as in Equation (3.14) [9, 120, 174].

$$\frac{C_t}{C_0} = \frac{1}{1 + \exp(k_{\text{Th}}/Q (q_0 m - C_0 V_{\text{eff}}))} \quad \text{Equation (3.14)}$$

where $q_{e,\text{max}}$ is the maximum adsorption capacity (mg/g), Q is the flow rate (mL/min), C_0 is initial concentration (mg/L), C_t is concentration at time t (mg/L), and m is the mass of the adsorbent within the column (mg), k_{Th} is the Thomas model adsorption rate

constant (mL/min mg), q_0 is the adsorption capacity (mg/g), and V_{eff} is effluent volume (mL).

Yoon-Nelson model is less useful to achieve process variables and to predict adsorption under variety conditions [150]. The linear form of Yoon-Nelson model is expressed as Equation (3.15) [9, 120, 174].

$$\ln\left(\frac{c_t}{c_0 - c_t}\right) = k_{\text{YN}}t - \tau k_{\text{YN}} \quad \text{Equation (3.15)}$$

where k_{YN} (1/min) is the rate constant and τ (min) is the time required for 50% adsorbate breakthrough.

3.2.4.3 Adsorption-microfiltration experiments

The pilot unit used for adsorption- microfiltration experiments is illustrated in Figures 3.3 and 3.4. The unit was designed as a single-channel tubular membrane. It was equipped with a feed tank, rotameters, control and drain valves, pressure gauges, and a feed pump. The feed tank was filled with heavy metal solution. Permeation and adsorption tests were performed at a gauge pressure of 1 psi. The volumetric flow rates of the feed were controlled by a flow meter at 2.5 and 5.0 mL/min. The samples (feed, retentate and permeate) were collected at pre-determined time. The heavy metals adsorption and water permeation through the CN- coated ceramic membrane were measured.

The experimental performance was studied having control experiment without various adsorbents. Samples of feed, retentate, and permeate were collected at various time interval. The heavy metal adsorption and water permeation through the adsorbent coated ceramic membrane were measured.

The permeate flux (L/m².h) was measured by using the Equation (3.16) [175].

$$J = \frac{Q}{A \cdot \Delta t} \quad \text{Equation (3.16)}$$

where J is permeate flux (L/m².h), V_p is volume of permeate (L), A is active surface

area of membrane (m^2), and Δt is time collecting the permeate (h).

The amount of heavy metals bound to adsorbent or uptake capacity (q_e , mg/g) can be calculated by Equations (3.12) and (3.13). The breakthrough curve and the adsorption kinetics of the column performance were analyzed using Thomas model (Equation (3.14)).

3.2.4.4 Desorption experiments

After the column saturation, the unadsorbed heavy metal was removed with the DI water by feeding through column. The heavy metal was then desorbed with 0.1 M H_2SO_4 solution at a flow rate of 10 mL/min for 1 hr. After desorption, the adsorption was repeated. The adsorption-desorption for heavy metal was repeated for three consecutive cycles.

The percent desorption is expressed as Equation (3.17).

$$\% \text{ Desorption} = \frac{Cu_{ads} - Cu_{des}}{Cu_{ads}} \times 100 \quad \text{Equation (3.17)}$$

where Cu_{ads} is the amount of Cu(II) adsorbed (mg), calculated using Equation (3.12), but without division by the sorbent mass, and Cu_{des} is the amount of Cu(II) desorbed (mg), calculated from the concentration of Cu(II) in the desorbed solution.

3.2.5 Analytical methods

3.2.5.1 Chitosan nanoparticles analysis

The prepared samples were characterized for their morphologies and sizes using a zetasizer nano ZS (Malvern Instruments, Worcestershire, UK), and an atomic force microscope (AFM) (Seiko Instrument Model SPI 4000). The size measurement from these techniques is called hydrodynamic size and dry sizes, respectively. pH and turbidity were measured using a pH meter (Mettler Toledo Model SG2 - SevenGo™) and a turbidity meter (TLEAD TU 001), respectively.

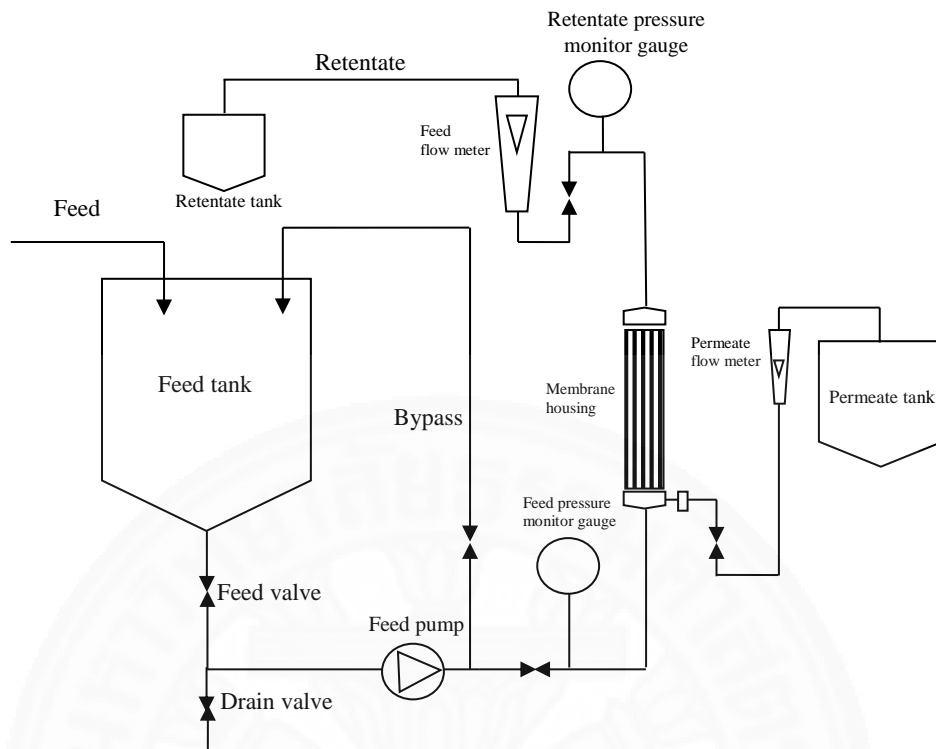


Figure 3.3 Flow diagram of the bench-scale membrane test unit



Figure 3.4 Picture of the bench-scale membrane test unit including: (a) feed tank, (b) permeate container, (c) membrane modules, (d) feed pump, (e) feed pressure gauge, (f) permeate flow meter, (g) pH and conductivity monitor, (h) control panel, and (i) retentate container

3.2.5.2 Surface analysis of supporting material

The functional groups of samples on surface were analyzed by Fourier transform infrared spectrometry (FTIR). The measurement was carried out using a Thermo Scientific Nicolet iD5 FT-IR spectrometer. The morphology of the chitosan nanoparticles, coated on supporting material, was examined by a scanning electron microscope (SEM) (Hitachi Model S-3400N) and field emission scanning electron microscope (FE-SEM) (JEOL Model JSM-7800F). The specific surface area was measured by Brunauer, Emmett and Teller (BET) (Micromeritics ASAP 2020). Element and chemical analysis was examined by Oxford Energy Dispersive Spectrometer (EDS/EDX) (LINK ISIS200).

3.2.5.3 Heavy metals analysis

The equilibrium concentration of metal was determined using an atomic absorption spectrometer (Perkin Elmer Analyst 200).

All the experiments were carried out in triplicate and data presented with these are the mean values. The relative standard deviation was less than 5%.

Chapter 4

Results and Discussion

4.1 Characterization of chitosan nanoparticles

4.1.1 Formation of chitosan nanoparticles

Chitosan nanoparticles (CN) were prepared by the ionic gelation of chitosan with sodium tripolyphosphate (TPP). High concentrations of TPP can gelatinize a great amount of chitosan. This effect can be seen in Table 4.1. To neutralize and concentrate the CN, for sizes in a similar range, a dialysis method using cellophane has been reported to be helpful [176]. Additionally, the dialysis method is effective in reducing the acidity of the CN solution, which contains dissolved acetic acid. According to Table 4.1, a clear solution of CN with TPP was observed in non-dialyzed conditions when the TPP and chitosan concentration were at 0.5 and 1-2 mg/mL, respectively. An opalescent suspension began to appear when the TPP concentration increased to 1 mg/mL. This opalescence was present in both dialyzed and non-dialyzed conditions at 1 mg/mL of chitosan. At higher concentrations of TPP and chitosan, the CN solutions were almost completely turbid due to the aggregation of CN at 3.0 mg/mL chitosan. The dialysates from dialysis exhibited turbidity because of two reasons: firstly, CN was concentrated more in the cellophane bag, and secondly, the acidity of the solution gradually decreased, inducing CN to aggregate in low charge-charge repulsion [177].

Table 4.1 Formation of the chitosan particles with addition of TPP

Chitosan (mg/mL)	TPP (mg/mL)					
	Dialyzed			Non-dialyzed		
	0.5	1	2	0.5	1	2
1	●	●	✱	○	●	●
2	✱	✱	✱	○	●	✱
3	✱	✱	✱	✱	✱	✱
	○ clear	● opalescent	✱ aggregate			

4.1.2 Size of chitosan nanoparticles

The observation of the CN solution agrees with the results obtained from the size measurement acquired from the Zetasizer instrument. The results shown in Figure 4.1 demonstrate the trend of size formation for CN from both dialyzed and non-dialyzed processes. An increase of chitosan concentration (Figure 4.1a), resulted in the increased CN hydrodynamic size from under 200 nm to above 1,200 nm. The size of CN in the dialyzed process was somewhat larger than that in the non-dialyzed case, except when the chitosan concentration was at 3 mg/mL. In accordance with the size measurement experiment (Figure 4.1b), the effect of TPP concentration in gelatinizing CN solution was predominant at high concentration (2 mg/mL). The hydrodynamic size of CN, rising to about 2,000 nm, was presumably derived from nanoparticle aggregation.

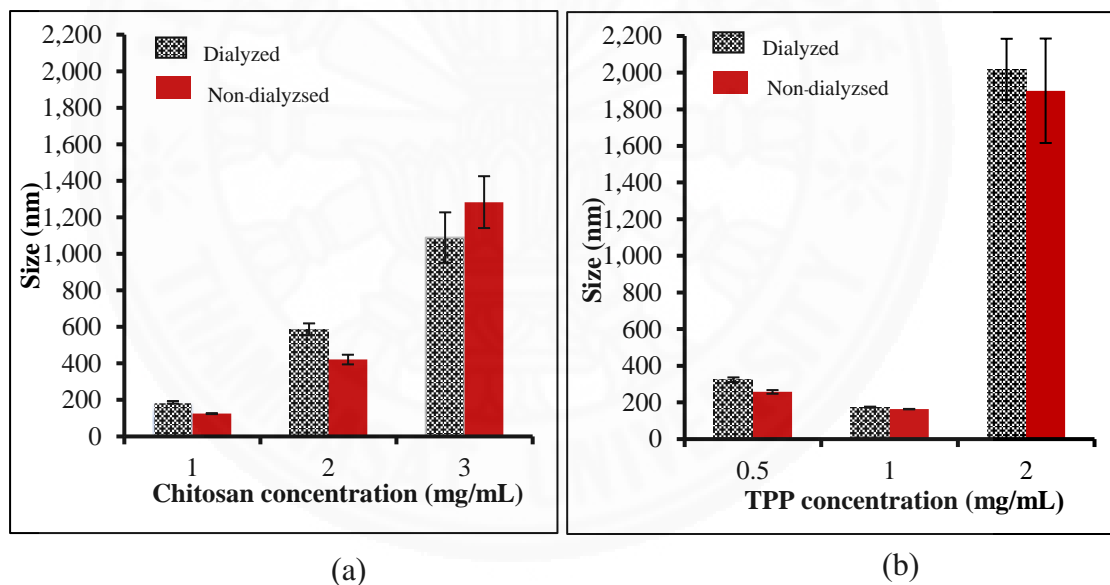


Figure 4.1 Influence of chitosan and TPP concentrations on the particle size: (a) at TPP concentration of 1 mg/mL and (b) at chitosan concentration of 1 mg/mL

The average CN hydrodynamic size was about 160 nm at a ratio of chitosan to TPP of 1:1 (w/w), while the average polydispersity index (PDI) was 0.629 and the zeta potential was positive. At this applicable ratio, the obtained CN was an acceptable nanometer size of 125-160 nanometer and the standard deviations was lower than 4%.

Hui and Changyou [178] and Gan et al. [179] found that a ratio of chitosan to TPP of 2:1 to 1:1 is optimal. The CN solution has an average particle size diameter of 250 to 800 nm with positive zeta potential at maximum and minimum chitosan concentrations applied [180]. The particle size and surface zeta potential can be manipulated by varying the fabrication conditions, such as chitosan to TPP ratio and concentration, solution pH, molar mass of the chitosan, and salt addition [178, 181]. The dry sizes of CN at a ratio of chitosan to TPP of 1:1 (w/w) and non-dialyzed processes were also investigated by topographical analysis with an atomic force microscope (AFM). Figure 4.2 presents the AFM image containing many spherical spots, attributable to CN with a smooth surface, separately dispersed on the sample holder. The size range of this CN was estimated to be 23-26 nm.

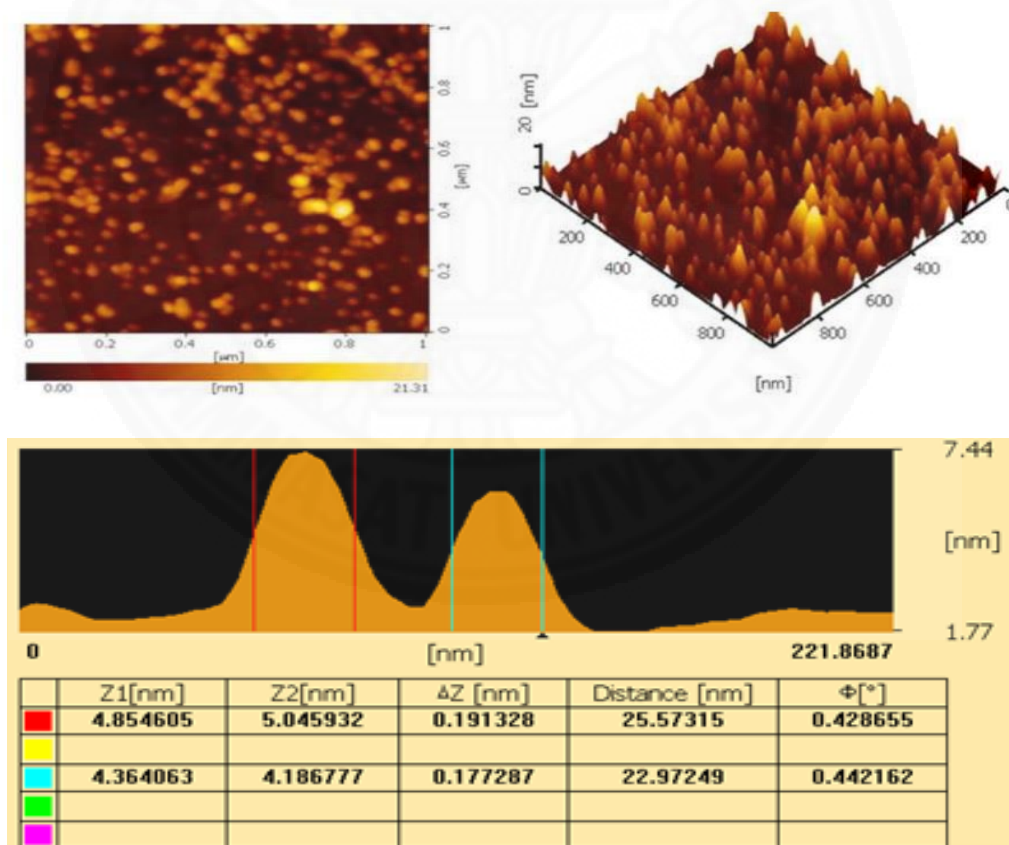


Figure 4.2 AFM images show the topographic and three-dimensional image of chitosan nanoparticles

The pH values of the studied CN solutions with non-dialyzed and dialyzed conditions were 3.22 and 6.02, while the turbidities were 20.8 and 41.9 NTU, respectively. These results are in agreement with those of Nasti et al. [182] who determined the influence of pH during the preparation of chitosan/TPP nanoparticles. It was found that at a pH of greater than 6, a decrease in chitosan charge density occurred, thus resulting in lowering not only the intensity of its electrostatic interactions, but also its solubility in water. The higher pH may induce some chitosan aggregation. Indeed, at high pH values, the zeta potential of the solution is critically low. This is also associated with partial chitosan deprotonation; the CN quickly aggregates to form micrometric complexes. This phenomenon was confirmed when the pH approached 7.0. As it was adjusted to 7.4, precipitation actually took place. These observations are consistent with the study of Nasti and colleagues [182], in determining the influence of pH on the preparation of chitosan/TPP nanoparticles. The solution pH value had effect on the stability of the chitosan nanoparticle system. The increase average particle size increased could be affected mostly by particle aggregation when solution pH value increased [179].

4.1.3 Summary

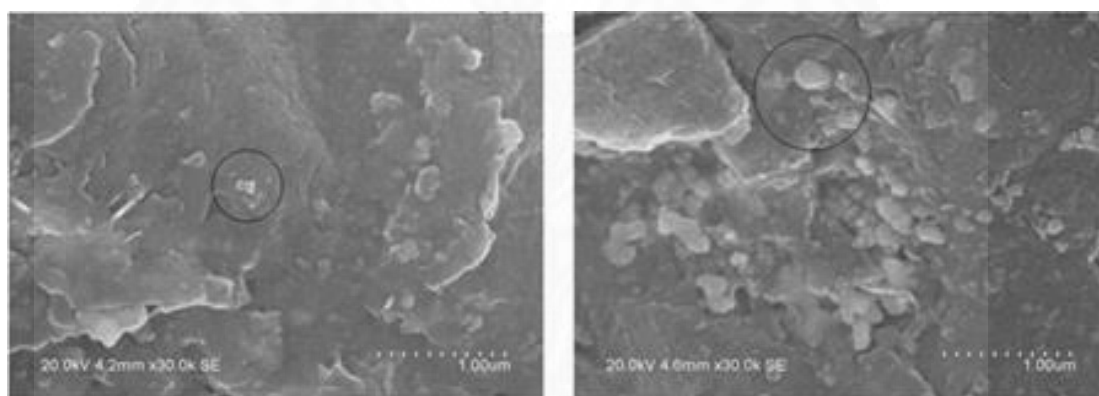
The sizes of the synthesized CN can be controlled by varying the concentration of the chitosan/reagents used. Increasing of chitosan concentration, resulted in the increased CN hydrodynamic size. The size of CN in the dialyzed process was larger than that in the non-dialyzed. The as-synthesized chitosan nanoparticles had a size range of 23-26 nm.

4.2 Characterization of adsorbent coated on supporting materials

Bituminous activated carbon (AC), alumina ceramic balls (CB), and microfiltration ceramic membrane (CM) were used as a support for CN. First, AC would be subsequently bound to CN via two deposition methods, wet impregnation and dip coating. Secondly, CB and CM were coated with CN by dip coating method.

4.2.1 By wet impregnation coating method

The deposition of CN from dialyzed and non-dialyzed solution was examined by weighing of the CN-coated AC, which turned out to increase approximately 24.6% and 32.3% respectively from the starting AC weight which there is difficulty to visualize the layer on the AC support it is possible to suppose that is very thin. However, the coating surface with non-dialyzed solution was better than dialyzed conditions because the surface charge density decreased with an increase in pH and a decrease in ionic strength [183]. The SEM images in Figure 4.3a and Figure 4.3b reveal a wrinkled appearance that is due to the CN layer adhering to the AC support. The CN exhibit a mainly spherical shape with an approximate hydrodynamic size of 200 nm (in the circle of images).



(a)

(b)

Figure 4.3 SEM images of bituminous activated carbon surface show morphology of chitosan nanoparticles: (a) non-dialyzed CN-AC and (b) dialyzed CN-AC

4.2.2 By dip coating method

Dip coating is a technique which has been used by a number of researchers [162, 184-186] due to its simplicity and low cost. In this experiment, the deposition of CN on supporting material (AC, CB and CM) was noted from the increased weight 19.4% and 17.9% of the dry weight of CN during non-dialyzed and dialyzed conditions. Figure 4.4 shows the SEM images, which reveal the evidence of CN from non-dialyzed (Figure 4.4a) and dialyzed (Figure 4.4b) conditions on the AC surface. The CN from the non-dialyzed process appear to be irregular in shape and smaller than the CN from the dialyzed process. The dialyzed CN exhibit a mainly spherical shape with an

approximate hydrodynamic size of 200 nm (in the circle of images). In comparison to the dry size obtained from AFM analysis, the size is relatively bigger. This may be a result of swelling after use. The distribution of CN on AC surface was quite random, and its deposition was small. The FTIR spectra showed no interaction between CN and AC.

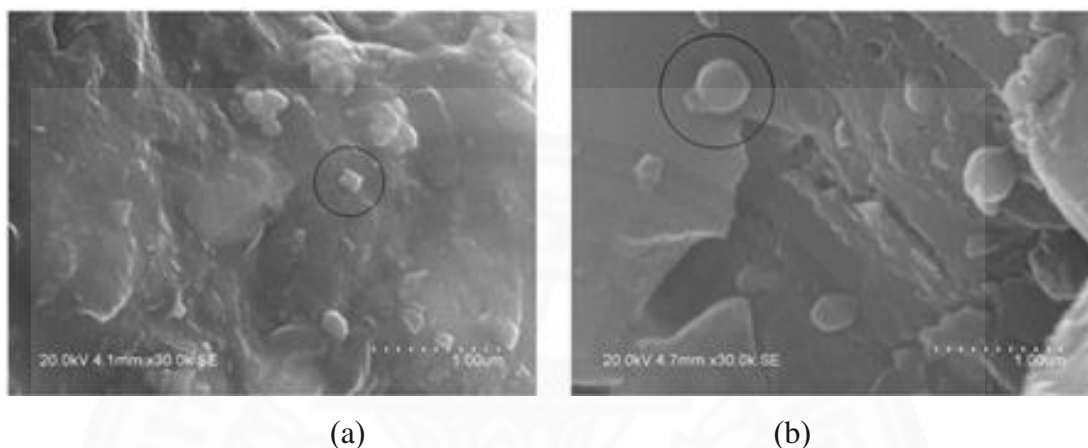


Figure 4.4 SEM images of bituminous activated carbon surface show morphology of chitosan nanoparticles: (a) non-dialyzed CN-AC (b) dialyzed CN-AC

According to Chen and Lin [183], the coating of CN on AC would be more plausible if the CN solution was not dialyzed. This is because the surface charge density tends to decrease as the pH of the solution increases from 3.22 to 6.02. In other words, the ionic strength of the solution becomes low when the acid-base conditions are close to neutral. As a result, the number of CN on AC, based on wet impregnation, would be higher than that with the dip coating method, which is consistent with the SEM results shown in Figure 4.3 and 4.4. CN solution continued to concentrate over time during evaporation, after the water had been removed. However, the deposition of CN on AC via wet impregnation and dip coating method was revealed that the wet impregnation easily caused aggregation of CN, which looked like a wrinkled form over the AC surface.

4.2.2.1 Characterization of adsorbent coated on alumina ceramic balls

Dip coating method was used to prepare chitosan nanoparticles (CN) coated alumina ceramic balls (CB) because of the greater adsorption performance and

difficulty aggregation of CN coated AC than wet impregnation method. Figure 4.5 exhibits the SEM micrographs of the bare and coated alumina balls at three different amount of nanochitosan loadings on the surface of alumina balls. Figure 4.5(a) depicts uncoated or bare ceramic balls, which display a pure and coarse surface. The film became thicker and smoother as the nanochitosan loading increased (Figure 4.5b-4.5d). The thick of film was indicated the amount of adsorbent, while the smooth surface show the low porous of adsorbent that indicate the decrease area for adsorb. The thickness film makes the surface smoother therefore, the 25 mg nanochitosan loading is the suitable loading for heavy metal removal. The surface of balls appeared to have less coarseness as more CN was coated onto the surface. A thin layer of CN can be seen over the surface of alumina balls at 15 mg of CN loading (Figure 4.5b). Figure 4.5c and 4.5d show a surface of balls covered by a film-like morphology.

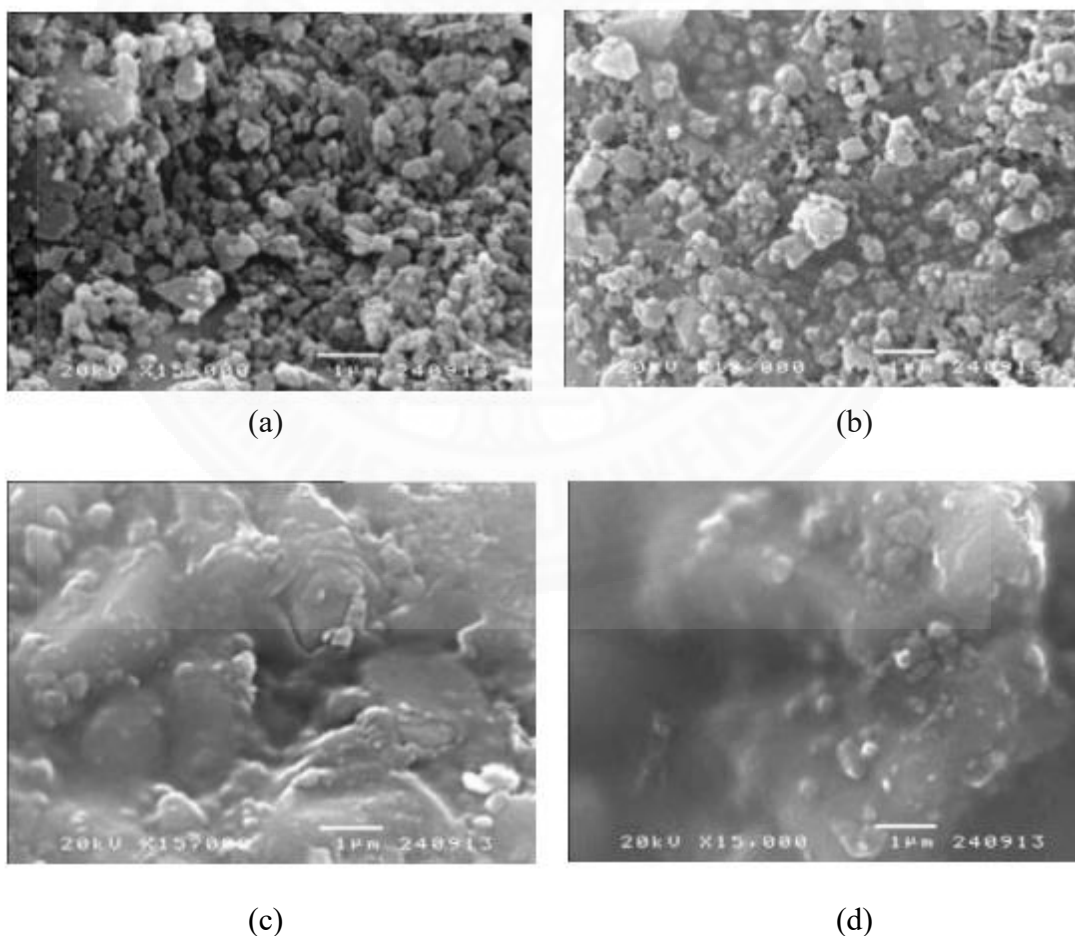


Figure 4.5 SEM images of alumina ceramic balls prepared at different amount of CN loadings: (a) 0 mg, (b) 15 mg, (c) 25 mg, and (d) 35 mg

4.2.2.2 Characterization of adsorbent coated on ceramic membrane

In order to shorten of treatment process and to improve the adsorption capacity for heavy metals removal. A simultaneous adsorption and filtration is established. The dip coating method was used for surface coating of ceramic membrane with CN. The SEM images of the uncoated and coated ceramic membranes at three different amounts of chitosan loadings on the surface of ceramic membrane are shown in Figure 4.6. From the figure, it is clear that the surface of the ceramic membrane was covered with the CN during the process. In comparison with these four SEM images, the film became thicker and smoother as the chitosan loading increased (Figure 4.6b-4.6d). At the 10 mg nanochitosan loading is the seemly loading optimal for thicker and smoother because it illustrations highest permeate flux and adsorption capacity. At higher thickness, resulting in surface is smoother but permeate flux decreased.

FTIR spectra showed no interaction between CN and supporting material. There is no additional peak in the spectra related to CN. The SEM pattern of uncoated ceramic membrane shows roughness surface and large pores. The membrane appears to have less roughness as more chitosan is coated onto the membrane. For 10 mg chitosan loading, the ceramic surface was partially covered by CN solution. Although ceramic surface seems probable a chitosan film covered, it still maintains the membrane because permeate flux remains flow (Figure 4.6). For 15 mg chitosan loading, a thin layer of chitosan can be seen over the top surface. For 20 mg chitosan loading, the surface appears to be covered by a film-like morphology. Due to the chitosan film, Figure 4.6c and 4.6d cannot see membrane particle anymore. With an increase in chitosan loading, the effective pore size of membrane was reduced. These occurred due to the penetration of chitosan molecules into the pores of the membrane [162, 187].

The membrane was coated with the selected modified chitosan solutions (CN, CN-GLA, or CN-PEG). The adsorbents were deposited onto the surface of the ceramic membrane (CM). This was to get a thin layer of chitosan on the ceramic surface to functionalize the membrane, thereby preparing the surface for chemical modification [188]. Figure 4.7 shows the morphology of the ceramic membrane surface with the three adsorbents characterized by SEM. Figure 4.7a depicts the pure and coarse

surface of the bare ceramic membrane. The surface when covered with CN became thicker and smoother (Figure 4.7b). Figure 4.7c and 4.7d, they indicate the coatings of the ceramic membrane with CN-GLA and CN-PEG, resulting in significant changes in the surface morphology from a coarse to smooth film-like morphology. When thickness and smoothness increase, the permeate flux was reduced due to decreasing of membrane effective pore size. The thickness and smoothness of ceramic membrane surface follows the order: CN<CN-GLA<CN-PEG.

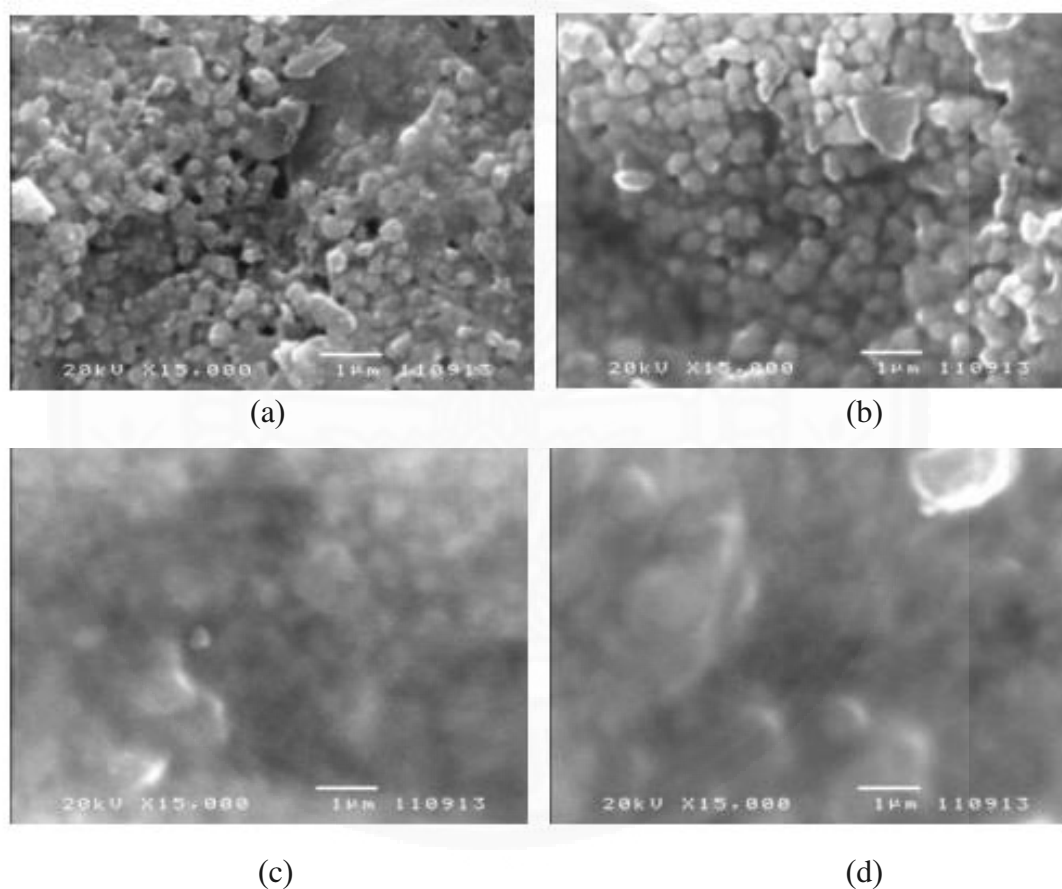


Figure 4.6 SEM images of membrane prepared at different amounts of chitosan loadings: (a) 0 mg, (b) 10 mg, (c) 15 mg, and (d) 20 mg

The difference of dried weights of ceramic membrane before and after adsorbent depositions on the surface was used to calculate the amount of adsorbent coated on the membrane. Figure 4.8 shows the thickness of CMCN, CMCN-GLA, and CMCN-PEG coated on the membrane, calculated according to Equation 3.2, which was 0.572 ± 0.05 , 0.669 ± 0.03 , and 0.692 ± 0.05 μm , respectively. The layer thickness is thin

when compare with the results of Steenkamp et al. [163], the layer thickness of the chitosan layer is about 30-50 μm by dipping in concentrate of chitosan solution (dissolving chitosan 1000 mg in 100 mL of 1 volume % aqueous acetic acid solution). Nevertheless, the layer thickness on ceramic membrane surface effects the volume of permeate flux when the more thickness, the permeate flux reduced. The amount of CMCN-PEG on the ceramic surface was the highest, probably due to the binding properties of PEG 1000. However, increasing the PEG amount may not always lead to thicker coating. Bhattarai et al. [189] and Hou et al. [190] investigated the grafting of PEG onto chitosan and observed that due to the hydrophilic nature of PEG, the resulting polymer may be able to dissolve in water better than the parent chitosan. Increasing the amount of PEG in the coating may therefore lead to the dissolution of the coating, which may not be a desirable property here. Based on the previous study on modified chitosan, GLA-crosslinked chitosan is more hydrophobic than native chitosan [191].

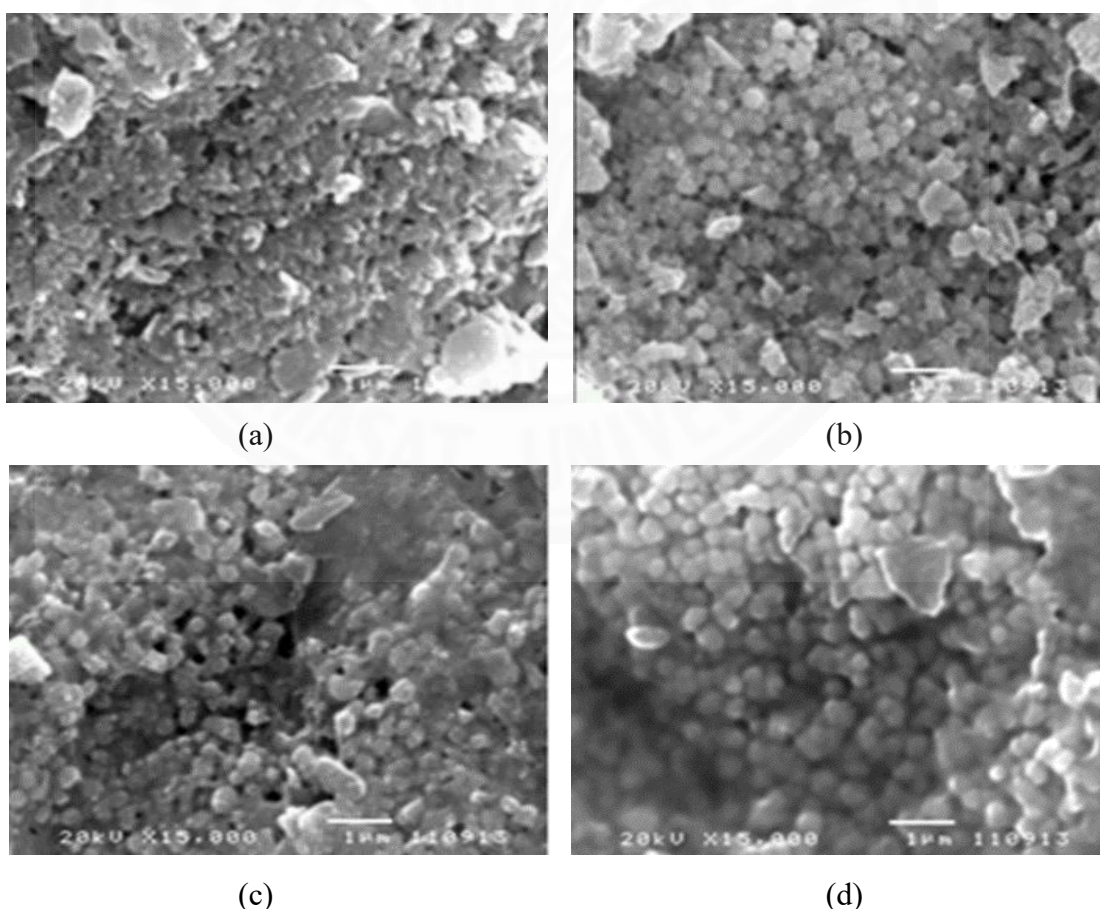


Figure 4.7 SEM images of membrane prepared at different adsorbents
(a) CM, (b) CMCN, (c) CMCN-GLA, and (d) CMCN-PEG

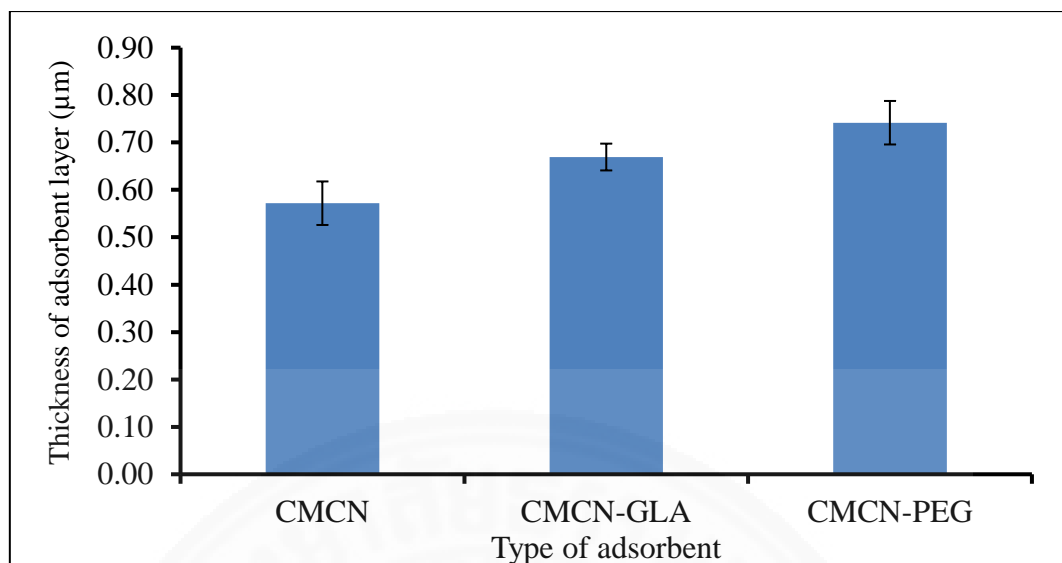


Figure 4.8 Thickness of adsorbent on ceramic membrane

4.2.3 Summary

The SEM images showed that the coated chitosan possessed film-like morphology which appears quite uniform over the supporting materials surface. Coating process was repeated many times to coat a sufficient amount of CN onto surface of supporting material. The porous structure of supporting material is regular and smooth. The film became thicker and smoother as the chitosan loading increased. The SEM pattern of uncoated supporting materials showed rough surface and large pores. The thickness of CMCN-PEG on the ceramic surface was the highest. However, an increasing amount of PEG in the coating may lead to the dissolution of the coating.

4.3 Cr(VI) removal using nanochitosan coated on bituminous activated carbon

The objective of this study is to investigate the possible enhancement of Cr(VI) removal from aqueous solution using chitosan nanoparticles (CN) coated bituminous activated carbon (AC) prepared by dip coating and wet impregnation methods. Cr(VI) removal, based on adsorption of the prepared CN coated AC, was studied in comparison with the original AC in terms of removal efficiency and adsorption capacity.

4.3.1 Properties of adsorption

Adsorption experiments were carried out by which the Cr(VI) in pH 5 solution were removed, based on physical and chemical sorptions upon a series of materials, including AC, Chitosan flake (CTS), CN, CN coated on AC by the dip coating method (CN-AC/DC), and wet impregnation method (CN-AC/WI). The adsorption results shown in Figure 4.9 demonstrates that CN-coated AC performs better for Cr(VI) removal than those of their original materials, such as AC, Chitosan flake (CTS), and CN. This indicates that the two-combined materials gained a synergistic effect, which was non-existent in the sole use of either AC or CN. This additional removal capacity, noted as a result of synergy from two materials, can be attributed to the dual interactions based on: 1) chemical affinity due to chelation between the NH₂ (or OH) groups of chitosan and Cr(VI) [113] and 2) physical adsorption due to the charge-charge interaction between positive charge existing on activated carbon and negative charge of anionic Cr₂O₇²⁻, dissociated from K₂Cr₂O₇ in a low pH solution [16, 124, 192]. About 5% difference in Cr(VI) removal efficiency can be observed between the CN-AC obtained from the two methods, dip coating and wet impregnation. The greater performance of CN-AC/DC can be seen as agreement with the above explanation, inferring that both CN and AC are involved in the adsorption mechanism with Cr(VI). The wet impregnation easily caused aggregation of CN, which looked like a wrinkled formed over the AC surface.

In this case, the CN solution continued to concentrate over time during evaporation, after the water had been removed. Although CN content was higher, CN was lost by dissipation on AC. Since the nano-form of CN would now no longer exist, the surface area of the particular adsorbent can be dramatically decreased. This higher concentration of CN had a similar effect as the higher concentration of Cr(VI) had in the adsorption process (Figures 4.9 and 4.10) where the adsorption efficacy tended to decrease when the initial concentration of Cr(VI) increased. Removal of Cr(VI) by the aforementioned adsorbents at pH 5 and initial Cr(VI) concentrations of 0.1 to 100 mg/L, is shown in Figures 4.9 and 4.10. This is based on the typical pH of wastewater from the electroplating industry [193]. Among the adsorbents evaluated, CN-AC/DC was the best adsorbent for Cr(VI). The BET results revealed that the surface area of CN-AC/DC and CN-AC/WI were 309.02 and 258.54 m²/g, respectively. For CN-AC/DC,

there were nanosize particles on the surface, while the CN-AC/WI was a film, which resulted in a decrease of surface area. Figure 4.9 demonstrates that the removal efficiencies of Cr(VI) decrease from 61.7% to 38.5% with an increase in concentration, while the amount of Cr(VI) adsorbed per unit mass, q_e , increases from 0.14 to 44.22 mg/g (Figure 4.10). It also appears that there was less Cr(VI) adsorbed onto the chitosan at lower concentrations than at higher concentrations.

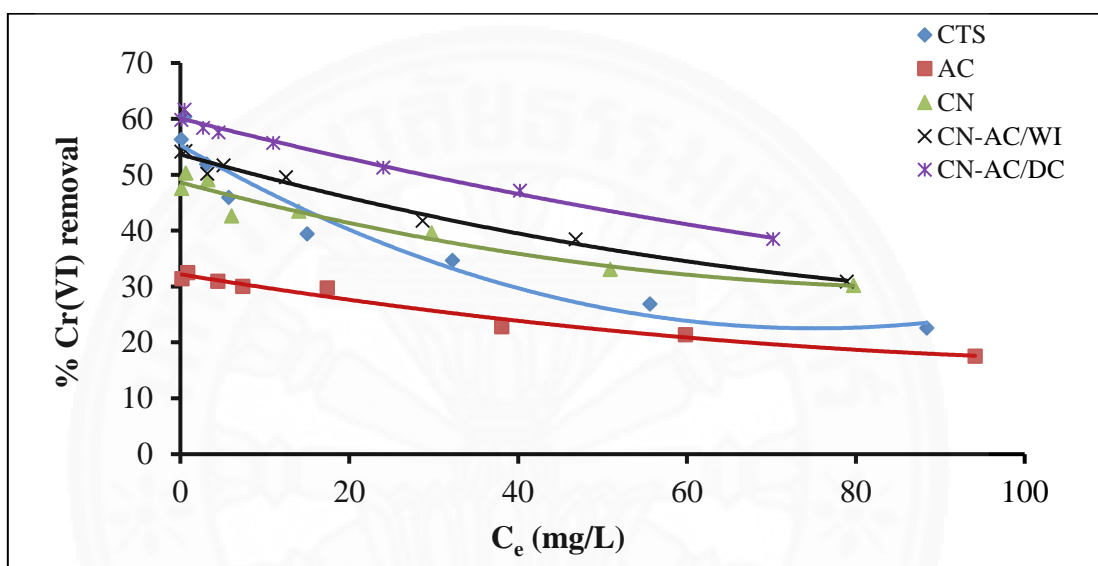


Figure 4.9 Relationship between C_e and % Cr (VI) removal for various adsorbents (at pH 5, adsorbent dose 1 g/L, contact time 3 h, agitation speed 100 rpm, and room temperature)

4.3.2 Adsorption isotherms

Langmuir and Freundlich adsorption isotherms were used to fit the experimental data (Appendix A). The Langmuir adsorption isotherm exhibits maximum adsorption capacities, which range from 32.57 to 77.52 mg/g, where its coefficient of determination (R^2) was 0.959-0.992. The greater values of K_L indicated higher affinity of adsorbent to the investigated materials and implied strong bonding characteristics of adsorbent. The R_L values in this study were from 0.147 to 0.999 (Table 4.2), indicating a highly favorable adsorption of Cr(VI) onto various adsorbents. The Freundlich isotherm generated a more linear fit (0.987-0.993) of the experiment data. Based on the R^2 values and sum of squared error (SSE) values, the Freundlich model fits slightly

better than the Langmuir model (Table 4.2). This observation suggests that the adsorption process took place as a multilayer adsorption on the heterogeneous surface, not a monolayer adsorption. The n values between 1.12-1.30 within the range under 10 indicated that the sorption process was favorable. Having $n > 1$ is common and may be due to a distribution of surface sites, or any factor that causes a decrease in adsorbent-adsorbate interaction with increasing surface density [4, 141].

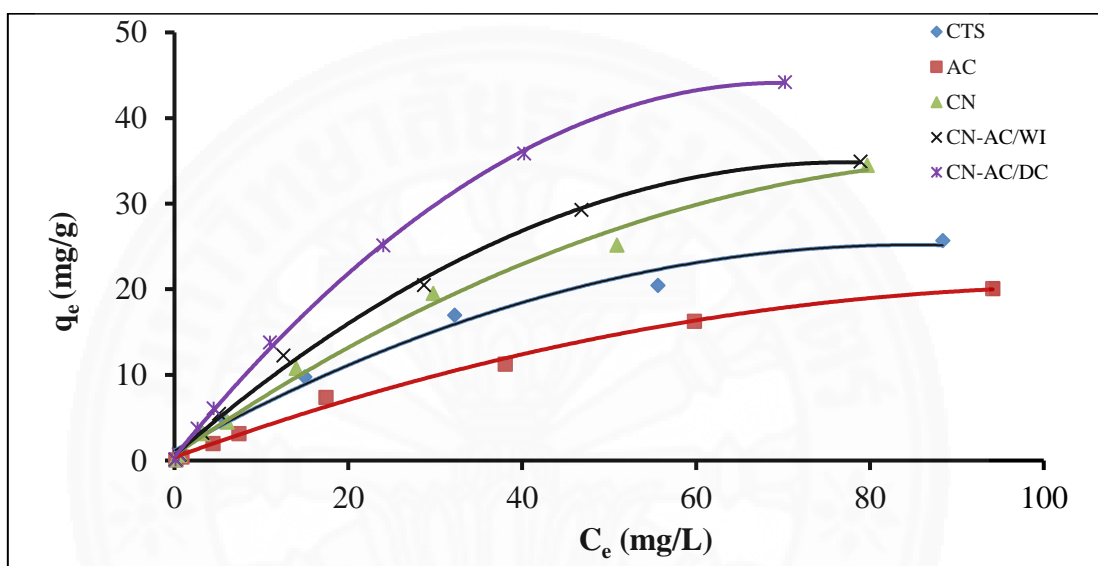


Figure 4.10 Relationship between C_e and adsorption capacities for various adsorbents (at pH 5, adsorbent dose 1 g/L, contact time 3 h, agitation speed 100 rpm, and room temperature)

4.3.3 Adsorption kinetics

Adsorption kinetics gives significant parameters of physicochemical, in order to calculate the abilities of a sorbent [124]. In order to clarify the mechanism of an adsorption process, several adsorption models were applied to evaluate the experimental data. For this purpose, the pseudo-first-order kinetic model, pseudo-second-order kinetic model, and intraparticle diffusion model were used to test the experimental data at an initial Cr(VI) concentration of 10.0 mg/L with two adsorbents namely, CN-AC/DC and CN-AC/WI, at adsorbent dosage of 20.0 mg.

Table 4.2 Equilibrium adsorption analysis for the adsorption of Cr(VI) on various adsorbents

Adsorbents	Langmuir isotherm					Freundlich isotherm			
	q_{\max} (mg/g)	K_L (L/mg)	R^2	SSE	R_L	K_F (mg/g)	n	R^2	SSE
CTS	32.57	0.0352	0.977	0.28	0.272- 0.997	1.084	1.30	0.987	0.23
AC	36.36	0.0131	0.982	0.14	0.147- 0.994	0.458	1.12	0.992	0.16
CN solution	61.35	0.0151	0.959	0.25	0.363- 0.998	0.890	1.13	0.993	0.23
CN-AC/WI	57.47	0.0203	0.992	0.21	0.402- 0.999	1.075	1.15	0.993	0.34
CN-AC/DC	77.52	0.0197	0.990	0.23	0.542- 0.998	1.397	1.13	0.991	0.41

The effect of contact time on Cr(VI) adsorbed by CN-AC/DC was also investigated at an initial Cr(VI) concentration of 10.0 mg/L. As seen in Figures 4.11, the adsorption capacity of the adsorbents increases rapidly with an increase of contact time from 0 to 840 min. More than 60 % of Cr(VI) in the solution were removed within 840 min. After 1,440 min, the adsorption capacity becomes a plateau approaching equilibrium. Additionally, the increasing in contact time did not show significant change in equilibrium concentration. It is indicated that the adsorption phase reached equilibrium. For CN-AC/WI adsorbent, the adsorption capacity increases rapidly with an increase of contact time from 0 to 1,080 min. More than 60 % of Cr(VI) in the solution were removed within 840 min (Figures 4.12). The difference in the range of adsorption may be because at firstly all sites on the adsorbent surface were available and the solute concentration gradient was relatively high.

Kinetic parameters for the adsorption of Cr(VI) were studied using CN-AC/DC and CN-AC/WI. The validities of the aforementioned kinetic models were checked which figure shows a good agreement between experimental data and a pseudo-second-order kinetic model (Appendix A). The values of the parameters and the R^2 value obtained from these three kinetic models are listed in Table 4.3 For kinetic parameters of the experimental adsorption of Cr(VI) using CN-AC/DC, it was found

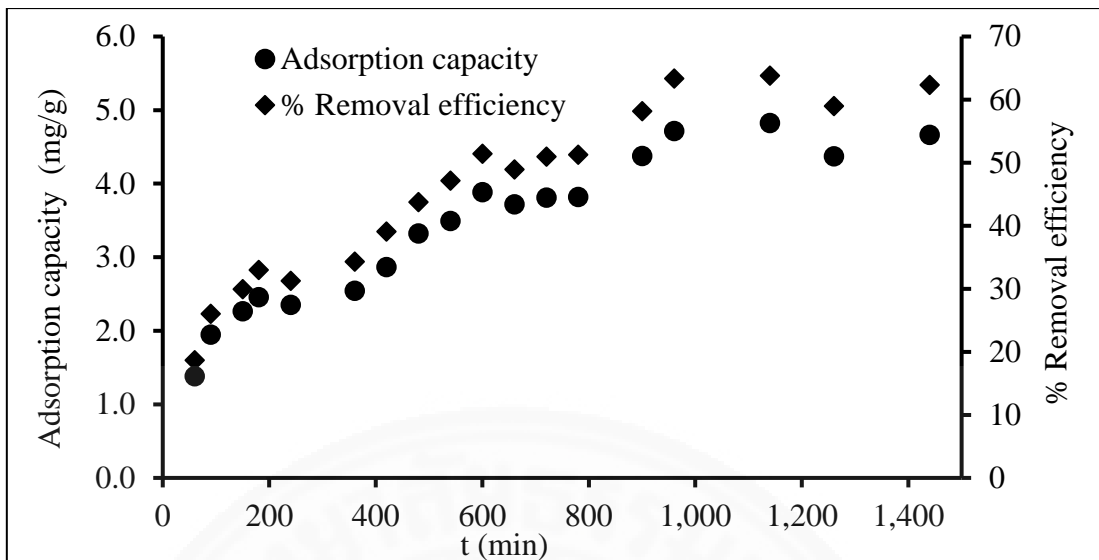


Figure 4.11 Adsorption capacity of CN-AC/DC for Cr(VI)

(at Cr(VI) initial concentration 10 mg/L, pH 5, adsorbent dose 1 g/L, agitation speed 100 rpm, and room temperature)

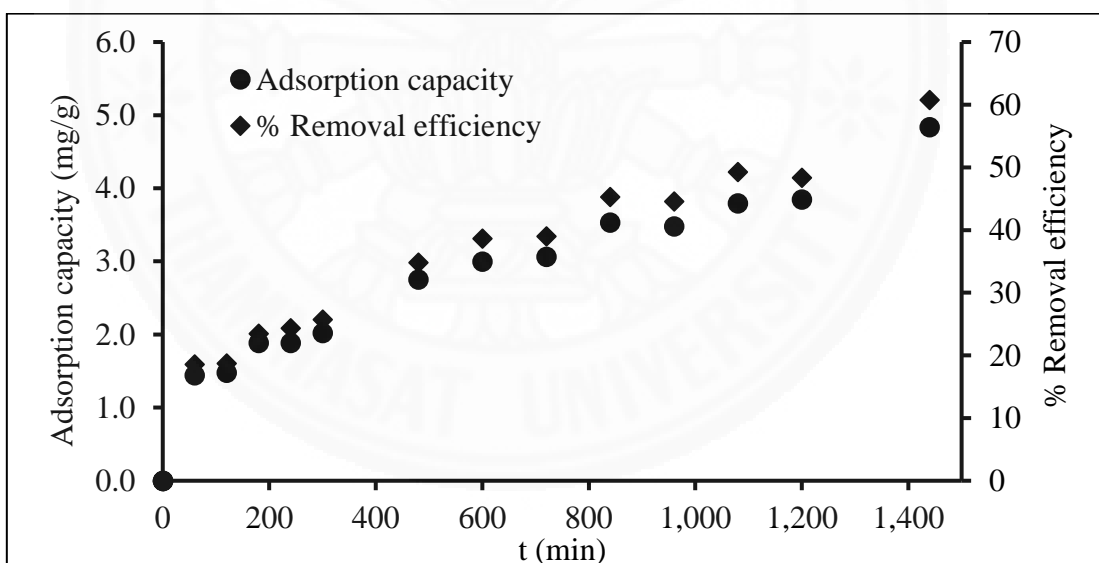


Figure 4.12 Adsorption capacity of CN-AC/WI for Cr(VI)

(at Cr(VI) initial concentration 10 mg/L, pH 5, adsorbent dose 1 g/L, agitation speed 100 rpm, and room temperature)

that the value of R^2 for a pseudo second-order kinetic model is higher than other models (greater than 0.990), followed by those of the intraparticle diffusion model, and the pseudo-first-order kinetic model. Moreover, the q_e (experiment: exp) values for the

pseudo-second order kinetic model are all consistent with the q_e (calculated: cal) values. For the adsorption of Cr(VI) by CN-AC/WI, the R^2 values for the pseudo-first order kinetic model and the intraparticle diffusion model are lower than that of the pseudo second-order kinetic model. There are large differences between experimental q_e values and the calculated q_e values. This indicates that the pseudo-first order kinetic model and the intraparticle diffusion model poorly fit the adsorption of Cr(VI) onto CN-AC/WI. For all regression cases, the SSE between the predicted values and the experimental data was calculated. The SSE value of CN-AC/DC and CN-AC/WI were 0.33 and 0.32, respectively (Table 4.3). The higher R^2 values and lower SSE values indicate that the sorption of Cr(VI) onto CN-AC/DC and CN-AC/WI followed a pseudo-second order kinetic model. This also implies that the mechanism is chemisorption [81, 194].

Table 4.3 Kinetic parameters for the adsorption of Cr(VI) by CN-AC/DC and CN-AC/WI

Kinetic models	Parameters	Unit	Adsorbents	
			CN-AC/DC	CN-AC/WI
Pseudo-first-order	q_e (exp)	mg/	4.84	4.66
	q_e (cal)	mg/g	3.59	2.86
	K_1	1/min	0.0009	0.0014
	R^2	-	0.963	0.866
	SSE	-	1.06	2.53
Pseudo-second-order	q_e (cal)	mg/g	4.83	4.57
	K_2	(g/mg)/min	0.00080	0.00099
	h	(mg/g)/min	0.021	0.019
	R^2	-	0.990	0.975
	SSE	-	0.33	0.32
Intraparticle diffusion	k_i	(mg/g)/min ^{0.5}	0.0046	0.0039
	R^2	-	0.974	0.831
	SSE	-	1.54	1.73

A comparison of adsorption capacity of adsorbents from this study with other modified activated carbons for Cr(VI) removal is given in Table 4.4. The

adsorption capacity of CN-AC/WI and CN-AC/DC was 57.47 and 77.52 mg/g, respectively, which is 4-5 times higher than commercial activated carbon [195, 196]. This was mainly because of the difference in technique used for surface modification of activated carbon and functional group formation. However, the results of this study are similar to those of chitosan coated and acid treated oil palm shell charcoal [91].

Table 4.4 Adsorption capacity of modification activated carbon for Cr(VI) removal in batch mode

Adsorbent	Adsorption capacity (mg/g)	pH	Reference
CN-AC/WI	57.47	5	Present study
CN-AC/DC	77.52	5	Present study
Commercial activated carbon	15.10	3	[195]
Commercial activated carbon	13.90	-	[196]
Chitosan coated acid treated oil palm shell charcoal	60.25	4	[91]
Chitosan coated oil palm shell charcoal	52.68	4	[91]
Acid treated oil palm shell charcoal	44.68	4	[91]

4.3.4 Summary

In this study, CN coated on AC was used as a biosorbent for the removal of Cr(VI). Langmuir and Freundlich isotherms were used for the mathematical description of the adsorption of Cr(VI) onto various adsorbents. Among various adsorbents investigated, CN-AC/DC gave the best results for adsorption with Cr(VI). The maximum adsorption capacity found in this study was 77.52 mg/g for CN coated on AC by dip coating. This was about 2.13 and 2.38 times higher in comparison to AC ($q_{\max} = 36.36$ mg/g) and CTS ($q_{\max} = 32.57$ mg/g), respectively. The adsorption kinetics results suggest that the adsorption processes of Cr(VI) onto CN-AC/DC and CN-AC/WI, follow pseudo-second-order kinetics. The results of this work show the potential to remove Cr(VI) from solution through adsorption onto CN coated AC, which can be used for scale-up and further research.

4.4 Cr(VI) removal using nanochitosan coated on alumina ceramic balls

In this work, chitosan nanoparticles were prepared by a facile ionic gelation method and then coated onto alumina ceramic ball supports that are usually used in water and wastewater treatment applications. The efficiency of coating, the performance of chitosan nanoparticle coated alumina ceramic balls (CN-CB) for Cr(VI) removal were studied in both the batch mode and continuous flow mode. The adsorption isotherms and adsorption kinetics were investigated to estimate the adsorption capacity and adsorption mechanism of the nanochitosan adsorbent for Cr(VI) removal. In the continuous flow mode, the removal and breakthrough of Cr(VI) is also studied.

4.4.1 Elemental analysis of adsorbent

Energy-dispersive X-ray spectroscopy (EDS) technique was used for the elemental analysis of adsorbent. The EDS spectra of the uncoated or bare alumina ceramic balls, CN-CB before Cr(VI) adsorption, and CN-CB after Cr(VI) adsorption are shown in Figures 4.13a, 4.13b, and 4.13c, respectively. The result indicates that the bare alumina ceramic balls consist mostly of Al and O with some carbon residual. After CN coating, significant amount of the carbon and nitrogen can be detected on the surface of the coated balls indicating the presence of the chitosan on its surface. After the Cr(VI) adsorption, Cr element can also be detected on the surface of the CN-CB with the amount of 0.10 % by weight.

4.4.2 Batch adsorption experiment

4.4.2.1. Adsorption isotherms

The influence of initial concentration on the adsorption capacity and the percent removal efficiency of the CN-CB are shown in Figure 4.14. The increase of Cr(VI) concentration leads to the increase in the adsorption capacity because of higher availability of Cr(VI) in the solution for the adsorption. At high initial concentration, the increase in the adsorption capacity is caused by the concentration gradient and increased driving force. The high concentration increased driving force to overcome

mass transfer resistance of Cr(VI) between the aqueous and solid phases resulting in higher probability of collision between Cr(VI) and CN-CB [140, 197]. The proportion of the initial amount of Cr(VI) to the available effective adsorption sites of the adsorbent is greater at low concentrations. However, the percent removal efficiency decreases from 91.2 to 15.0 % as the initial concentration is increased from 1 to 25 mg/L.

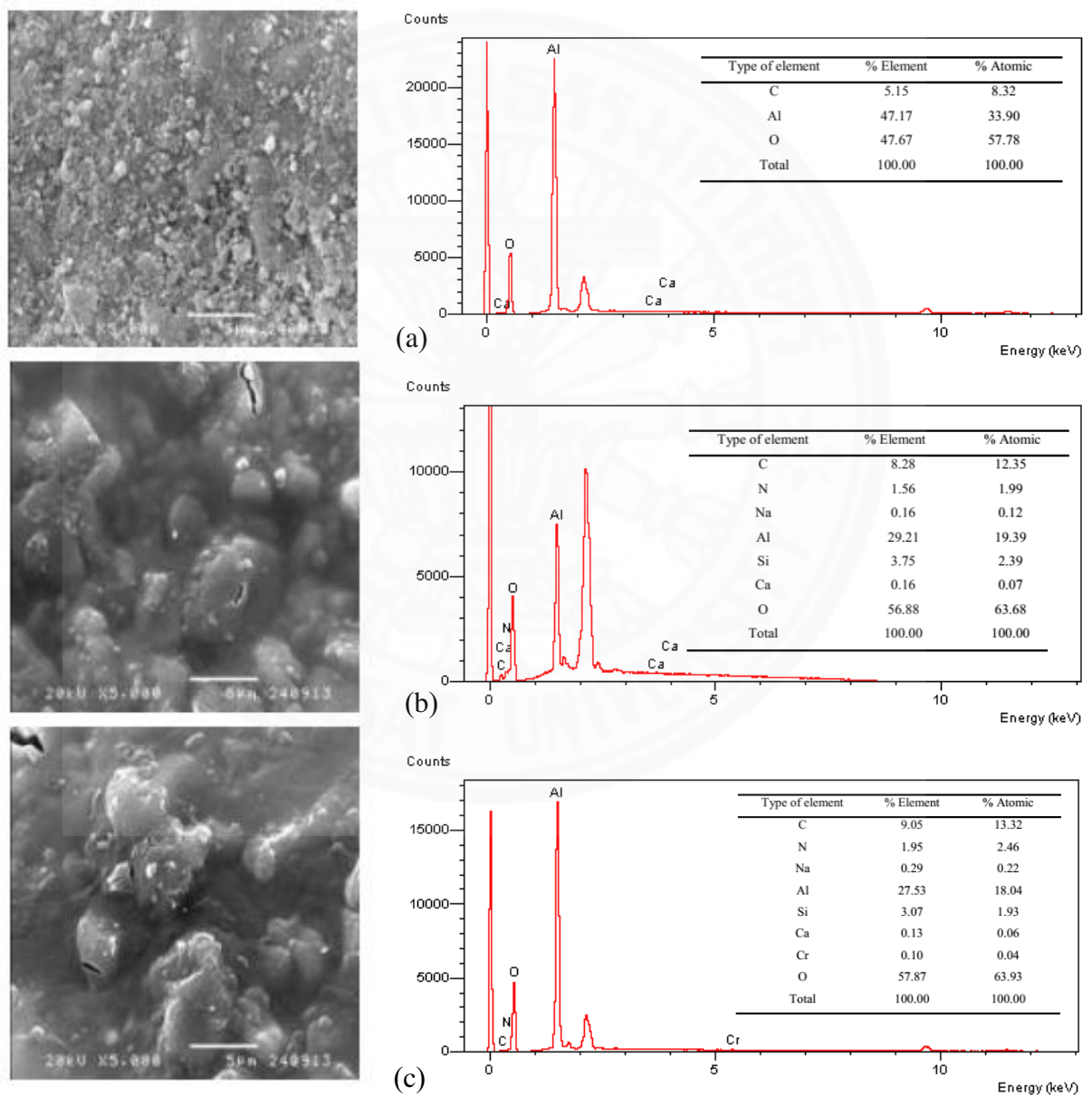


Figure 4.13 The SEM images of CN-CB at 5,000x and the corresponding EDS:

- (a) bare alumina ceramic balls, (b) CN-CB before Cr(VI) adsorption, and
- (c) CN-CB after Cr(VI) adsorption

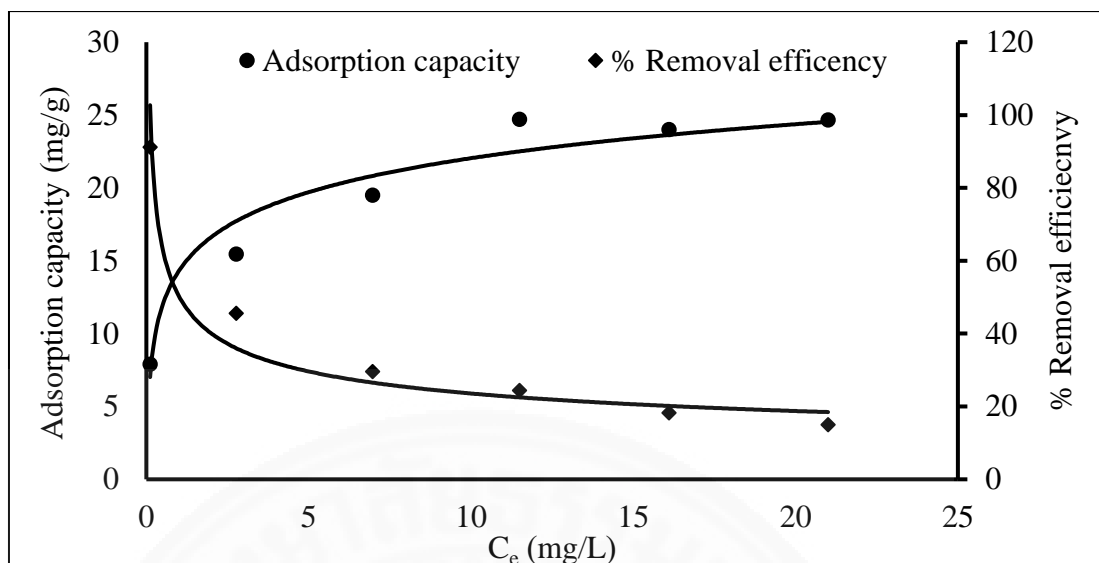


Figure 4.14 Adsorption capacity and removal efficiency of Cr(VI) on CN-CB (at pH 5, adsorbent dose 1.0 g/L, agitation speed 100 rpm, and room temperature)

The linearized adsorption isotherms of Cr(VI) removal by CN-CB according to the Langmuir and Freundlich models are shown in Appendix B. The parameters of the adsorption isotherm models are given in Table 4.5. The Langmuir isotherm yields the maximum adsorption capacity, which is 25.97 mg/g with the R^2 value of 0.991. The Langmuir affinity constant (K_L) was calculated from the fit to be about 2×10^{-3} L/mg indicating good Cr(VI) affinity of the prepared CN-CB. The R_L values in this study were from 0.040 to 0.768, indicating a favorable adsorption of Cr(VI) onto adsorbents (The R_L value of $R_L > 1$, $0 < R_L < 1$, and $R_L = 0$ suggests that adsorption is unfavorable, favorable and irreversible, respectively) [169].

The Freundlich model fits slightly worse than the Langmuir model with the R^2 of 0.986. The Freundlich constant k_F and n of 12.81 mg/g and 4.38, respectively. The value of n between 1 and 10 represents a favourable adsorption [198].

4.4.2.2 Adsorption kinetics

The kinetics of the adsorption were tested against various kinetics models of the adsorption which are the pseudo-first-order kinetic model, the pseudo-second-order kinetic model, the intraparticle diffusion model and the Elovich kinetic model. The fits of the data to these kinetic models are presented in Appendix B. The

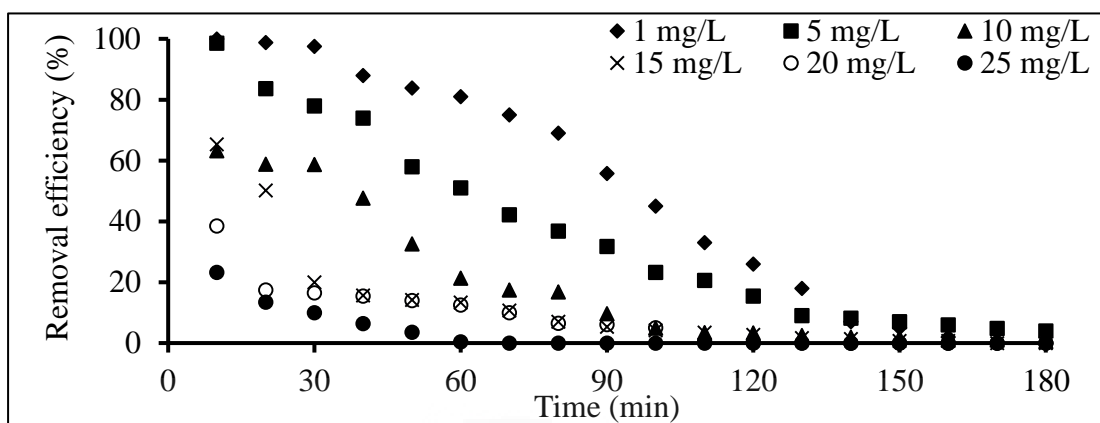
Table 4.5 Equilibrium adsorption analysis for the adsorption of Cr(VI) on adsorbents

Adsorbent	Langmuir isotherm				Freundlich isotherm		
	q_{\max} (mg/g)	K_L (L/mg)	R^2	R_L	K_F (mg/g)	n	R^2
CN-CB	25.97	0.002	0.991	0.040-0.768	12.81	4.38	0.986

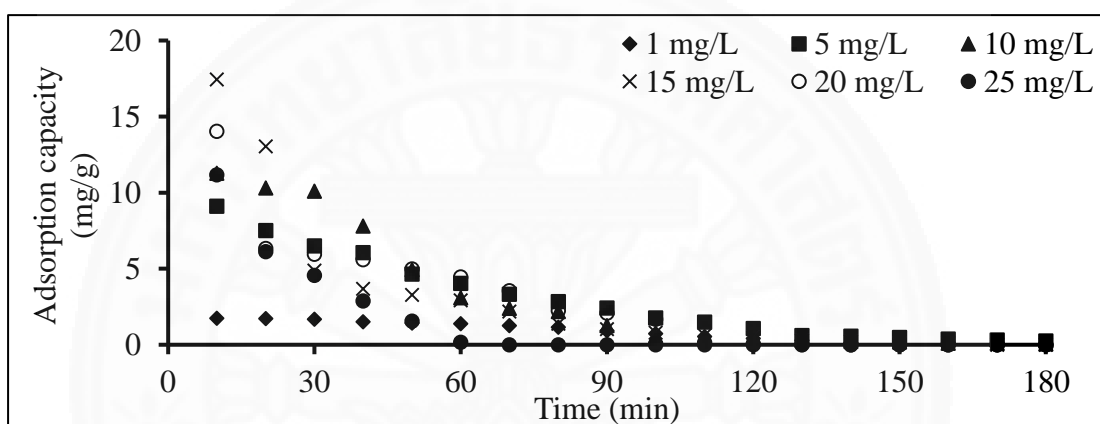
values of the model parameters obtained from the fits are summarized in Table 4.6. It can be seen that the simple pseudo-first order model with the lowest R^2 value cannot quite adequately describe the data. The pseudo-second order model offers the best fit to the data with the highest R^2 of 0.99 which is much higher than other models. The q_e (experiment: exp) values for the pseudo-second order kinetic model is consistent with the q_e (calculated: cal) values. For the pseudo-first order kinetic model are large differences between experimental q_e values and the calculated q_e values. Both the elovich and the intraparticle diffusion models can also describe the data quite well. The actual sorption processes may consist of several complex steps including the chemisorption steps as well as the intraparticle diffusion into the chitosan coating layer. Within the range of our kinetics data, the sorption is best described using the pseudo-second order model.

4.4.3 Fixed-bed column adsorption experiment

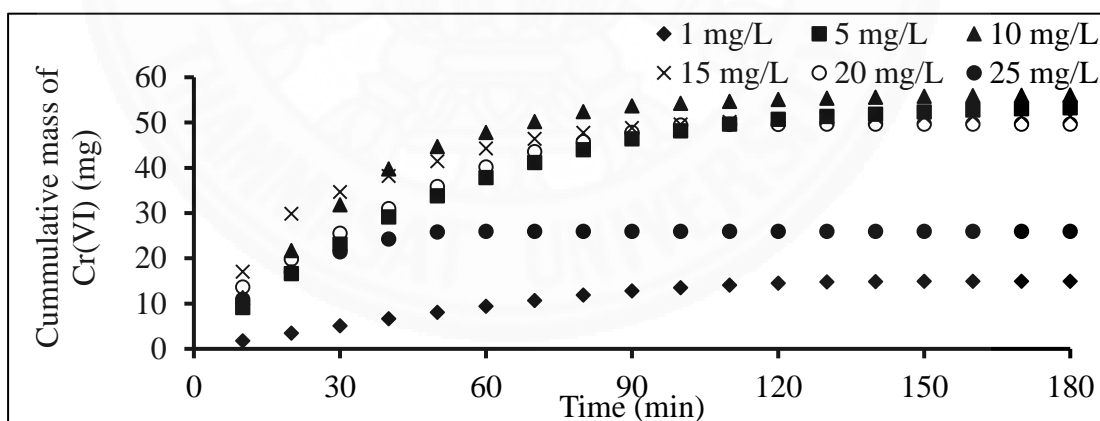
The extensive experiment consideration was conducted to evaluate fixed-bed column performance for the removal of Cr(VI) by CN-CB at flow rate at 2.5 mL/min with various initial concentrations, the results shown that Cr(VI) removal up to 100% was accomplished by the CN-CB with 1.0 mg/L of initial concentration. At a higher initial concentration, more of Cr(VI) passing through adsorbent, which increased. The cumulative adsorption. However, note that at high concentration of Cr(VI) exhaustion time decreases. This result indicates that that adsorbent gets saturated faster at higher concentrations. The specific adsorption capacity (mg Cr/g chitosan) was 14.97, 53.29, 55.72, 52.45, 51.07 and 26.46 mg/g chitosan at 1, 5, 10, 15, 20 and 25 mg/L of initial concentration, respectively (Figure 4.15).



(a)



(b)



(c)

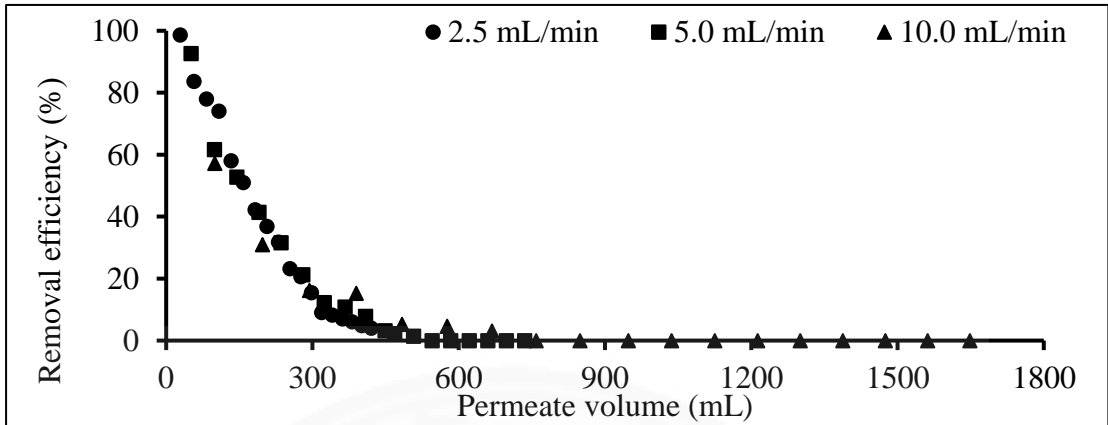
Figure 4.15 Adsorption of the Cr(VI) on CN-CB at various concentrations:

- (a) time course of Cr(VI) removal efficiency,
- (b) adsorption capacity of Cr(VI) as a function of initial concentration of Cr(VI), and
- (c) Time course of the cumulative Cr(VI) mass removed
(at pH 5, flow rate 2.5 mL/min, and room temperature)

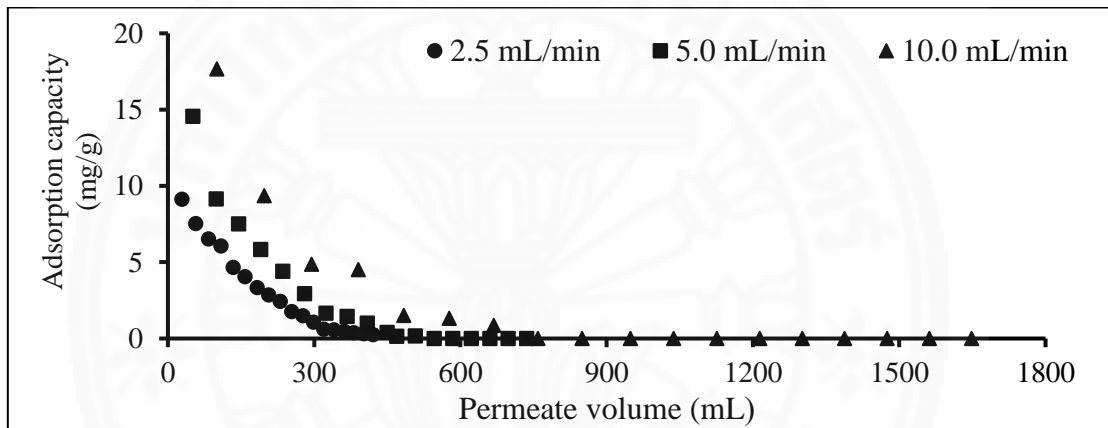
Table 4.6 The kinetic parameters for the adsorption of Cr(VI) by CN-CB

Parameters	Unit	Pseudo-first-order kinetic model	Pseudo-second-order kinetic model	Intraparticle diffusion model	Elovich kinetic model
q_e (exp)	mg/g	14.28	14.28	14.28	14.28
q_e (cal)	mg/g	223.10	15.08	-	-
K_1	min ⁻¹	0.0055	-	-	-
K_2	g/mg-min	-	0.0005	-	-
h	mg/g-min	-	0.1064	-	-
k_i	(mg/g)/min ^{0.5}	-	-	3.5329	-
α	((mg/g)/min)	-	-	-	0.6006
β	g/mg	-	-	-	0.4298
R^2	-	0.959	0.991	0.975	0.977

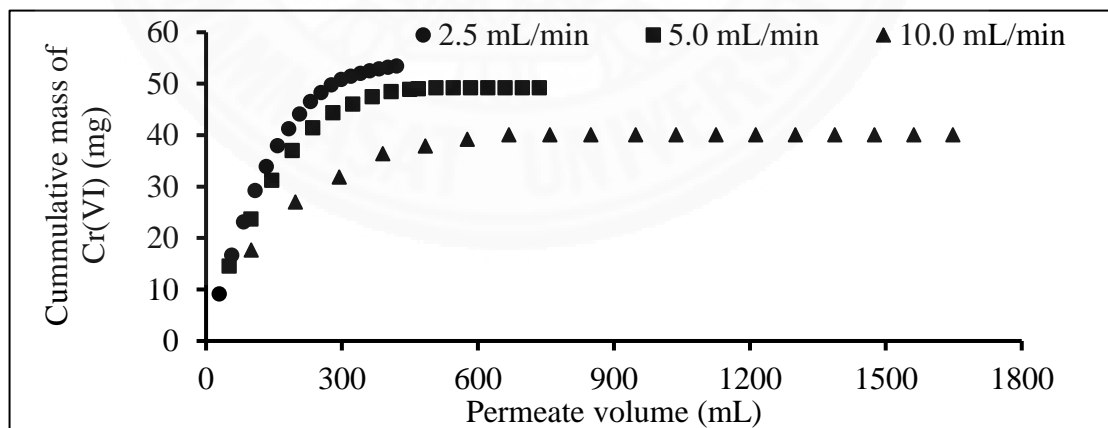
Figure 4.16 displays the results at flow rates of 2.5, 5.0 and 10.0 mL/min (or 3.9, 7.9 and 15.7 cm/min of linear velocity, respectively) and holding initial concentration of 5.0 mg/L, more of Cr(VI) passing through adsorbent, which decreased the cumulative adsorption owing to the permeate volume between the CN-CB and Cr(VI) is reduced at a higher flow rate. The removal efficiency was decreased from 98.6% to 92.6% and 57.2% at the beginning of operation when changing the flow rate from 2.5 to 5.0 and 10.0 mL/min, respectively (Figure 4.16a). Additionally, the specific adsorption capacity was 27.20, 25.51, and 20.77 mg/g chitosan, respectively. The specific adsorption capacity (mg Cr/g chitosan) decreased with an increase in flow rate. At a high rate of flow, Cr(VI) did not have enough time to contact with CN-CB and resulted in a lower removal of Cr(VI) at lower flow rate or longer contact time would be required (Figure 4.16b). Although Cr(VI) adsorption started to level off after 60 min of operation time, adsorption approached steady state conditions for Cr(VI) removal for nearly 340, 470 and 580 mL of permeate volume or 140, 110 and 60 min of operation time at flow rate 2.5, 5.0 and 10.0 mL/min respectively of operation (Figure 4.16c). At a higher flow rate or permeate volume, more of Cr(VI) passing through adsorbent, which quickly accessed and saturated.



(a)



(b)



(c)

Figure 4.16 Adsorption of the Cr(VI) on CN-CB at various flow rates: (a) removal efficiency of Cr(VI), (b) adsorption capacity of Cr(VI), and (c) cumulative of Cr(VI) mass (at Cr(VI) initial concentration 10 mg/L, pH 5, and room temperature)

4.4.3.1 Influence of initial concentration on the breakthrough curve

curve

The breakthrough curves of varying initial Cr(VI) concentration with 1, 5, 10, 15, 20 and 25 mg/L at pH 5, 2.5 mL/min flow rate and room temperature are given in Figure 4.17. The curves from Figure 4.17 shows that the adsorbent become saturated faster at higher concentrations used. The exhaustion time decreases with increasing initial concentration. The results showed that during the interval of 60 min, the value of C_t/C_0 reached 0.19, 0.49, 0.79, 0.87, 0.88 and 1.00 when the influent concentrations were 1,5, 10, 15, 20 and 25 mg/L, respectively. The breakthrough curve comes out late at lower concentrations, may be because of the non-linear adsorption. The breakthrough point was reached at higher concentration. At lower concentrations, the value of ratio of Cr(VI) uptake (in mg/g) to the initial Cr(VI) concentration (q/C_0) will be higher than that at higher initial concentrations [199]. The time of breakthrough point time was found to decline with increasing Cr(VI) concentration as the binding sites became more rapidly saturated in the column. The breakthrough curves illustrate that decreasing the concentration of Cr(VI) extends the breakthrough times [200, 201].

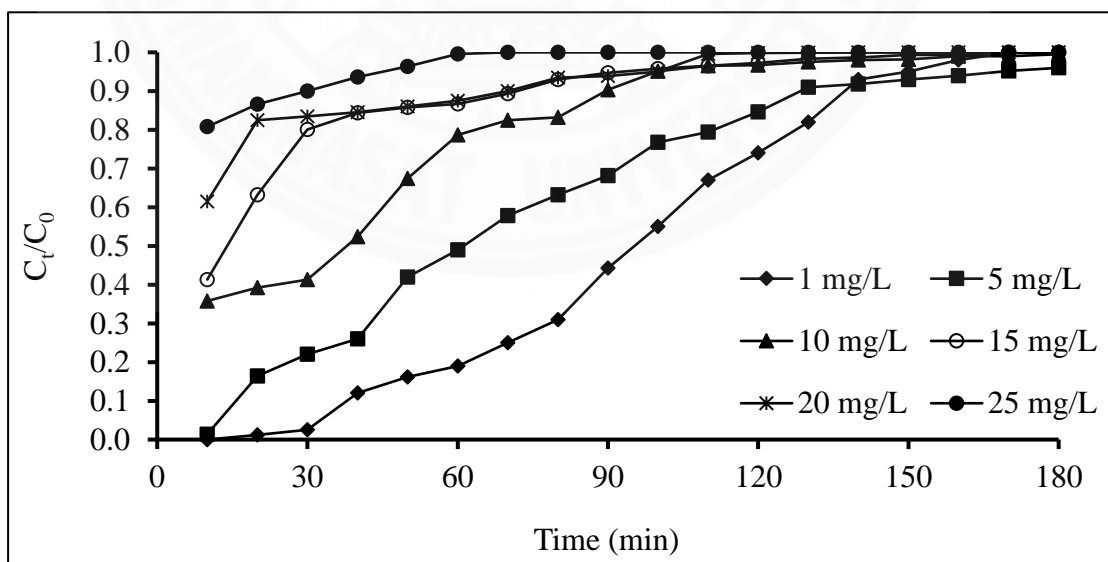


Figure 4.17 The breakthrough curve of Cr(VI) adsorption on CN-CB with different initial concentrations

(at pH 5, flow rate 2.5 mL/min, and room temperature)

The decreasing of inlet concentration provided an extended breakthrough curve, indicating that a more volume of Cr(VI) solution could be treated. This is because of the fact that lower concentration gradient affected a slower transport as a result of a decline in diffusion coefficient or mass transfer coefficient [202].

4.4.3.2 Influence of flow rate on the breakthrough curve

Different flow rates were conducted at 2.5, 5.0 and 10.0 mL/min at pH 5 and room temperature, while the initial concentration of Cr(VI) was kept constant at 5.0 mg/L. The breakthrough curves are illustrated in Figure 4.18. It was showed that the breakthrough occurred faster with higher flow rate and fixed-bed column implemented well at the lower flow. Breakthrough time reaching saturation was increased with a decreased in the flow rate. From Figure 4.18b, at the interval of 90 min, the value of C_t/C_0 reached 0.68, 0.92 and 1.00 when flow rate was 2.5, 5.0 and 10.0 mL/min, respectively.

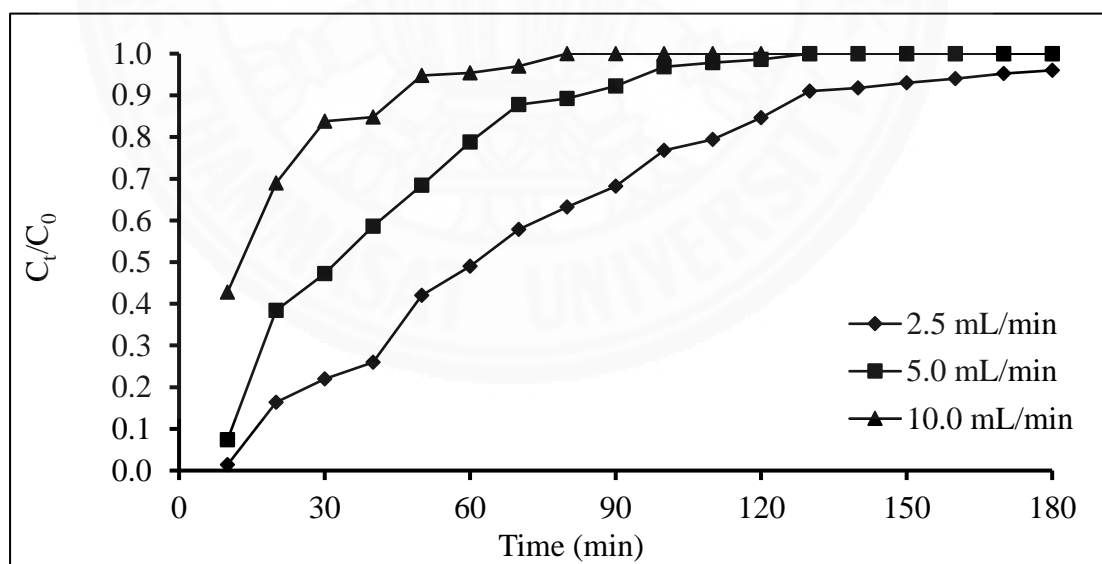


Figure 4.18 The breakthrough curve of Cr(VI) adsorption on CN-CB with different flow rates

(at Cr(VI) initial concentration 5.0 mg/L, pH 5, and room temperature)

At a low rate of C_t/C_0 , Cr(VI) had more time to contact with CN-CB in column that resulted in higher removal efficiency of Cr(VI) [203]. The increasing of flow rate sources a decrease in residence time, which lowers removal efficiency of Cr(VI). At higher flow rate more steeper curve with quite rapid breakthrough and exhaustion time caused fewer adsorption capacity [202]. The breakthrough curve is saturated earlier when the flow rate is increased that similar trends have been reported from literatures [9, 204, 205]. It appears that rapid uptake of Cr(VI) took place at the beginning of operation and rate decreased thereafter and finally reached saturation.

4.4.3.3 Application of model

The Thomas model was used to evaluate the adsorption kinetics of experiment with different initial concentrations and flow rates [206]. The Thomas model, which assumes Langmuir kinetics of adsorption-desorption and no axial dispersion is derived with the adsorption that the rate driving force obeys second-order reversible reaction kinetics [207]. The Thomas rate constant was used for design of a column adsorption process. By fitting data using the model, characteristic parameters for model were examined. Table 4.7 shows the results from Thomas model.

The behavior of the column by using the Thomas model showed the linear regression (R^2) was 0.796 - 0.985 of experimental data for initial concentration with 1, 5, 10, 15, 20 and 25 mg/L at flow rate 2.5 mL/min. The R^2 values ranged from 0.951 to 0.992 for the flow rates of 2.5, 5.0 and 10.0 mL/min. The Thomas rate constant (k_{Th}) decreased with an increase in concentration of Cr(VI) from 1 to 10 mg/L. However, increasing the concentration to 15, 20 and 25 mg/L the rate constant increased. This indicates that the Cr(VI) reaction with increasing concentration of Cr(VI) is not uniform and the reaction becomes slightly slower at higher concentration. The results also revealed that the Thomas rate constant (k_{Th}) increased with increase of the flow rates while the adsorption capacity (q_0) decreased. The q_0 increased with the initial concentration increased (1, and 5 mg/L). Increasing in the flow rate, the specific adsorption capacity also increased because there are more Cr(VI) flow through. However, at high initial concentration (10, 15, 20 and 25 mg/L), The k_{Th} decreased with increase of the initial concentrations while the adsorption capacity fluctuates. The kinetics study revealed that adsorption of Cr(VI) onto CN-CB is well

described by the Thomas model. At this point, the mass transfer limiting mechanism occurred in the first adsorption stage due to surface reaction [207]. The Cr(VI) adsorption increased quickly at the beginning because chitosan active surface was quickly accessed and saturated. In the second slower adsorption stage, the Cr(VI) already adsorbed on the chitosan surface may slowly diffuse into the inner part of the chitosan film, and hence slowly released the outer sites for further Cr(VI) adsorption.

Table 4.7 Characteristic parameters of Thomas model for Cr(VI) adsorption onto CN-CB

Initial concentration (mg/L)	Flow rate (mL/min)	q_{ex} (mg/g)	k_{Th} (mL/min mg)	$q_{0,Th}$ (mg/g)	R^2
1	2.5	4.97	0.0519	14.89	0.973
5	2.5	3.29	0.0061	49.11	0.985
10	2.5	5.72	0.0035	38.98	0.983
15	2.5	2.45	0.0020	14.30	0.981
20	2.5	1.07	0.0025	28.37	0.796
25	2.5	6.46	0.0029	17.32	0.843
5	5.0	9.18	0.0096	40.75	0.992
5	10.0	1.84	0.0122	26.00	0.951

To compare with the results of literature, the adsorption capacity of CN-CB developed by this study for batch and continuous fixed-bed column system. From the Table 4.8, adsorption capacity of present study shows the lower adsorption capacity of Cr(VI) onto CN-CB than literature in batch system. Schmuhl et al. [16] studied the adsorption capacity of chitosan for Cr(VI) removal in batch processes. They revealed 78.0 mg/g of the maximum adsorption capacity. Nevertheless, it is difficult to compare the results because of the differences in the conditions and technique used for surface modification of experimental such as pH, flow rates, and initial concentrations used. In the column study, Sugashini et al. [148] showed that the capacity was 52.7 mg/g of ethylamine modified chitosan carbonized rice husk composite beads for Cr(VI)

removal. The fixed-bed column experiment allows more effective application of the adsorption capacity than the batch process since isotherms are unable to provide accurate data for scale up because a flow in the column is not at equilibrium [208]. At higher pH, the concentration of OH⁻ ions increases and overall charge on the sorbent surface becomes negative which causes limitation in the sorption of negatively charged Cr such as Cr₂O₇²⁻ and CrO₄²⁻ results in the decreased sorption of Cr(VI) [197]. Moreover, the difference in technique used for surface modification and functional group formation is the main reason of difference capacity.

Table 4.8 Comparative adsorption capacity results from literature and experimental data of Cr(VI) onto batch and fixed-bed column experiments

Adsorbents	Concentration (mg/L)	pH	Adsorption capacity (mg/g)		References
			Batch	Column	
CN-CB	10	5.0	-	55.72	Present study
CN-CB	1-25	5.0	25.97	-	Present study
Chitosan coated acid treated oil palm shell charcoal	5 - 25	4.0	60.25	-	[91]
Amino-functionalized	-	-	11.24	-	[113]
Non-cross-linked chitosan	-	-	78.00	-	[16]
Chitosan/montmorillonite-Fe ₃ O ₄	6-60	5.0	58.82	-	[124]
Ethylamine modified chitosan	300	2.0	-	52.7	[148]
carbonized rice husk composite beads	-	-	-	-	-
Chitosan onto ceramic alumina.	5,000	4.0	35.40	-	[5]
Chitosan cross-linked with epichlorohydrin	100	3.0	11.30	-	[209]
Chitosan cross-linked with ethylene glycol diglycidyl ether	1,000	5.5	56.8	-	[210]
Chitosan-based polymeric surfactants	-	5.3	180	-	[211]
Chemically modified chitosan beads	-	3.0	625	-	[139]

4.4.4 Summary

The adsorption of Cr(VI) on CN-CB in batch systems was fitted with the Langmuir isotherm. Batch systems found that the initial concentration effect to adsorption capacity and the adsorption mechanism can be described by the pseudo-second-order kinetic model. CN-CB is an effective adsorbent to remove Cr(VI) in the column systems. The exhaustion times and breakthrough curves were reached, when the initial concentration and flow rate were increased. This was due to the adsorbent get saturated faster at higher concentrations and reduce in the contact time at high flow

rate, which limited the contact of Cr(VI) to the CN-CB. The Thomas model is used to describe column performance for predicting breakthrough curves. It assumes Langmuir model for adsorption processes where the external and internal diffusions are not the limiting step. Moreover, the Thomas model presumes the rate driving force follows second order kinetics. It was found to be suitable for the experimental data. The adsorption capacity of fixed-bed column was higher in comparison to the batch experiment. Fixed-bed column do not essentially work under equilibrium situations as the contact time is not sufficiently long for the achievement of equilibrium.

4.5 Cu(II) removal from aqueous solutions by nanochitosan coated alumina balls in fixed-bed column

There are few reports on the application of nanochitosan coated on supporting materials for heavy metal removals. To prepare the surface layer over the support, many techniques were reported such as spray coating [212], grafting [213], spin coating [214], self-assembly [215], dip coating [212] and vapor deposition [216]. Among these methods, dip coating is simple, inexpensive and thus most desirable choice for industrial purpose [3]. Since the earlier studies found that the batch system lower efficiency than fixed-bed column system. Moreover, the continuous process and fixed-bed column are usually used for the industries wastewater treatment. In this study, CN was coated onto alumina balls and packed in the column in order to study its adsorption capacity. The main objective is to investigate the adsorption mechanism of Cu(II) by nanochitosan coated alumina balls (CN-CB).

4.5.1 Parameters affecting the column performance

4.5.1.1 Effect of initial concentration on breakthrough curve

A series of experiments were conducted at varying initial Cu(II) concentrations of 5, 10 and 30 mg/L at pH 5 and room temperature, while the flow rate of 2.5 mL/min and dose of CN-CB of 25 mg were maintained. Figure 4.19, the breakthrough curves illustrate that the exhaustion time decreases by increasing the initial concentration, indicating that binding sites become more quickly saturated and adsorbent gets saturated faster at higher concentrations in the column [199, 202]. The

total adsorption capacity (q_e) are 54.3, 105.4 and 187.4 mg/g at initial Cu(II) concentrations of 5, 10, and 30 mg/L, respectively (Figure 4.20).

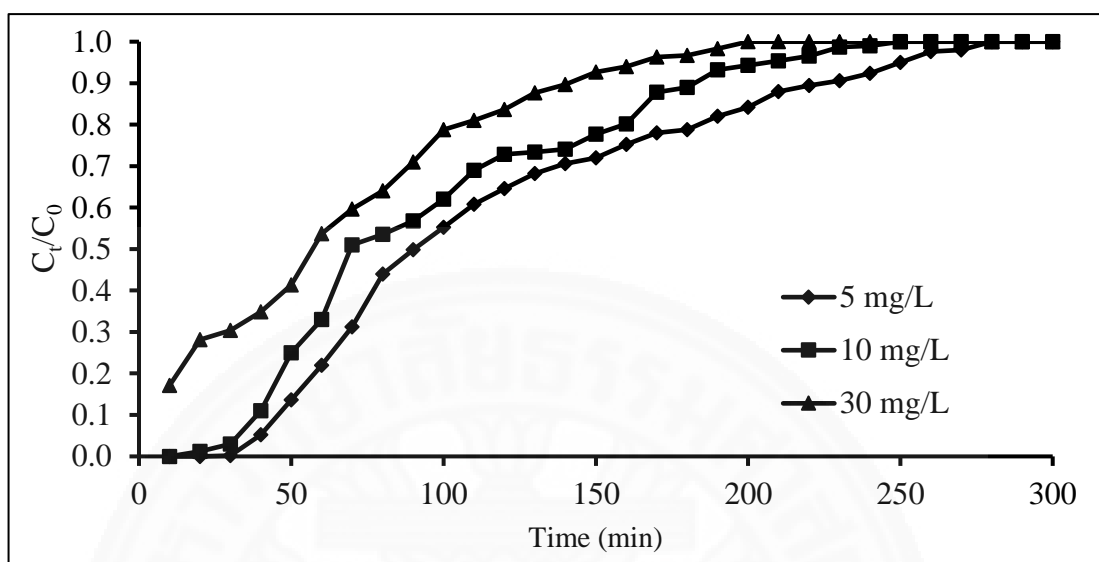


Figure 4.19 Breakthrough curve of Cu(II) at different initial concentrations (at pH 5, flow rate 2.5 mL/min, CN-CB dose 25 mg, and room temperature)

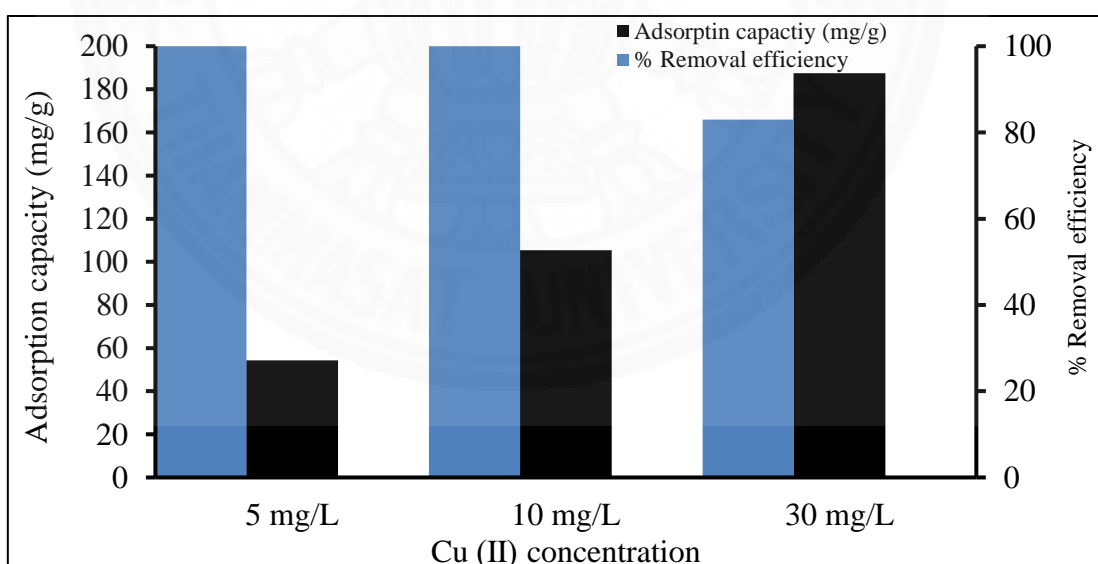


Figure 4.20 Adsorption capacity and % removal efficiency of Cu(II) at different initial concentrations (at pH 5, flow rate 2.5 mL/min, CN-CB dose 25 mg, and room temperature)

It was found that the total adsorption capacity increased with increasing initial Cu(II) concentration up until a plateau but the rate decreased. It is possible owing to most of the sites are already occupied when the concentration is high and the uptake rate becomes slower, indicating that the driving force for adsorption is concentration gradient [217]. A larger concentration gradient caused a faster transport due to an increase of diffusion coefficient or mass transfer coefficient [201].

4.5.1.2 Effect of flow rate on breakthrough curve

To investigate the effect of flow rate on the breakthrough curve, the flow rate was varied ranging from 2.5 to 10.0 mL/min at pH 5 and room temperature. The initial concentration of 10 mg/L and dose of CN-CB of 25 mg were set constant. The flow rates have a significant effect on the shape of breakthrough curve [217]. A plot of breakthrough curves related between C_t/C_0 and time at different flow rates was shown in Figure 4.21. As shown in the Figure, early breakthrough and exhaustion occurred at higher flow rates. Similar trends have been reported from literatures [9, 204, 205] at which the breakthrough curve is saturated earlier when flow rate increased. Flow rates of 5.0 and 10.0 mL/min were recognized to have a faster movement of adsorption zone.

When the flow rate was double to 5 and 10 mL/min, the specific adsorption capacity (q_e) decreased. The q_e is 105.4, 90.4 and 66.4 mg/g for the flow rates of 2.5, 5.0 and 10.0 mL/min, respectively (Figure 4.22). By increasing the flow rate, the removal efficiency decreased from 100.0% at 2.5 mL/min to 58.5% and 34.9% at 5 and 10 mL/min, respectively. The reduction of percentage can be attributed to the insufficient time for diffusion of Cu(II) into the inner pores of CN-CB through intraparticle diffusion [149, 204].

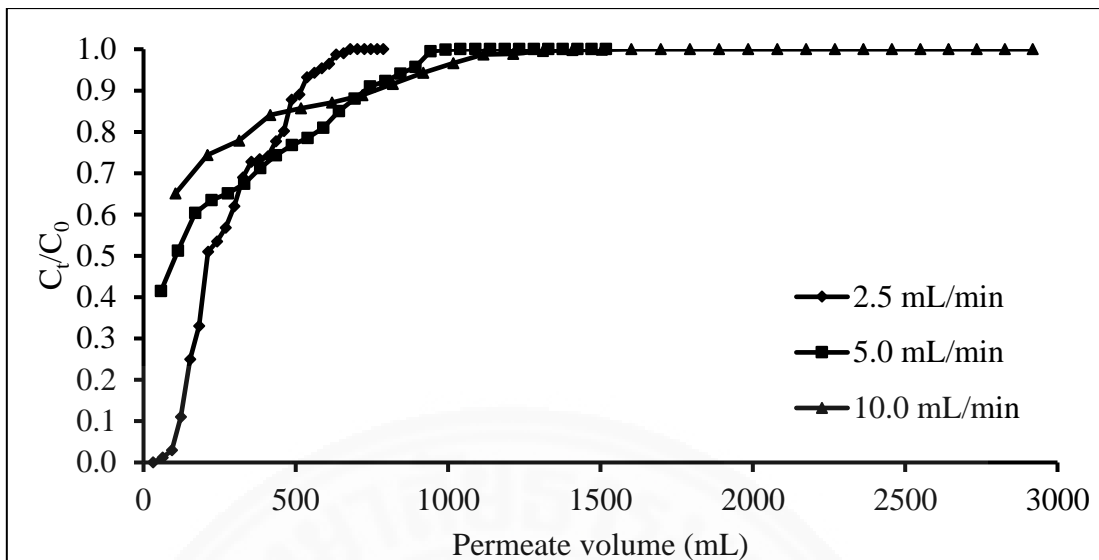
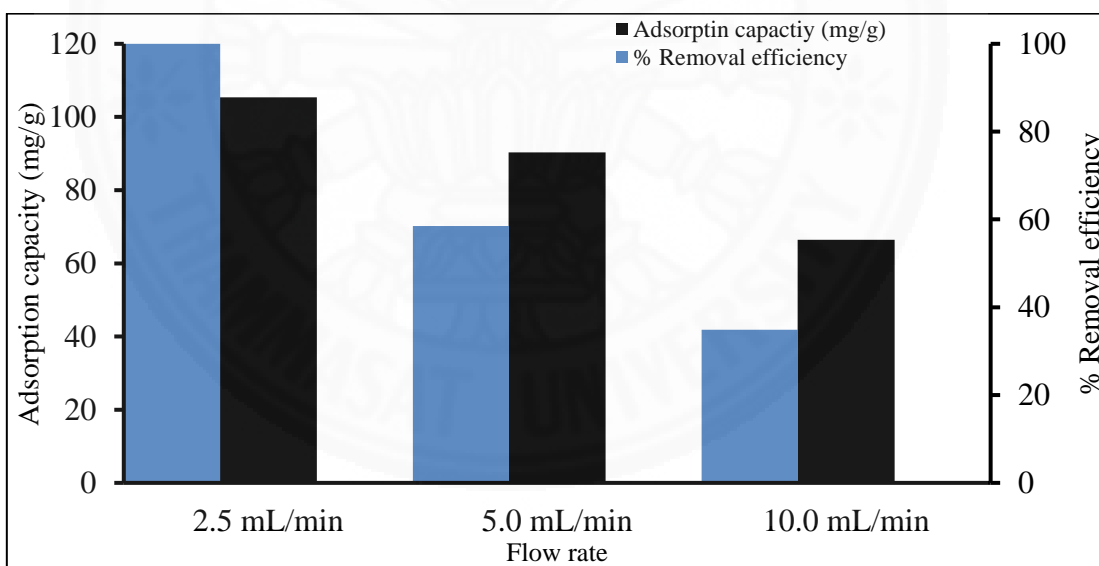


Figure 4.21 Breakthrough curve of Cu(II) at different flow rates (at Cu (II) initial concentration 10 mg/L, pH 5, CN-CB dose 25 mg, and room temperature)



(b)

Figure 4.22 Adsorption capacity and % removal efficiency of Cu(II) at different flow rates (at Cu (II) initial concentration 10 mg/L, pH 5, CN-CB dose 25 mg, and room temperature)

4.5.1.3 Effect of nanochitosan loading on breakthrough curve

Figure 4.23 illustrates the breakthrough curves accomplished at various nanochitosan loadings of CN-CB in column with a constant flow rate of 2.5 mL/min and initial concentration 10 mg/L. At nanochitosan loadings of 15, 25 and 35 mg, the total adsorption capacity was 118.1, 105.4, and 71.3 mg/g, respectively (Figure 4.24). While the amount of nanochitosan loading increased, the surface area also increased due to the change from particle-like morphology to film-like morphology of nanochitosan on the alumina ball support. This result indicates that the sorption of Cu(II) took place mostly on the nanochitosan surface.

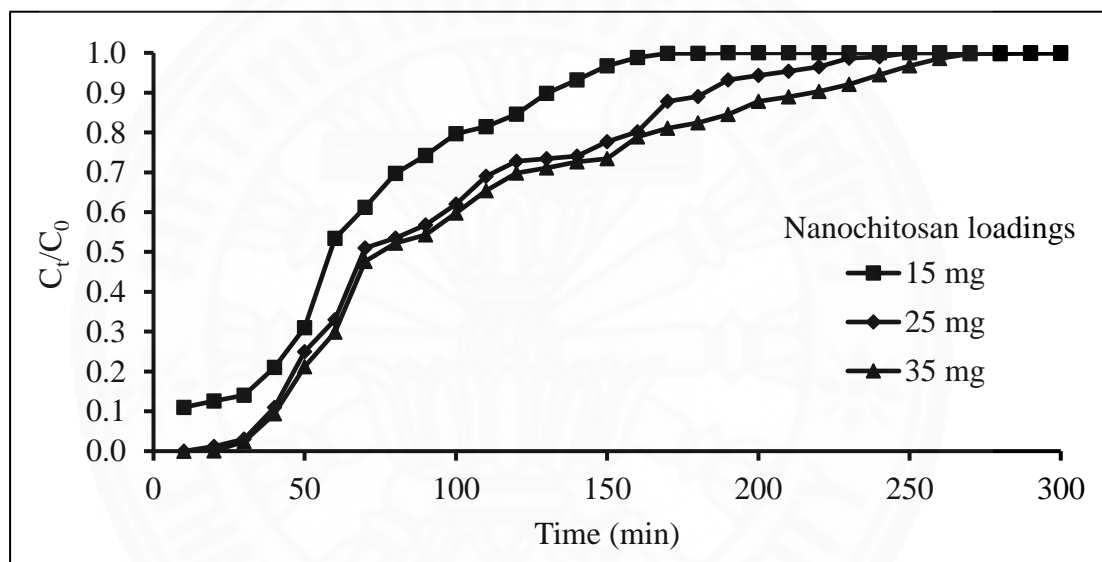
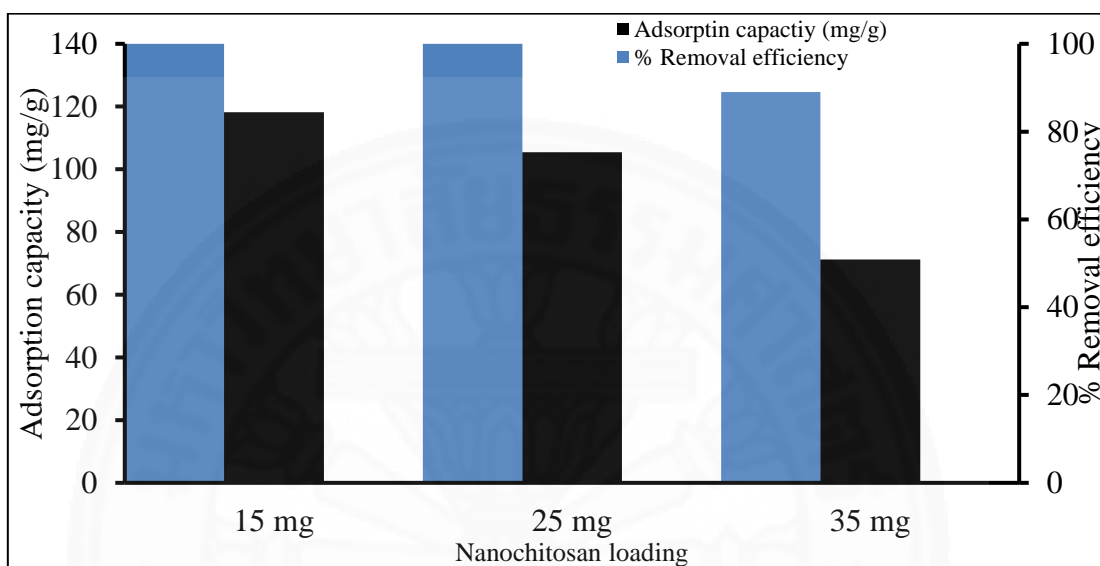


Figure 4.23 Breakthrough curve of Cu(II) at different nanochitosan loadings (at Cu (II) initial concentration 10 mg/L, flow rate 2.5 mL/min, pH 5, and room temperature)

For comparative study, data were collected from literature for chitosan-coated on supporting materials, as listed in Table 4.9. This study presents an adsorption capacity of 187.4 mg/g which is 2.6 times lower when compared to chitosan-immobilized bentonite in columnar system [149]. This is mainly because of the differences in the experimental conditions such as pH, flow rates, and initial concentrations used. The flow rate used in this study was 12.5 times higher than that of Futralan et al [149], resulting in less contact time between Cu(II) and the sorbents. Thus, less sorption capacity was obtained. Nevertheless, it is relatively higher than chitosan

coated on various supporting materials in batch system such as magnetic nanoparticles [20], sand [140], and PVC beads [19], but nearly similar to chitosan-coated perlite [95] which its conditions are pH 5, and adsorbent doses 0.3 g. Moreover, the removal efficiency of Cu(II) in column system exhibited higher than Cr(VI) in the earlier study.



(b)

Figure 4.24 Adsorption capacity and % removal efficiency of Cu(II) at different nanochitosan loadings (at Cu(II) initial concentration 10 mg/L, flow rate 2.5 mL/min, pH 5, and room temperature)

4.5.1.4 Application of Thomas and Yoon-Nelson model

The behavior of columnar adsorption was evaluated using the Thomas and Yoon-Nelson models. The coefficient of determination and model parameters are shown in Table 4.10 with variation of initial concentrations, flow rates and nanochitosan loadings.

A measure of the proportion of variability in data set to the Thomas model, accounted by R^2 , ranges from 0.8899 to 0.9935 indicating a good agreement between the experimental data and the column data generated using the Thomas model. The Thomas rate constant (k_{Th}) decreased with an increase initial concentration and chitosan loading. As flow rate increased, the value of q_0 decreased while k_{Th}

increased which indicates that the mass transport resistance decreases as a result of different driving force for adsorption between CN-CB and Cu(II) solution [149, 201]. The direct effect on mass transfer resistance took place from the thickness of liquid film on the CN-CB surface [172].

Table 4.9 Adsorption capacity of chitosan-coated on various supporting materials for Cu(II) removal

Adsorbent	System	Adsorption capacity (mg/g)	pH	References
CN-CB	Column	187.40	5.0	Present study
Chitosan-immobilized bentonite	Column	480.97	4.0	[149]
Chitosan-coated magnetic nanoparticles	Batch	65.67	4.5-5.0	[20]
Chitosan-coated sand	Batch	8.18	-	[140]
Chitosan-coated PVC beads	Batch	87.90	4.0	[19]
Chitosan-coated perlite	Batch	196.07	5.0	[95]

So lower flow rate and lower nanochitosan loading would increase the adsorption of Cu(II) on the CN-CB column. This shows that the Cu(II) reaction with increasing amount of chitosan is not uniform and the reaction becomes somewhat slower at higher amount of chitosan. The specific adsorption capacity (q_0) decreased as the nanochitosan loading increased. With an increase in the initial concentration, the specific adsorption capacity also increased because there are more Cu(II) ions flow through. The Thomas model was suitable for prediction of column performance because the specific adsorption capacity is also in the same trend as that calculated by using mass balance indicating that the external and internal diffusions will not be the limiting step of mass transfer [207].

By fitting data using the Yoon-Nelson model, the Yoon-Nelson model provided fit to the experimental data with R^2 values ranging from 0.8304 to 0.9935. k_{YN} and τ values were used to determine the breakthrough curve. From Table 4.10, the value of k_{YN} increases with respect to Cu(II) concentration. This is due to an increase of initial concentration thereby increases the competition between molecules of Cu(II) for the

adsorption sites. Thus, an uptake rate increased. The value of k_{YN} increases while τ decreases with an increase in the flow rate. The τ value decreases with increasing of flow rate and Cu(II) initial concentration but increases with increasing nanochitosan loading. At high flow rate, the number of Cu(II) molecules passing through a particular CN-CB is more, which increases the adsorption rate [120]. These values have a similar trend to the Cr(VI) removal in the aforementioned study. Additionally, the values also similar trend to the reported earlier [120, 174, 207].

Clearly, the experimental data fitted well to the both models. The rate constants, adsorption capacity, and τ were dependent on flow rate, initial ion concentration and nanochitosan loading.

Table 4.10 Thomas and Yoon-Nelson model parameters at different flow rates, initial concentrations and doses for Cu(II) adsorption onto CN-CB

C_0 (mg/L)	Dose (mg)	Q (mL/min)	$q_e(\text{exp})$	Thomas model			Yoon-Nelson model		
				q_0 (mg/g)	K_{Th} (mL/mg min)	R^2	K_{YN} (l/min)	τ (min)	R^2
5	25	2.5	54.3	52.1	0.0045	0.9337	0.0224	112.14	0.9337
10	25	2.5	105.4	93.8	0.0027	0.9552	0.027	89.85	0.9552
30	25	2.5	187.4	170.3	0.0010	0.9935	0.0288	59.42	0.9935
10	25	5	90.4	70.6	0.0028	0.9780	0.019	20.95	0.9757
10	25	10	66.4	28.1	0.0042	0.9313	0.0396	3.76	0.9281
10	15	2.5	118.1	109.6	0.0040	0.9728	0.0403	66.95	0.9728
10	35	2.5	71.3	84.2	0.0030	0.8899	0.0335	118.62	0.8304

4.5.2 Summary

Cu(II) removal through a fixed-bed column was dependent on the initial concentration, flow rate and the nanochitosan loading on the surface of alumina balls. The maximum adsorption capacity, 187.4 mg/g, was achieved at 30 mg/L of initial concentration, 2.5 mL/min and 25 mg nanochitosan loading. Thomas models provided more preferable results for describing the behavior of Cu(II) adsorption in a fixed-bed column than Yoon-Nelson models. It can be used as an effective tool for prediction and design of an adsorption column for removal of Cu(II) concentration in water. Nevertheless, modified Thomas model parameters may be required.

4.6 Ni(II) removal from aqueous solutions by chitosan coated ceramic membrane in adsorption-filtration membrane

The earlier study demonstrates the performance of chitosan and CN solution for heavy metal removal by adsorption process. However, the adsorption process needs an additional stage to separate adsorbent from treated wastewater. The combination of adsorption process and membrane filtration is of interest. Membrane filtration is widely used for heavy metals removal, particularly ultrafiltration, nanofiltration, reverse osmosis, and electrodialysis [10] . Membrane processes illustrates great ability for heavy metal removal, high permeate fluxes, convenient operation, and space saving [10, 37] . Moreover, using membrane filtration allows continuous operation and can be simply integrated with other methods [7, 37].

In this investigation an attempt was made to overcome the mass transfer limitations by coating biosorbents, chitosan, on the surface of ceramic membrane. The efficiency for uptake Ni(II) onto continuous flow of chitosan coated ceramic membrane was explored. The effect of flow rate and chitosan loading were investigated. Continuous flow adsorption studies were conducted to obtain breakthrough curve and to evaluate the column adsorption performance by using the kinetic model.

4.6.1 Ni(II) removal

Removal efficiencies of Ni(II) by the method of simultaneous filtration and adsorption is shown in Figure 4.25. Ni(II) removal up to 76% was accomplished by the CN-coated ceramic membrane with 20 mg chitosan loading at flow rate 2.5 mL/min (Figure 4.25a). The specific adsorption capacity (mg Ni/g chitosan) decreased with an increase in chitosan loading. At chitosan loadings of 10, 15 and 20 mg, the specific adsorption capacity was 89.0, 85.1, and 74.2 mg/g chitosan, respectively. When the flow rate was double to 5 mL/min, the specific adsorption capacity was then increased to 123.0, 113.8, and 100.6 mg/g chitosan, respectively (Figure 4.25b). At a higher flow rate, more of Ni(II) passing through adsorbent, which increased the cumulative adsorption. However, note that the cumulative amount of Ni(II) adsorbed increased with an increase in chitosan loading, while the adsorption capacity (amount of

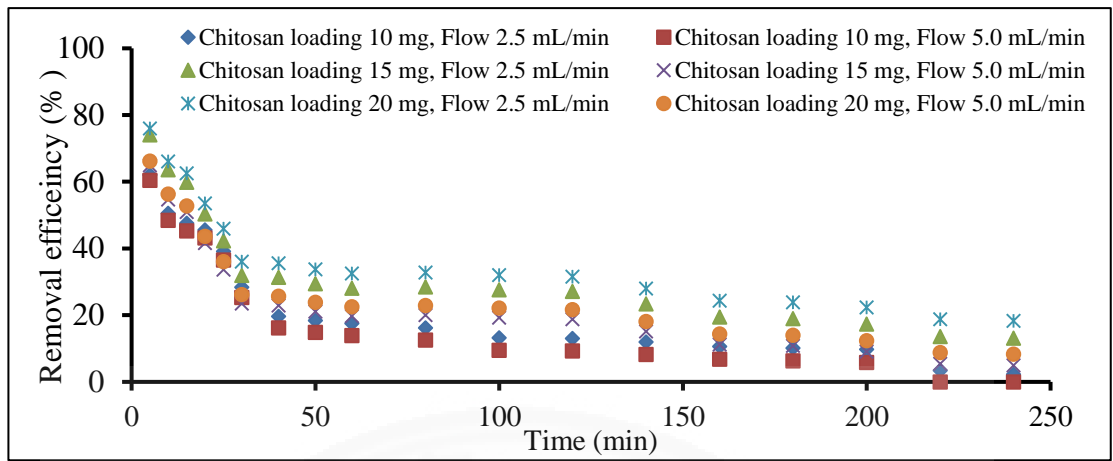
Ni/chitosan loading) decreased. This result indicates that the sorption of Ni(II) took place primarily on the chitosan surface. When the amount of chitosan coating increased, the surface area also increased but at slower rate due to the change from the particle-like morphology to film-like morphology of chitosan on the membrane support. Although Ni(II) adsorption started to level off after 60 min of operation, adsorption approached steady state conditions for Ni(II) removal for nearly 240 min of operation (Figure 4.25c). It appears that rapid uptake of Ni(II) was observed at the beginning of operation and rate decreased thereafter and finally reached saturation.

4.6.2 Permeate flux

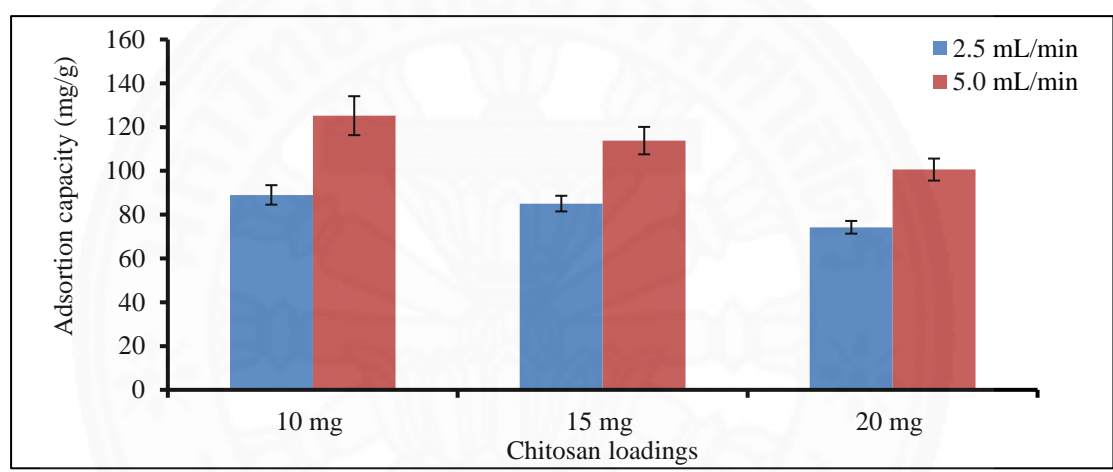
The permeate flux of all conditions decreased with time and leveled off around 100 min) Figure 4.26. (The condition chitosan loading of 10 mg and flow rate 5.0 mL/min seemed to be suitable in term of its highest flux. The flux decreased to 52.02 L/m². h from the initial 61.28 L/m². h. Initially, the permeate flux of all conditions slightly decreased and then the decrease became steady. Although permeate flux approached steady state conditions for Ni(II) removal around 100 min of operation, measurements carried on for 240 min. With an increase in chitosan loadings, the permeate flux decreases because of thicker chitosan layer on membrane surface and the concentration polarization [162]. [This tendency showed that interaction between the ceramic membrane and chitosan led to the formation of a chitosan layer on the membrane ceramic and induced a reduction of the membrane pore size. Membrane compaction and fouling apparently caused a reduction in permeate flux during this period.

4.6.3 Adsorption kinetics and breakthrough curves

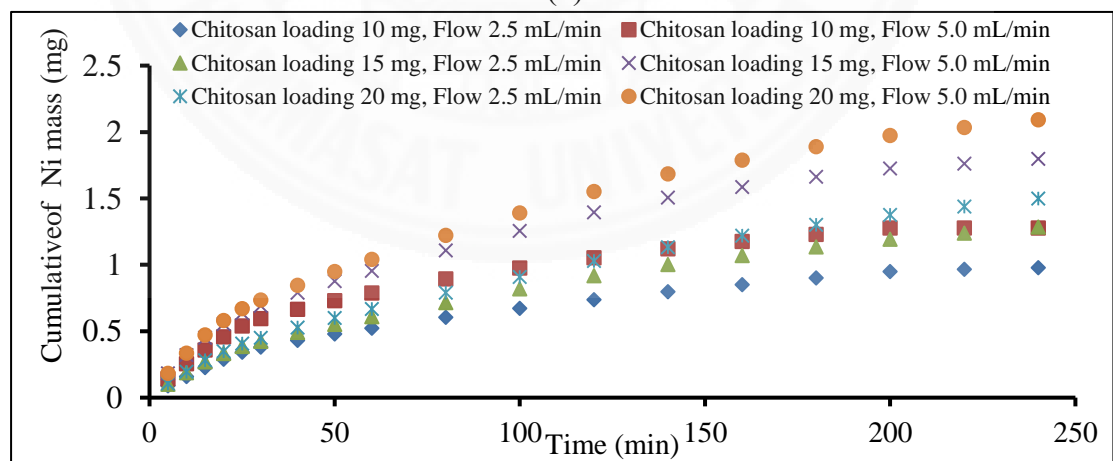
As adsorption and filtration continues, the chitosan-coated membranes gradually become saturated with Ni(II). The plot of C_t/C_0 versus permeate volume as shown in Figure 4.27 can be used to indicate capacity of this membrane. The breakthrough curves were obtained for the chitosan loadings at 10, 15 and 20 mg with flow rates between 2.5 and 5.0 mL/min. As the chitosan loading on ceramic membrane was increased, the break point time decreased. Decreasing the inflow rate increased the breakthrough volume or breakthrough time. The results also showed that the shape of the breakthrough curve reached saturation (became flat) faster for a higher chitosan



(a)



(b)



(c)

Figure 4.25 Adsorption of the Ni(II) on CN-coated ceramic membrane at various chitosan loadings and flow rate: (a) time course of Ni(II) removal efficiency, (b) adsorption capacity of Ni(II), and (c) time course of the cumulative Ni(II) mass (at Ni(II) initial concentration 10 mg/L, pH 5, and room temperature)

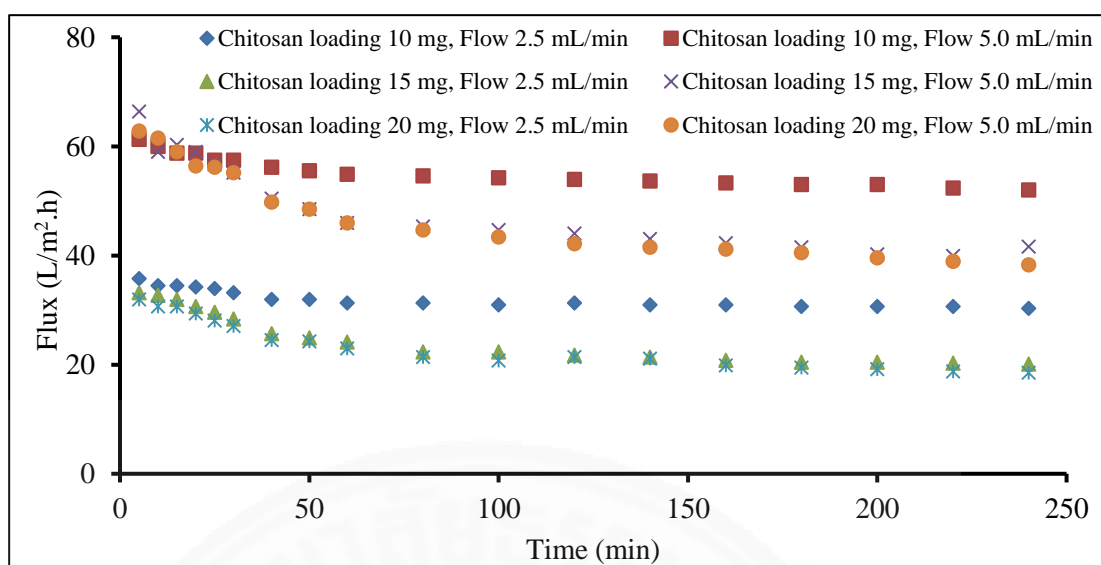
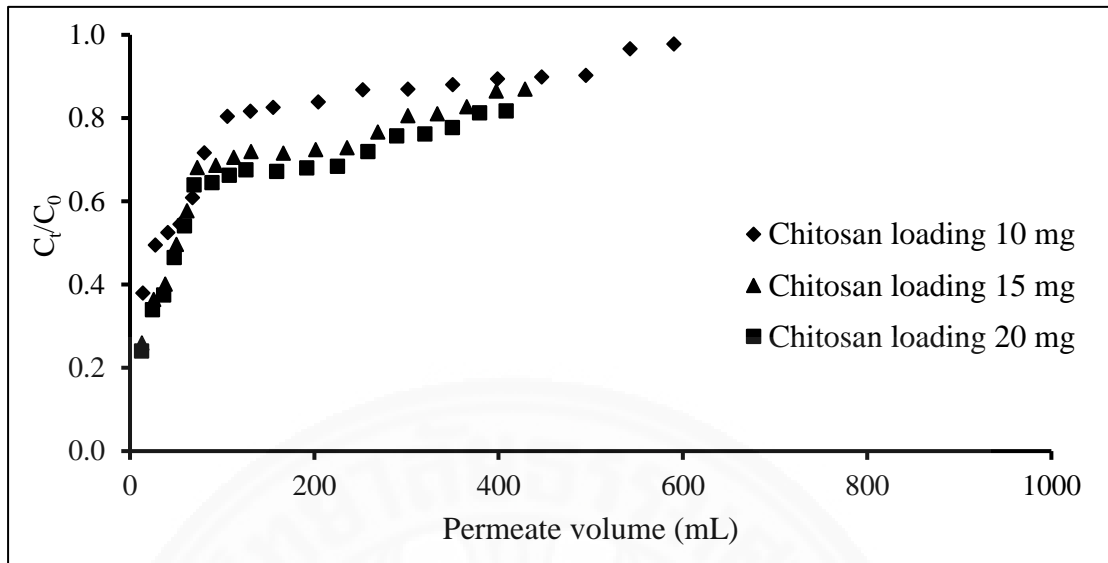


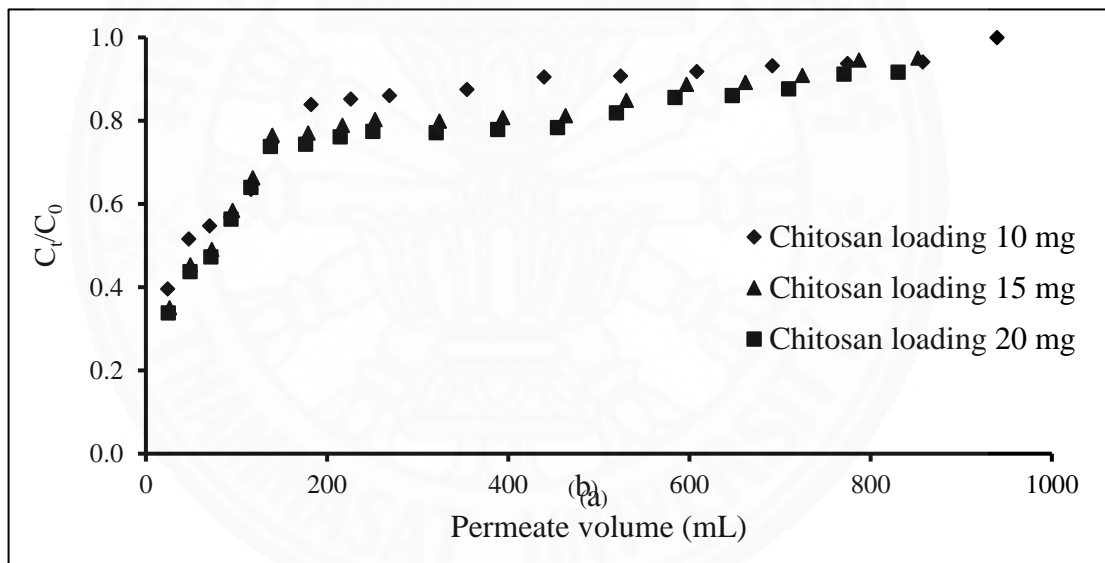
Figure 4.26 Flux decline profiles of Ni(II) concentration with different chitosan loadings and flow rates (at Ni(II) initial concentration 10 mg/L, pH 5, and room temperature)

loading. This was because the front of the adsorption zone quickly reached the top of membrane surface [9]. This indicates that the adsorption took place mainly on the chitosan film's surface that is, in turn, controlled by surface area of the membrane. From the shapes of the curves, adsorption may occur in two stages: a rapid rise and a slow rise. The initial rapid rise of breakthrough Ni(II) may be due to the saturation of the chitosan active surface across the membrane. After these easily access chitosan sites have been taken, the concentration of the breakthrough Ni(II) increases slowly. This may be due to the second slower adsorption of Ni(II) by the more difficult to access sites of chitosan, and possibly also to the diffusion of Ni(II) already adsorbed on the outer surface of the chitosan film to the inner pores of the chitosan film. For high chitosan loadings of 15 and 20 mg, a turnover point occurred sooner than the 10 mg chitosan loading. A sharp turning point is an indication that there are likely at least two different adsorption mechanisms such as a rapid rise and a slow rise involved here.

The adsorption kinetics from these column studies at different chitosan loadings and flow rates were then analyzed using the Thomas and the Yoon-Nelson models [206]. By fitting data using the two models, characteristic parameters for each model were determined and shown in Table 4.11. The Thomas model provided fit to



(a)



(b)

Figure 4.27 Influence of chitosan loadings on the breakthrough curve of Ni(II) adsorption on CN-coated ceramic membrane: (a) flow rate of 2.5 mL/min and (b) flow rate of 5.0 mL/min (at Ni(II) initial concentration 10 mg/L, pH 5, and room temperature)

the experimental data with R^2 values ranging from 0.969 to 0.985 for flow rate 5.0 mL/min and from 0.889 to 0.974 for the flow rate of 2.5 mL/min. The Thomas rate constant (k_{Th}) decreased with an increase in chitosan loading with 10 and 20 mg. This

indicates that the Ni(II) reaction with increasing amount of chitosan is not uniform and the reaction becomes somewhat slower at higher amount of chitosan. The specific adsorption capacity (q_0) decreased as the chitosan loadings increased. With an increase in the flow rate, the specific adsorption capacity also increased because there are more Ni(II) flow through. This specific adsorption capacity is also in the same trend as that calculated by using mass balance indicating applicability of Thomas model in predicting column performance. The Yoon-Nelson model fitting to the data was somewhat less satisfactory compared to that provided by the Thomas model with the R^2 ranging between 0.839-0.938 for the 5 mL/min flow rate, and 0.915-0.974 for the 2.5 mL/min flow rate.

Table 4.11 Characteristic parameters of kinetic model for the adsorption of Ni(II) onto CN-coated ceramic membrane

Chitosan loading	mg	10.0	15.0	20.0	10.0	15.0	20.0
Flow rate	mL/min	2.5	2.5	2.5	5.0	5.0	5.0
Thomas model							
k_{Th}	mL/min mg	0.0015	0.0016	0.0008	0.0016	0.0013	0.0011
q_0	mg/g	78.10	66.39	57.39	81.79	69.62	63.59
R^2	-	0.974	0.933	0.889	0.969	0.985	0.976
Yoon and Nelson model							
k_{YN}	L/min	0.0157	0.0112	0.0100	0.0163	0.0116	0.0114
τ	min	13.45	48.83	63.75	0.83	19.23	14.80
q_{YN}	mg/g	32.22	66.78	65.59	3.54	50.89	30.02
R^2	-	0.974	0.933	0.915	0.933	0.839	0.938

The kinetics study revealed that adsorption of Ni(II) onto CN-coated ceramic membrane is better described by the Thomas model rather than the Yoon-Nelson model. Here, the mass transfer limiting mechanism occurred in the first adsorption stage due to surface reaction. The Ni(II) adsorption rose rapidly because chitosan active surface was quickly accessed and saturated. In the second slower adsorption stage, the Ni(II) already adsorbed on the chitosan surface may slowly diffuse into the inner part of the chitosan film, and hence slowly released the outer sites for further Ni(II) adsorption.

4.6.4 Summary

A novel technique for Ni(II) removal from aqueous solution was developed which allowed simultaneous filtration and adsorption using chitosan-coated ceramic membrane. The chitosan-coated membrane in this work has maximum adsorption capacity of 123 mg Ni/g of coated chitosan, comparable to that of using chitosan nanoparticles but without the difficulty of needing to separate chitosan from treated water. Two Ni adsorption mechanisms were observed from column studies and breakthrough curves, which are the rapid sorption of Ni(II) onto chitosan surface followed by the slower intraparticle diffusion of Ni(II) inside chitosan structure. Thomas model can also be used to provide good description of the column performance with change in process parameters like chitosan loading and flow rates.

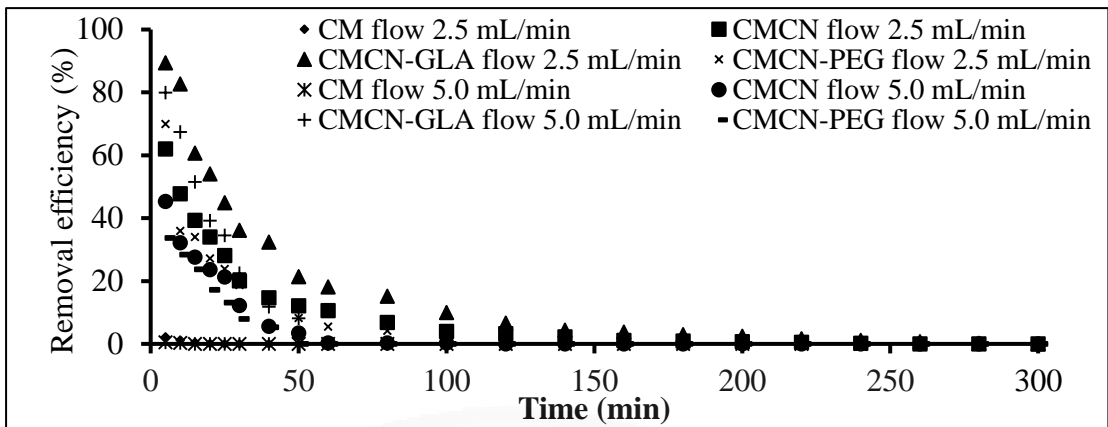
4.7 Cu(II) removal by modified nanochitosan coated ceramic membrane in adsorption-filtration membrane

Membrane processes illustrates great ability for heavy metal removal, high permeate fluxes, convenient operation, and space saving [10, 37]. Moreover, using membrane filtration allows continuous operation and can be simply integrated with other methods [7, 37]. The combination of adsorption process and membrane filtration is of interest. In this study, ceramic microfiltration membrane was used as filter and support material for nanochitosan. The earlier study shows the high Ni(II) removal by simultaneous filtration and adsorption using chitosan-coated ceramic membrane. In order to shorten treatment process and to improve the adsorption capacity of the chitosan for Cu(II) removal, nanochitosan was coated on the surface of membrane which led to an increase in hydrophilicity and high water permeability [218]. Chelation was used to overcome the mass transfer limitations by coating biosorbents, nanochitosan, and modified chitosan GLA and PEG, on the surface of ceramic membrane. Their efficiencies for Cu(II) adsorption were explored. Continuous flow adsorption studies were conducted to obtain breakthrough curves and to evaluate the column adsorption performance by using the kinetic model.

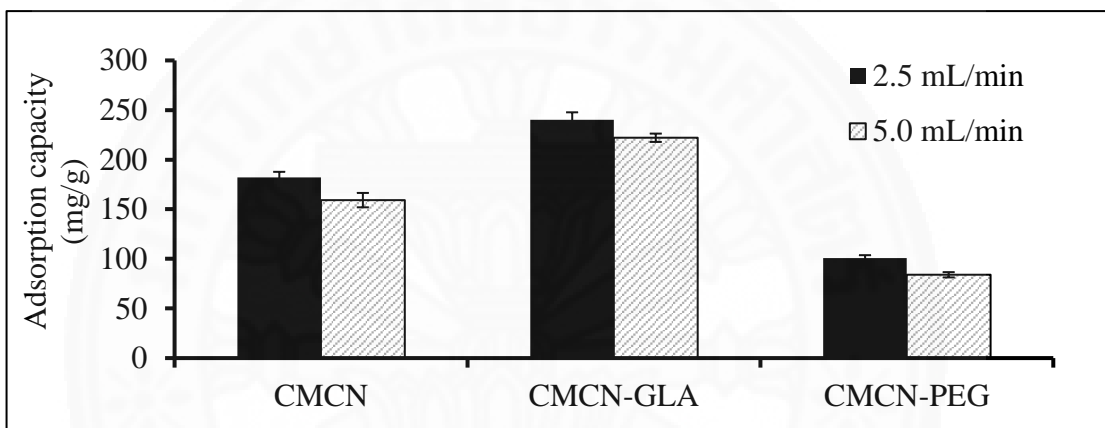
4.7.1 Cu(II) removal

The achievements of simultaneous removal of Cu(II) by the filtration and adsorption are illustrated in Figure 4.25. Cu(II) was unable to be removed by the bare ceramic membrane but adsorbed by the interaction with nanochitosan and modified nanochitosan. Cu(II) removal up to 89.38% was accomplished by CMCN-GLA at a flow rate of 2.5 mL/min (Figure 4.28a). The specific adsorption capacity (mg Cu/g chitosan) was 240.3 mg/g, which is 2.4 times higher when compared to the simultaneous adsorption-filtration study using native chitosan by Steenkamp et al. [163]. When the flow rate was doubled to 5.0 mL/min, the specific adsorption capacity was then decreased to 222.1 mg/g chitosan (Figure 4.28b). At a higher flow rate, a greater amount of Cu(II) passed by the adsorbent, resulting in an increase in Cu(II) on the sorbent. For CMCN and CMCN-PEG, at a flow rate of 2.5 mL/min, the removal was achieved with specific adsorption capacities of 182.0 and 100.7 mg/g of chitosan, respectively. The adsorption capacity decreased to 159.2 and 84.0 mg/g, respectively, at a flow rate of 5.0 mL/min for CMCN and CMCN-PEG. When the surface of the membrane changes from a particle-like morphology to a film-like morphology, the adsorption rate decreased as the surface area also decreased. The decreased percentage and adsorption capacity can be attributed to the insufficient time for Cu(II) diffusion into the inner pores of the adsorbent [149, 204].

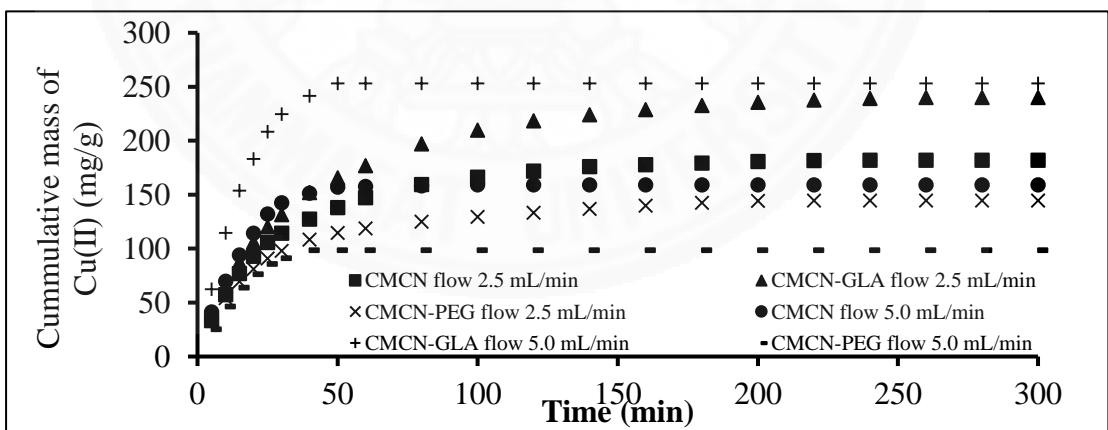
Moreover, nanochitosan becomes more hydrophobic and can also play an active role in Cu(II) sorption via free aldehyde groups. This is because the chemical modification with GLA [191], results in negative species to bind with Cu(II) [174, 219]. Although a chitosan grafted copolymer with PEG can be used to recover cations from solution [220], this results in greater water solubility, and therefore, there could be swelling [221]. However, note that the cumulative amount of Cu(II) adsorbed increased with an increase in flowrate, while the adsorption capacity (amount of Cu(II)/adsorbent loading) decreased. This result indicates that the sorption of Cu(II) took place primarily on the adsorbent surface. The Cu(II) adsorption started to level off after 60 min of operation, and then approached steady state conditions, after nearly 300 min of operation (Figure 4.28c). It appears that rapid uptake of Cu(II) occurred at the beginning of operation, and the rate decreased thereafter and finally reached saturation.



(a)



(b)



(c)

Figure 4.28 Adsorption of the Cu(II) by various adsorbents coated on ceramic membrane for difference flow rates: (a) Time course of Cu(II) removal efficiency, (b) adsorption capacity of Cu(II), and (c) Time course of the cumulative Cu(II) mass (at Cu (II) initial concentration 50 mg/L, adsorbent dose 20 mg, pH 5, and room temperature)

A membrane study for three consecutive adsorption-desorption cycles shows the stability of coated adsorbents on the membrane surface and the ease of desorption. Desorption of adsorbents can be successfully accomplished for three consecutive cycles using 0.1 M H₂SO₄ solution. The mechanism of desorption involves H⁺ from H₂SO₄. The bound Cu(II) undergoes both electrostatic and complexation reactions, affected by the ionic strength of solutions [139, 219]. Thus, the electrostatic interaction between chitosan and Cu(II) becomes weaker, causing the release of adsorbed Cu(II) and the adsorption sites to be evacuated. Similar desorption data were also reported by Wambu et al. [222].

In addition, the membrane coating stability was evaluated based on the difference of the dry weight before and after use of the coated membrane. Assuming that the detachment during operation was the prime mechanism for weight loss, it was found that the coating adhered to the membrane surface quite well with most of the weight losses occurring during the initial flow. At the flow rate of 2.5 mL/min, the weight loss after 180 min of operation was about 15%. Additional loss of 3% occurred towards 300 min of run time. The loss of weight during initial flow was suspected to associate with the loose particles on the membrane surface. At higher flow rate of 5.0 mL/min, the weight loss was slightly larger of about 18% during the first 180 min. Increasing run time to 300 min caused only 2% further loss of weight.

The chemical composition of the ceramic membrane with various adsorbents, as determined by EDS, is presented in Figure 4.29. Figure 4.29(a) shows that the peaks assigned to Ti and O were dominant (more than 90% of the total composition) for the ceramic membrane. The EDS composition after Cu(II) adsorption provides the composition of Ti, C, and O, which were major constituents of chitosan and the ceramic membrane. Figure 4.29(b), 4.29(c), and 4.29(d) show direct evidence for Cu(II) uptake by various adsorbents after adsorption (0.32, 0.85 and 0.16 % by weight with CMCN, CMCN-GLA, and CMCN-PEG, respectively).

4.7.2 Permeate flux

Figure 4.30 shows the permeate flux evolution for various adsorbents coated on a ceramic membrane. As indicated, the flux is inversely proportional to the thickness of adsorbent in the order of CM > CMCN > CMCN-GLA > CMCN-PEG. A

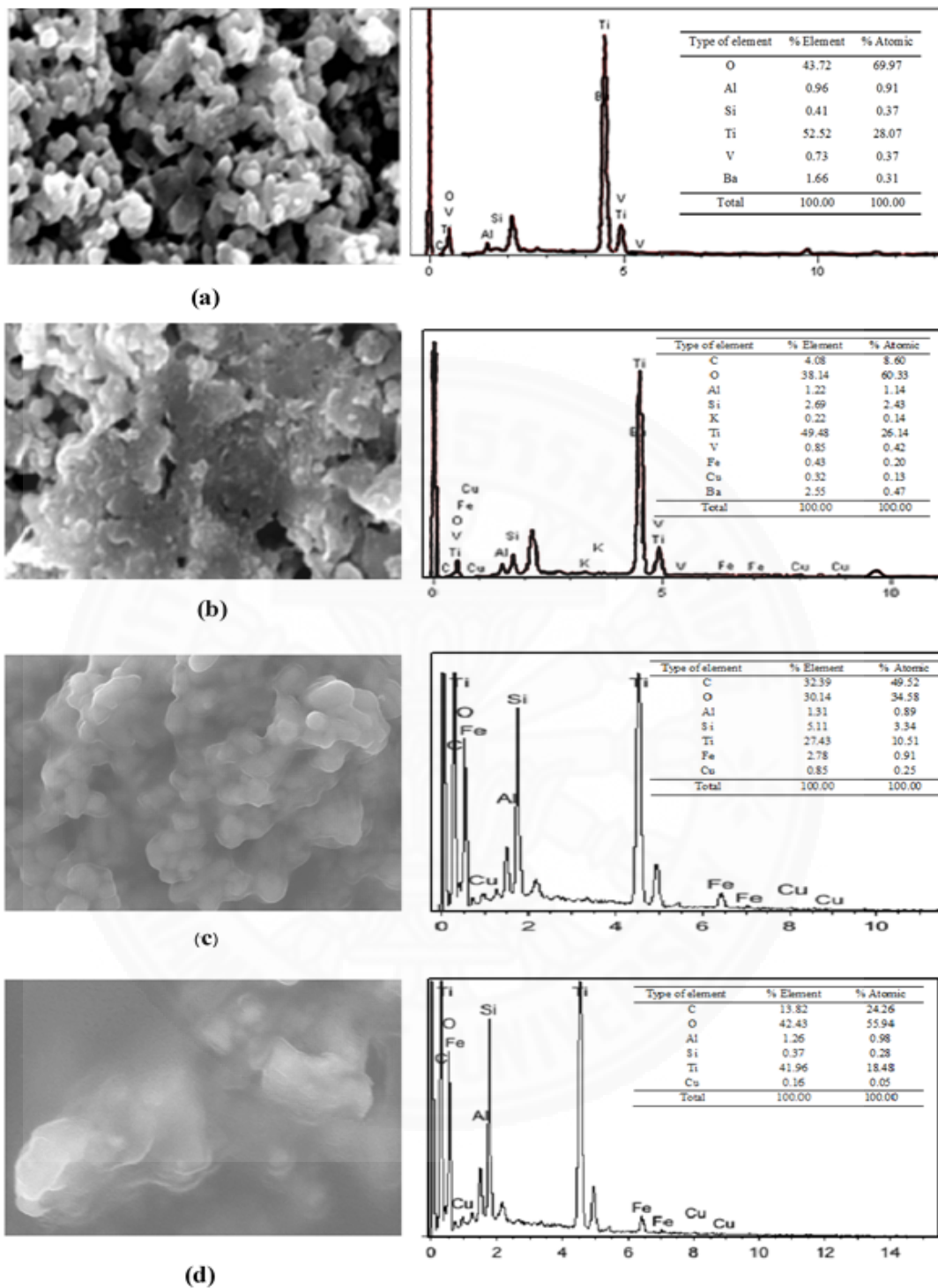


Figure 4.29 SEM images of ceramic membrane surface coated with different adsorbents after Cu(II) adsorption at 15,000X, and EDS analysis: (a) CM, (b) CMCN, (c) CMCN-GLA, and (d) CMCN-PEG

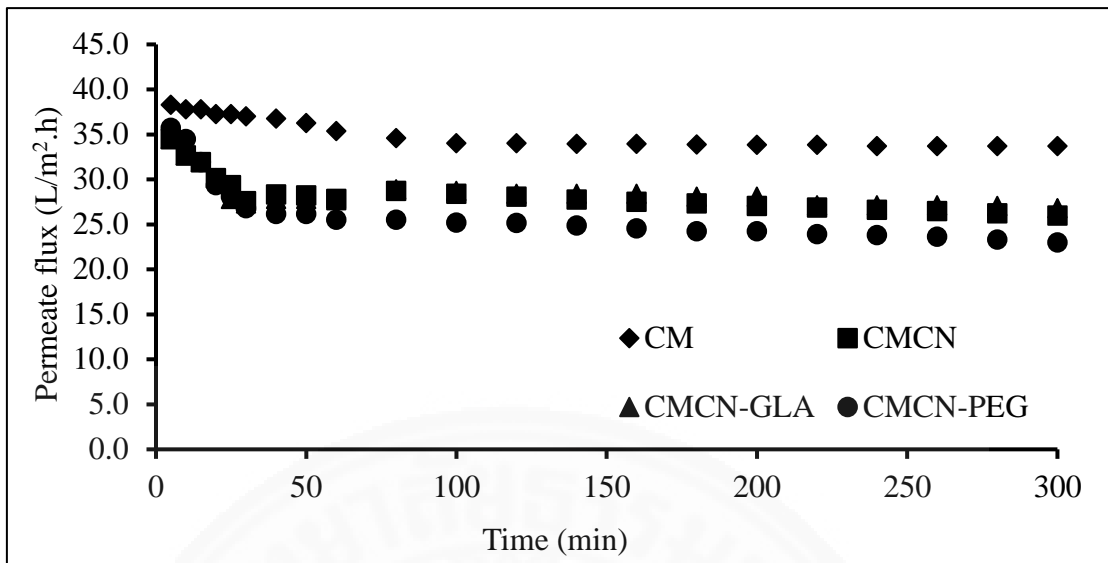
rapid decline of flux occurred during the first 60 min and slowly decreased thereafter until 100 min, then relatively stabilized toward the end of the experiment at 300 min. This initial decrease in flux may be due to the swelling of chitosan, resulting in a reduced pore size and decreased flux from the initial values. After 100 min, a slight decrease in flux may be caused by membrane fouling and compaction. CMCN-PEG has the lowest permeate flux, which may be associated with a film-like morphology on the surface and the hydrophilicity of the PEG, causing large film swelling and reduced pore size [212]. The use of the hydrophilic polymer PEG, may therefore, offer good filtration, but with more resistance to flow. As reported by Jana et al [162], a slow decrease of flux may be due to a thicker chitosan layer on the membrane surface, concentration polarization, and membrane fouling.

4.7.3 Breakthrough curves

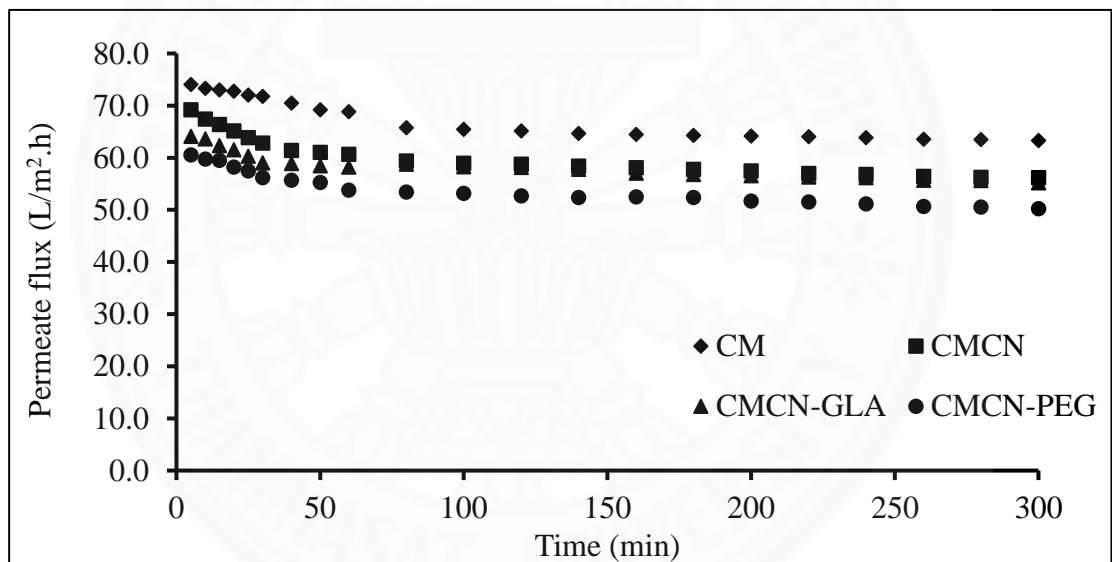
The profile and slope of the breakthrough curves as indicated in Figure 4.31 shows slight differences for the adsorbents. The CMCN-PEG saturated earlier than other adsorbents. The breakthrough times of all adsorbents decreased with an increase in flow rate. At a high flow rate, Cu(II) solution leaves the membrane before equilibrium occurs. There is insufficient contact time for Cu(II) adsorption, leading to a poor removal efficiency and uptake capacity [149, 223, 224]. This mechanism can be attributed to the fact that earlier saturation leads to a shorter breakthrough time [15]. The results indicate that there was an overflow of the adsorbate in the membrane at a flow rate exceeding 5.0 mL/min. The CMCN-GLA took a longer time to approach saturation. This result indicates that the sorption occurred mainly on the adsorbent surface.

4.7.4 Kinetic models

The kinetics study shows the adsorption capacity of Cu(II) onto several adsorbents coated ceramic membranes, which is described by the Thomas model. The R^2 values are in a range of 0.920-0.990 and 0.880-0.972, at flow rates of 2.5 and 5.0 mL/min, respectively. The coefficient of determination and model parameters are presented in Table 4.12 with variation of adsorbents and flow rates. Noticeably, an increase of flow rate from 2.5 to 5.0 mL/min led to a reduction of adsorption capacity



(a)

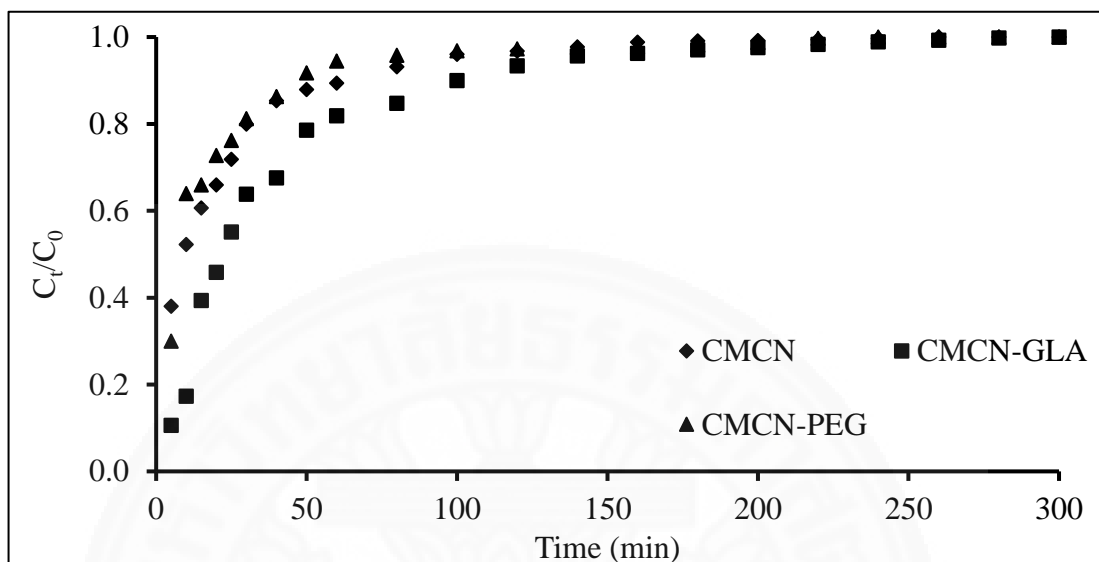


(b)

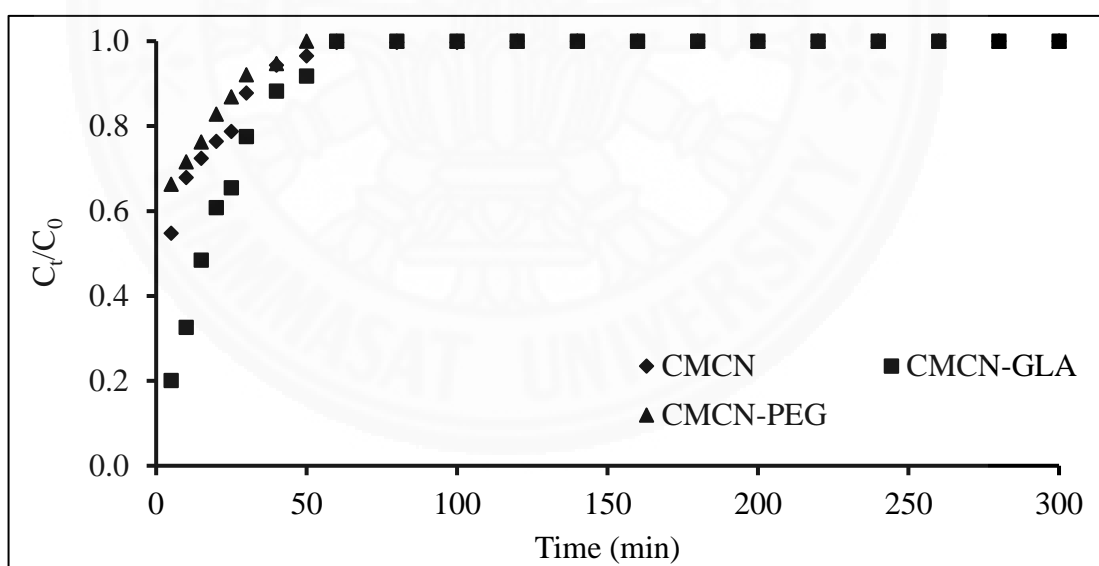
Figure 4.30 The permeate flux of various adsorbents at
 (a) 2.5 mL/min and (b) 5.0 mL/min
 (at Cu (II) initial concentration 50 mg/L, adsorbent dose 20 mg, pH 5, and
 room temperature)

for all adsorbents. Although the Thomas model fits well all experimental types and flow rates, good prediction of adsorption capacity occurred only for CMCN and CMCN-GLA, at a low flow rate of 2.5 mL/min. The great discrepancy between the predicted and actual adsorption capacity for other adsorbents was probably due to a high

superficial velocity. For the CMCN-PEG, a poor prediction may be associated with its solubility, which results in a detachment of adsorbent on the supported membrane.



(a)



(b)

Figure 4.31 The breakthrough curves for various adsorbents at (a) 2.5 mL/min and (b) 5.0 mL/min (at Cu (II) initial concentration 50 mg/L, adsorbent dose 20 mg, pH 5, and room temperature)

Table 4.12 Characteristic parameters of Thomas model for the adsorption of Cu(II) onto several adsorbents

Adsorbent type	Flow rate (mL/min)	q_{ex} (mg/g)	k_{Th} (mL/mg·min)	$q_{0,Th}$ (mg/g)	R^2
CMCN		181.95	0.00054	184.73	0.920
CMCN-GLA	2.5	240.28	0.00053	264.96	0.990
CMCN-PEG		100.71	0.00048	179.92	0.986
CMCN		159.20	0.00220	93.61	0.972
CMCN-GLA	5.0	222.05	0.00190	183.56	0.923
CMCN-PEG		83.97	0.00170	45.92	0.880

4.7.5 Simulation of adsorption-filtration membrane for Cu(II) removal

From the experiment, CMCN- GLA provided the highest adsorption capacity for Cu(II). The kinetics study was described by the Thomas model. The R^2 values are 0.990 and 0.923 at flow rate of 2.5 and 5.0 mL/min, respectively. The mass balance of Cu(II) in the system was used for developing the equation which the schematic was displayed in Figure 4.32.

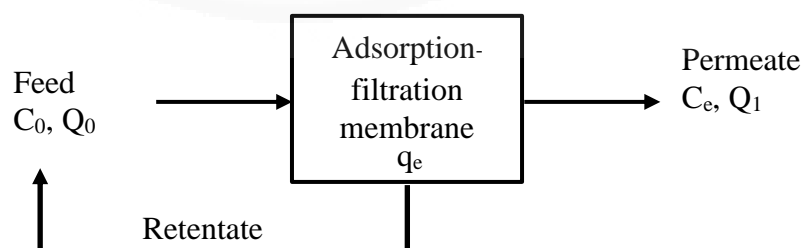


Figure 4.32 Schematic of adsorption-filtration membrane unit

For the adsorption-filtration membrane unit, the Cu(II) mass balance can be written as Equation (4.1)-(4.2).

$$Q_0C_0 - Q_1C_e = Mq_e \quad \text{Equation (4.1)}$$

When $Q_0 = Q_1$ is considered ($Q_0 = Q_1 = Q$)

$$Q(C_0 - C_e) = Mq_e \quad \text{Equation (4.2)}$$

where C_0 and C_e is the initial and equilibrium concentration (mg/L), M is mass of adsorbent (mg), q_e is adsorption capacity from the Thomas model (mg/g) and Q_0 and Q_1 are the feed and permeate volume, respectively.

In order to apply the adsorption-filtration membrane for Cu(II) removal, the surface area of membrane for CMCN-GLA deposition was developed as Equation (4.3).

$$A = \frac{kM}{m} \quad \text{Equation (4.3)}$$

A is active surface area of membrane, k is the surface area of the membrane from experiment (0.0047 m^2) and m is the mass of CN from experiment (11.19 mg).

According to Equation (4.3), the design of membrane unit was calculated by using CMCN-GLA. The values of Q , C_0 , and C_e are given which C_e value follows the industrial effluent standards of Cu(II) in Thailand not more than 2.0 mg/L . At 2.5 mL/min , the results present the amount of adsorbent on the membrane surface and surface area of membrane 90.6 g and 35.8 m^2 , respectively with 500 L and 50 mg/L of volume and initial concentration of Cu(II), respectively. As initial concentration of Cu(II) increased, the surface area of membrane also increased (Table 4.13). The expected amount of adsorbent based on experimental data can use for wastewater treatment plant design to obey with the industrial effluent standards of Thailand. However, the results can be useful for further applications of tertiary wastewater treatment system design at low concentration of Cu(II) from industrial effluents prior to their discharge.

4.7.6 Summary

A new hybrid nanosorption/ceramic microfiltration membrane offers an alternative and efficient means for Cu(II) removal. The ceramic membrane coated CN, crosslinked with GLA, showed the highest adsorption capacity of 240.3 mg/g, at the flow rate 2.5 mL/min. The breakthrough curves were dependent on flow rate and illustrated good performance for CMCN-GLA. The experimental data correlated well with the Thomas model. The membrane parameters can be used for the design of treatment systems to remove Cu(II) from wastewater. Desorption studies showed the operation can be repeated up to at least three cycles of adsorption-desorption for CMCN, CMCN-GLA, and CMCN-PEG. This limitation may be overcome by application of membrane re-coat using more durable coating techniques such as those involving chemical bonding between the CN and the supporting membrane. The system also works well for treatment of low concentration of Cu(II) and may thus find suitable applications in the design for tertiary wastewater treatment system.

Table 4.13 The estimated amount of mass adsorbent at various scenarios based on experimental data

Scenarios	Flow rate (mL/min)	Q (L)	C ₀ (mg/L)	C _e (mg/L)	q _e (mg/g)	M (g)	Surface area of membrane (m ²)
1			50.0		264.96	90.6	35.8
2	2.5	500	10.0	2.0	264.96	15.1	6.0
3			5.0		264.96	5.7	2.2
4			50		183.56	130.7	51.6
5	5.0	500	10	2.0	183.56	21.8	8.6
6			5		183.56	8.2	3.2

Chapter 5

Conclusions and Recommendations

5.1 Conclusions

The main objective of this study was to develop the effective treatment methodology for the removal of heavy metal from synthetic wastewater. In this study, it was found that simultaneous filtration and adsorption by coating modified chitosan nanoparticles on ceramic microfiltration membrane had high efficiency to remove heavy metal from synthetic wastewater. The conditions applied in the simultaneous filtration and adsorption process are based on optimum conditions from adsorption process in batch and fixed column system. Based on the results of this study, the conclusions were summarized as follows:

5.1.1 CN was prepared by TPP cross-linking. The dry sizes of nanochitosan were in the range of 23- 26 nm based on atomic force microscope examination. The sizes can be controlled by varying the concentration of the chitosan/reagents used.

5.1.2 The surface morphology of supporting material showed the significant changes on the surface from a coarse to smooth uniform surface of film-like morphology. The film became thicker and smoother as the CN loading increased. FTIR spectra showed no interaction between CN and supporting material. There is no additional peak in the spectra related to CN. The EDS composition before and after heavy metal adsorption provides the direct evidence for heavy metal adsorption by adsorbent. The efficiency of removal was tested by three different heavy metals which are Cr(VI), Cu(II), and Ni(II).

5.1.3 The CN-coated AC demonstrated an increase in Cr(VI) removal efficiency. The adsorption capacity of the CN-coated AC (77.52 mg/g) was more than twice that of the uncoated AC (36.36 mg/g), or pure chitosan (32.57 mg/g). The adsorption isotherms are better described using the Freundlich rather than the Langmuir model and are in agreement with the heterogeneity of the surfaces. Adsorption kinetics

followed that of the pseudo-second-order kinetics, suggesting chemisorption as a rate limiting step.

5.1.4 CN coated on alumina balls (CN-CB) were used for Cu(II) removal using a fixed-bed column. The adsorption capacity increased with an increase of initial concentration, but decreased with increase of flow rate and CN loading. The adsorption capacity was 187.4 mg/g with the initial concentration 30 mg/L, flow rate 2.5 mL/min and CN loading 25 mg. The Thomas and Yoon-Nelson models were both successfully used to predict the breakthrough curves, indicating that CN coated alumina balls are suitable for a columnar design.

5.1.5 CN-CB were investigated for the Cr(VI) removal. The maximum Cr(VI) adsorption capacity according to this model is 25.97 mg/g in batch mode. In the continuous fixed-bed column experiment, the adsorption capacity was 55.72 mg/g. The exhaustion times and breakthrough curves were reached, when the initial concentration and flow rate were increased. The Cr(VI) removal efficiency decreases with the increase in the flow rate but increased with an increase of initial concentration. A comparison of the results of the batch with column systems showed that continuous fixed-bed column exhibited greater adsorption capacity than batch system for Cr(VI) removal.

5.1.6 CN was introduced onto the ceramic membrane. These coated membranes were then tested for Ni(II) removal at various flow rates. At constant flow rate of 2.5 mL/min and 10, 15 and 20 mg chitosan loadings, the amount of Ni(II) removed were 89.0, 85.1, and 74.2 mg/g chitosan, respectively. When the flow rate was doubled, the amount of Ni(II) removed became 123.0, 113.8, and 100.6 mg/g chitosan, respectively. The amount of Ni(II) removed increased with an increase in flow rate due to larger flow, but decreased with an increase in the amount of chitosan loading, indicating that the adsorption takes place mainly on the surface of chitosan film which, in turn, is controlled by surface area of the membrane. The adsorption kinetics can be well described using the Thomas model.

5.1.7 The Cu(II) removal was investigated using simultaneous filtration and adsorption by coating modified nanochitosan on ceramic microfiltration membrane. CMCN-GLA provided the highest adsorption capacity of 240.3 mg/g at a flow rate of 2.5 mL/min. It is greater than a 30% improvement of adsorption capacity,

as compared to native nanochitosan. This is about 2.4 times higher, as compared to a previous study on simultaneous adsorption-filtration method. The experimental data was found to fit well with the Thomas model.

5.2 Recommendations

5.2.1 The membrane filtration system should be tested with the suspension adsorbent of nanochitosan coated on bituminous activated carbon

5.2.2 The study is necessary to investigate the removal efficiency for heavy metal from actual wastewater and to explore the membrane fouling and compaction between the ceramic membrane and various adsorbents.

5.2.3 This study results should be used in order to design and control for large scale heavy metals of industrial wastewater.

5.2.4 The study of removal efficiency is required for the combined metals with different conditions such as type of metal, pH, concentration and flow rate.

5.2.5 Economical study is needed in order to compare with existing technologies for wastewater treatment.

References

- [1] J.S. Kim, S. Akeprathumchai, S.R. Wickramasinghe, Flocculation to enhance microfiltration, *J. Membr. Sci.*, 182 (2001) 161-172.
- [2] H.A. Qdais, H. Moussa, Removal of heavy metals from wastewater by membrane processes: A comparative study, *Desalination*, 164 (2004) 105-110.
- [3] S. Jana, M.K. Purkait, K. Mohanty, Preparation and characterization of low-cost ceramic microfiltration membranes for the removal of chromate from aqueous solutions, *Appl. Clay Sci.*, 47 (2010) 317-324.
- [4] C. Yuwei, W. Jianlong, Preparation and characterization of magnetic chitosan nanoparticles and its application for Cu(II) removal, *Chem. Eng. J. (Lausanne)*, 168 (2011) 286-292.
- [5] V.M. Boddu, K. Abburi, J.L. Talbott, E.D. Smith, Removal of hexavalent chromium from wastewater using a new composite chitosan biosorbent, *Environ. Sci. Technol.*, 37 (2003) 4449-4456.
- [6] T. Panayotova, M. Dimova Todorova, I. Dobrevsky, Purification and reuse of heavy metals containing wastewaters from electroplating plants, *Desalination*, 206 (2007) 135-140.
- [7] Z. Wang, G. Liu, Z. Fan, X. Yang, J. Wang, S. Wang, Experimental study on treatment of electroplating wastewater by nanofiltration, *J. Membr. Sci.*, 305 (2007) 185-195.
- [8] M. Owlad, M.K. Aroua, W.A.W. Daud, S. Baroutian, Removal of hexavalent chromium-contaminated water and wastewater: A review, *Water, Air, Soil Pollut.*, 200 (2008) 59-77.
- [9] P. Suksabye, P. Thiravetyan, W. Nakbanpote, Column study of chromium(VI) adsorption from electroplating industry by coconut coir pith, *J. Hazard. Mater.*, 160 (2008) 56-62.
- [10] F. Fu, Q. Wang, Removal of heavy metal ions from wastewaters: A review, *J. Environ. Manage.*, 92 (2011) 407-418.
- [11] C.P. Athanasekou, S.K. Papageorgiou, V. Kaselouri, F.K. Katsaros, N.K. Kakizis, A. A. Sपालidis, N. K. Kanellopoulos, Development of hybrid

- alginate/ceramic membranes for Cd²⁺ removal, *Microporous Mesoporous Mater.*, 120 (2009) 154-164.
- [12] P.A. Kumar, S. Chakraborty, Fixed-bed column study for hexavalent chromium removal and recovery by short-chain polyaniline synthesized on jute fiber, *J. Hazard. Mater.*, 162 (2009) 1086-1098.
- [13] V.K. Gupta, A. Rastogi, A. Nayak, Adsorption studies on the removal of hexavalent chromium from aqueous solution using a low cost fertilizer industry waste material, *J. Colloid Interface Sci.*, 342 (2010) 135-141.
- [14] M.L.P. Dalida, A.F.V. Mariano, C.M. Futralan, C.-C. Kan, W.-C. Tsai, M.-W. Wan, Adsorptive removal of Cu(II) from aqueous solutions using non-crosslinked and crosslinked chitosan-coated bentonite beads, *Desalination*, 275 (2011) 154-159.
- [15] S. Chen, Q. Yue, B. Gao, Q. Li, X. Xu, K. Fu, Adsorption of hexavalent chromium from aqueous solution by modified corn stalk: A fixed-bed column study, *Bioresour. Technol.*, 113 (2012) 114-120.
- [16] R. Schmuhl, H. Krieg, K. Keizer, Adsorption of Cu(II) and Cr(VI) ions by chitosan: Kinetics and equilibrium studies, *Water SA*, 27 (2001) 1-8.
- [17] L. Monser, N. Adhoum, Modified activated carbon for the removal of copper, zinc, chromium and cyanide from wastewater, *Sep. Purif. Technol.*, 26 (2002) 137-146.
- [18] R.S. Juang, H.J. Shao, A simplified equilibrium model for sorption of heavy metal ions from aqueous solutions on chitosan, *Water Res.*, 36 (2002) 2999-3008.
- [19] S.R. Popuri, Y. Vijaya, V.M. Boddu, K. Abburi, Adsorptive removal of copper and nickel ions from water using chitosan coated PVC beads, *Bioresour. Technol.*, 100 (2009) 194-199.
- [20] Y.T. Zhou, H.L. Nie, C. Branford White, Z.Y. He, L.M. Zhu, Removal of Cu²⁺ from aqueous solution by chitosan-coated magnetic nanoparticles modified with α -ketoglutaric acid, *J. Colloid Interface Sci.*, 330 (2009) 29-37.
- [21] G. Crini, Non-conventional low-cost adsorbents for dye removal: A review, *Bioresour. Technol.*, 97 (2006) 1061-1085.

- [22] M. Dakiky, M. Khamis, A. Manassra, M. Mer'eb, Selective adsorption of chromium(VI) in industrial wastewater using low-cost abundantly available adsorbents, *Adv. Environ. Res.*, 6 (2002) 533-540.
- [23] S.S. Baral, S.N. Das, P. Rath, Hexavalent chromium removal from aqueous solution by adsorption on treated sawdust, *Biochem. Eng. J.*, 31 (2006) 216-222.
- [24] A.K. Bhattacharya, T.K. Naiya, S.N. Mandal, S.K. Das, Adsorption, kinetics and equilibrium studies on removal of Cr(VI) from aqueous solutions using different low-cost adsorbents, *Chem. Eng. J. (Lausanne)*, 137 (2008) 529-541.
- [25] M.N.V. Ravi Kumar, A review of chitin and chitosan applications, *React. Funct. Polym.*, 46 (2000) 1-27.
- [26] W. Tan, Y. Zhang, Y. S. Szeto, L. Liao, A novel method to prepare chitosan/montmorillonite nanocomposites in the presence of hydroxy-aluminum oligomeric cations, *Compos. Sci. Technol.*, 68 (2008) 2917-2921.
- [27] F.C. Wu, R.L. Tseng, R.S. Juang, A review and experimental verification of using chitosan and its derivatives as adsorbents for selected heavy metals, *J. Environ. Manage.*, 91 (2010) 798-806.
- [28] T.F. Lin, J.K. Wu, Adsorption of Arsenite and Arsenate within Activated Alumina Grains: Equilibrium and Kinetics, *Water Res.*, 35 (2001) 2049-2057.
- [29] B. Daus, R. Wennrich, H. Weiss, Sorption materials for arsenic removal from water: A comparative study, *Water Res.*, 38 (2004) 2948-2954.
- [30] S. Babel, T.A. Kurniawan, Low-cost adsorbents for heavy metals uptake from contaminated water: A review, *J. Hazard. Mater.*, 97 (2003) 219-243.
- [31] K.V. Harish Prashanth, R.N. Tharanathan, Chitin/chitosan: modifications and their unlimited application potential-An overview, *Trends Food Sci. Technol.*, 18 (2007) 117-131.
- [32] N.M. Alves, J.F. Mano, Chitosan derivatives obtained by chemical modifications for biomedical and environmental applications, *Int. J. Biol. Macromol.*, 43 (2008) 401-414.
- [33] M. Kong, X.G. Chen, K. Xing, H.J. Park, Antimicrobial properties of chitosan and mode of action: A state of the art review, *Int. J. Food Microbiol.*, 144 (2010) 51-63.

- [34] Z.X. Tang, J.Q. Qian, A.E. Shi, Preparation of chitosan nanoparticles as carrier for immobilized enzyme, *Appl. Biochem. Biotechnol.*, 136 (2007) 77-96.
- [35] Y.B. Onundi, A.A. Mamun, M.F.A. Khatib, M.A.A. Saadi, A.M. Suleyman, Heavy metals removal from synthetic wastewater by a novel nano-size composite adsorbent, *Int. J. Environ. Sci. Technol.*, 8 (2011) 799-806.
- [36] J.A. Suarez, J.M. Veza, Dead-end microfiltration as advanced treatment for wastewater, *Desalination*, 127 (2000) 47-58.
- [37] J. Landaburu Aguirre, V. García, E. Pongrácz, R. Keiski, Applicability of membrane technologies for the removal of heavy metals, *Desalination*, 200 (2006) 272-273.
- [38] M.A. Barakat, New trends in removing heavy metals from industrial wastewater, *Arabian J.Chem.*, 4 (2011) 361-377.
- [39] J. Dong, F. Wu, R. Huang, G. Zang, A chromium-tolerant plant growing in Cr-contaminated land, *Int. J. Phytorem.*, 9 (2007) 167-179.
- [40] S. Madala, S.K. Nadavala, S. Vudagandla, V.M. Boddu, K. Abburi, Equilibrium, kinetics and thermodynamics of cadmium(II) biosorption on to composite chitosan biosorbent, *Arabian J.Chem*, in press (2013) 1-11.
- [41] P. Miretzky, A.F. Cirelli, Hg(II) removal from water by chitosan and chitosan derivatives: A review, *J. Hazard. Mater.*, 167 (2009) 10-23.
- [42] Q. Liu, Y. Bei, F. Zhou, Removal of lead(II) from aqueous solution with amino-functionalized nanoscale zero-valent iron, *Cent. Eur.J. Chem.*, 7 (2008) 79-82.
- [43] C.M. Simonescu, M. Ferdes, Fungal biomass for Cu(II) uptake from aqueous system, *Pol. J. Environ. Stud.*, 21 (2012) 1831-1839.
- [44] Y. Ku, I.L. Jung, Photocatalytic reduction of Cr(VI) in aqueous solutions by UV irradiation with the presence of titanium dioxide, *Water Res.*, 35 (2001) 135-142.
- [45] Q.Y. Chen, Z. Luo, C. Hills, G. Xue, M. Tyrer, Precipitation of heavy metals from wastewater using simulated flue gas: sequent additions of fly ash, lime and carbon dioxide., *Water Res.*, 43 (2009) 2605-2614.
- [46] D. Fang, R. Zhang, W. Deng, J. Li, Highly efficient removal of Cu(II), Zn(II), Ni(II) and Fe(II) from electroplating wastewater using sulphide from sulphidogenic bioreactor effluent, *Environ. Technol.*, 33 (2012) 1709-1715.

- [47] L. Semerjian, G.M. Ayoub, High- pH-magnesium coagulation-flocculation in wastewater treatment, *Adv. Environ. Res.*, 7 (2003) 389-403.
- [48] I. Licskó, Realistic coagulation mechanisms in the use of aluminium and iron(III) salts, *Water Sci. Technol.*, 36 (1997) 103-110.
- [49] L.K. Wang, D.A. Vaccaari, Y.Li, N.K. Shammass (2004), Chemical precipitation, In: Wang, L.K., Hung, Y.T. and Shammass, N.K., Eds., *Physicochemical Treatment Processes*, Vol. 3, Humana Press; 2004. 141-198.
- [50] A. Dąbrowski, Z. Hubicki, P. Podkościelny, E. Robens, Selective removal of the heavy metal ions from waters and industrial wastewaters by ion- exchange method, *Chemosphere*, 56 (2004) 91-106.
- [51] S. Y. Kang, J. U. Lee, S. H. Moon, K. W. Kim, Competitive adsorption characteristics of Co^{2+} , Ni^{2+} , and Cr^{3+} by IRN-77 cation exchange resin in synthesized wastewater, *Chemosphere*, 56 (2004) 141-147.
- [52] T.A. Kurniawan, G.Y.S. Chan, W.H. Lo, S. Babel, Physico-chemical treatment techniques for wastewater laden with heavy metals, *Chem. Eng. J. (Lausanne)*, 118 (2006) 83-98.
- [53] M. Cerna, Use of solvent extraction for the removal of heavy metals from liquid wastes, *Environ. Monit. Assess.*, 34 (1995) 151-162.
- [54] B. R. Reddy, D.N. Priya, J.R. Kumar, Solvent extraction of cadmium (II) from sulphate solutions using TOPS 99, PC 88A, Cyanex 272 and their mixtures, *Hydrometallurgy*, 74 (2004) 277-283.
- [55] B. R. Reddy, D.N. Priya, J. R. Kumar, Solvent extraction and separation of Cd(II), Ni(II) and Co(II) from chloride leach liquors of spent Ni–Cd batteries using commercial organo-phosphorus extractants, *Hydrometallurgy*, 77 (2005) 253-261.
- [56] T.K. Tran, H.J. Leu, K.F. Chiu, C. Y. Lin, Electrochemical treatment for wastewater contained heavy metal the removing of the COD and heavy metal ions, *Int. J. Eng. Res. Sci.*, 1 (2015) 96-101.
- [57] G. Chen, Electrochemical technologies in wastewater treatment, *Sep. Purif. Technol.*, 38 (2004) 11-41.
- [58] X. Chen, G. Huang, J. Wang, Electrochemical reduction/oxidation in the treatment of Heavy metal wastewater, *J. Metall. Eng.*, 2 (2013) 161-164.

- [59] X.Z. Yuan, Y. T. Meng, G.M. Zeng, Y. Y. Fang, J.G. Shi, Evaluation of tea-derived biosurfactant on removing heavy metal ions from dilute wastewater by ion flotation, *Colloids Surf., A.*, 317 (2008) 256-261.
- [60] H. Polat, D. Erdogan, Heavy metal removal from waste waters by ion flotation, *J. Hazard. Mater.*, 148 (2007) 267-273.
- [61] A.A. Mohammed, S.E. Ebrahim, A.I. Alwared, Flotation and sorptive-flotation methods for removal of lead ions from wastewater using SDS as surfactant and barley husk as biosorbent, *J. Chem.*, 2013 (2013) 1-7.
- [62] G. Crini, Recent developments in polysaccharide-based materials used as adsorbents in wastewater treatment, *Prog. Polym. Sci.*, 30 (2005) 38-70.
- [63] M. Ruiz, A.M. Sastre, E. Guibal, Palladium sorption on glutaraldehyde-crosslinked chitosan, *React. Funct. Polym.*, 45 (2000) 155-173.
- [64] E. Samper, M. Rodríguez, M.A. De la Rubia, D. Prats, Removal of metal ions at low concentration by micellar-enhanced ultrafiltration (MEUF) using sodium dodecyl sulfate (SDS) and linear alkylbenzene sulfonate (LAS), *Sep. Purif. Technol.*, 65 (2009) 337-342.
- [65] M. Mohsen Nia, P. Montazeri, H. Modarress, Removal of Cu^{2+} and Ni^{2+} from wastewater with a chelating agent and reverse osmosis processes, *Desalination*, 217 (2007) 276-281.
- [66] L. Zhang, Y. Wu, X. Qu, Z. Li, J. Ni, Mechanism of combination membrane and electro-winning process on treatment and remediation of Cu^{2+} polluted water body, *J. Environ. Sci.*, 21 (2009) 764-769.
- [67] J. Tanninen, M. Mänttari, M. Nyström, Nanofiltration of concentrated acidic copper sulphate solutions, *Desalination*, 189 (2006) 92-96.
- [68] L. Cifuentes, I. García, P. Arriagada, J.M. Casas, The use of electrodialysis for metal separation and water recovery from $\text{CuSO}_4\text{-H}_2\text{SO}_4\text{-Fe}$ solutions, *Sep. Purif. Technol.*, 68 (2009) 105-108.
- [69] Y.C. Sharma, Cr(VI) removal from industrial effluents by adsorption on an indigenous low-cost material, *Colloids Surf., A*, 215 (2003) 155-162.
- [70] M. Kobya, Removal of Cr(VI) from aqueous solutions by adsorption onto hazelnut shell activated carbon: Kinetic and equilibrium studies, *Bioresour. Technol.*, 91 (2004) 317-321.

- [71] E. Guibal, Interactions of metal ions with chitosan-based sorbents: A review, *Sep. Purif. Technol.*, 38 (2004) 43-74.
- [72] R.F. Tabor, J. Eastoe, P.J. Dowding, A two-step model for surfactant adsorption at solid surfaces, *J. Colloid Interface Sci.*, 346 (2010) 424-428.
- [73] S.N.A. Abas, M.H.S. Ismail, M.L.K. a.S. Izhar, Adsorption process of heavy metals by low-cost adsorbent: A review, *World Appl Sci J.*, 28 (2013) 1518-1530.
- [74] G.P. Rao, C. Lu, F. Su, Sorption of divalent metal ions from aqueous solution by carbon nanotubes: A review, *Sep. Purif. Technol.*, 58 (2007) 224-231.
- [75] P. Yin, Q. Xu, R. Qu, G. Zhao, Removal of transition metal ions from aqueous solutions by adsorption onto a novel silica gel matrix composite adsorbent, *J. Hazard. Mater.*, 169 (2009) 228-232.
- [76] S. Zhu, N. Yang, D. Zhang, Poly(N,N-dimethylaminoethyl methacrylate) modification of activated carbon for copper ions removal, *Mater. Chem. Phys.*, 113 (2009) 784-789.
- [77] S.E. Bailey, T.J. Olin, R.M. Bricka, D.D. Adrian, A review of potentially low-cost sorbents for heavy metals, *Water Res.*, 33 (1999) 2469-2479.
- [78] L. Lorenzen, J.S.J. van Deventer, W.M. Landi, Factors affecting the mechanism of the adsorption of arsenic species on activated carbon, *Miner. Eng.*, 8 (1995) 557-569.
- [79] A.J. Varma, S.V. Deshpande, J.F. Kennedy, Metal complexation by chitosan and its derivatives: a review, *Carbohydr. Polym.*, 55 (2004) 77-93.
- [80] J.C.Y. Ng, W.H. Cheung, G. McKay, Equilibrium studies of the sorption of Cu(II) ions onto chitosan, *J. Colloid Interface Sci.*, 255 (2002) 64-74.
- [81] F.C. Wu, R.L. Tseng, R.S. Juang, Enhanced abilities of highly swollen chitosan beads for color removal and tyrosinase immobilization, *J. Hazard. Mater.*, 81 (2001) 167-177.
- [82] E.P. Kuncoro, J. Roussy, E. Guibal, Mercury recovery by polymer-enhanced ultrafiltration: comparison of chitosan and poly(Ethylenimine) used as macroligand, *Sep. Sci. Technol.*, 40 (2005) 659-684.

- [83] W.S. Wan Ngah, A. Kamari, Y.J. Koay, Equilibrium and kinetics studies of adsorption of copper (II) on chitosan and chitosan/PVA beads, *Int. J. Biol. Macromol.*, 34 (2004) 155-161.
- [84] J.D. Merrifield, Synthesis and characterization of thiol grafted chitosan beads for mercury removal [master's thesis]. The University of Maine, 2002. 101 p.
- [85] R.A. Gil, S. Cerutti, J.A. Gásquez, R.A. Olsina, L.D. Martinez, Preconcentration and speciation of chromium in drinking water samples by coupling of on-line sorption on activated carbon to ETAAS determination, *Talanta*, 68 (2006) 1065-1070.
- [86] T. Y. Hsien, G.L. Rorrera, Effects of acylation and crosslinking on the material properties and cadmium ion adsorption capacity of porous chitosan beads, *Sep. Sci. Technol.*, 30 (1995) 2455–2475.
- [87] L. Jin, R. Bai, Mechanisms of lead adsorption on chitosan/PVA hydrogel beads, *Langmuir*, 18 (2002) 9765–9770.
- [88] I.M.N. Vold, K.M. Vårum, E. Guibal, O. Smidsrød, Binding of ions to chitosan-selectivity studies, *Carbohydr. Polym.*, 54 (2003) 471-477.
- [89] H.S. Kas, Chitosan: Properties, preparations and application to microparticulate systems, *J. Microencapsulation*, 14 (1997) 689-711.
- [90] V. Mohanasrinivasan, M. Mishra, J.S. Paliwal, S.K. Singh, E. Selvarajan, V. Suganthi, C. Subathra Devi, Studies on heavy metal removal efficiency and antibacterial activity of chitosan prepared from shrimp shell waste, *Biotech*, 4 (2014) 167-175.
- [91] S.M. Nomanbhay, K. Palanisamy, Removal of heavy metal from industrial wastewater using chitosan coated oil palm shell charcoal *J. Biotechnol.*, 8 (2005) 43-53.
- [92] R. Ramya, P. Sankar, S. Anbalagan, P.N. Sudha, Adsorption of Cu(II) and Ni(II) ions from metal solution using crosslinked chitosan-g-acrylonitrile copolymer, *International Int. J. Environ. Sci.*, 1 (2011) 13-23.
- [93] K. Vijayalakshmi, T. Gomathi, S. Latha, T. Hajeeth, P.N. Sudha, Removal of copper(II) from aqueous solution using nanochitosan/ sodium alginate/microcrystalline cellulose beads, *Int. J. Biol. Macromol.*, 82 (2016) 440-452.

- [94] K. Swayampakula, V. M. Boddu, S. K. Nadavala, K. Abburi, Competitive adsorption of Cu (II), Co (II) and Ni (II) from their binary and tertiary aqueous solutions using chitosan-coated perlite beads as biosorbent, *J. Hazard. Mater.*, 170 (2009) 680-689.
- [95] S. Kalyani, J.A. Priya, P.S. Rao, A. Krishnaiah, Removal of copper and nickel from aqueous solutions using chitosan coated on perlite as biosorbent, *Sep. Sci. Technol.*, 40 (2005) 1483-1495.
- [96] W. X. Zhang, Nanoscale iron particles for environmental remediation: An overview, *J. Nanopart. Res.*, 5 (2003) 323-332.
- [97] T. Tuutijärvi, J. Lu, M. Sillanpää, G. Chen, As(V) adsorption on maghemite nanoparticles, *J. Hazard. Mater.*, 166 (2009) 1415-1420.
- [98] P.G. Tratnyek, R.L. Johnson, Nanotechnologies for environmental cleanup, *Nano Today*, 1 (2006) 44-48.
- [99] J. Hu, I.M. Lo, G. Chen, Fast removal and recovery of Cr(VI) using surface-modified jacobsite ($MnFe_2O_4$) nanoparticles, *Langmuir*, 21 (2005) 11173-11179.
- [100] C. Govindarajan, S. Ramasubramaniam, T. Gomathi, A. Narmadha Devi, P.N. Sudha, Sorption studies of Cr (VI) from aqueous solution using nanochitosan-carboxymethyl cellulose blend, *Arch. Appl. Sci.Res.*, 3 (2011) 127-138.
- [101] K. Kurita, Controlled functionalization of the polysaccharide chitin, *Prog. Polym. Sci.*, 26 (2001) 1921-1971.
- [102] Y.C. Chang, D.H. Chen, Preparation and adsorption properties of monodisperse chitosan-bound Fe_3O_4 magnetic nanoparticles for removal of Cu(II) ions, *J. Colloid Interface Sci.*, 283 (2005) 446-451.
- [103] A. Findona, G. McKaya, H.S. Blaira, Transport studies for the sorption of copper ions by chitosan, *J Environ. Sci. Heal. A.*, 28 (1993) 173–185.
- [104] C. Huang, Y.C. Chung, M.R. Liou, Adsorption of Cu(II) and Ni(II) by pelletized biopolymer, *J. Hazard. Mater.*, 45 (1996) 265-277.
- [105] R.B. da Silva, A.F. Lima Neto, L.S. Soares dos Santos, J.R. de Oliveira Lima, M.H. Chaves, J.R. dos Santos Jr, G.M. de Lima, E.M. de Moura, C.V.R. de Moura, Catalysts of Cu(II) and Co(II) ions adsorbed in chitosan used in transesterification of soy bean and babassu oils - A new route for biodiesel syntheses, *Bioresour. Technol.*, 99 (2008) 6793-6798.

- [106] J.F. Liu, Z.S. Zhao, G.B. Jiang, Coating Fe₃O₄ magnetic nanoparticles with humic acid for high efficient removal of heavy metals in water, *Environ. Sci. Technol.*, 48 (2008) 6949-6954.
- [107] Y.T. Zhou, C. Branford White, H.L. Nie, L.M. Zhu, Adsorption mechanism of Cu²⁺ from aqueous solution by chitosan-coated magnetic nanoparticles modified with α -ketoglutaric acid, *J. Colloid Interface Sci.*, 74 (2009) 244-252.
- [108] W.S. Wan Ngah, C.S. Endud, R. Mayanar, Removal of copper(II) ions from aqueous solution onto chitosan and cross-linked chitosan beads, *React. Funct. Polym.*, 50 (2002) 181-190.
- [109] A. Heidari, H. Younesi, Z. Mehraban, Removal of Ni(II), Cd(II), and Pb(II) from a ternary aqueous solution by amino functionalized mesoporous and nano mesoporous silica, *Chem. Eng. J. (Lausanne)*, 153 (2009) 70-79.
- [110] R. Qu, C. Sun, F. Ma, Y. Zhang, C. Ji, Q. Xu, C. Wang, H. Chen, Removal and recovery of Hg(II) from aqueous solution using chitosan-coated cotton fibers, *J. Hazard. Mater.*, 167 (2009) 717-727.
- [111] K. Inoue, K. Yoshizuka, K. Ohto, Adsorptive separation of some metal ions by complexing agent types of chemically modified chitosan, *Anal. Chim. Acta*, 388 (1999) 209-218.
- [112] B.J. McAfee, W.D. Gould, J.C. Nadeau, A.C.A.d. Costaa, Biosorption of metal ions using chitosan, chitin, and biomass of *Rhizopus Oryzae*, *Sep. Sci. Technol.*, 36 (2001) 3207-3222.
- [113] S.H. Huang, D.H. Chen, Rapid removal of heavy metal cations and anions from aqueous solutions by an amino-functionalized magnetic nano-adsorbent, *J. Hazard. Mater.*, 163 (2009) 174-179.
- [114] Y.M. Hao, C. Man, Z.B. Hu, Effective removal of Cu (II) ions from aqueous solution by amino-functionalized magnetic nanoparticles, *J. Hazard. Mater.*, 184 (2010) 392-399.
- [115] J. Wang, S. Zheng, Y. Shao, J. Liu, Z. Xu, D. Zhu, Amino-functionalized Fe₃O₄@SiO₂ core-shell magnetic nanomaterial as a novel adsorbent for aqueous heavy metals removal, *J. Colloid Interface Sci.*, 349 (2010) 293-299.

- [116] S. Tan, Y. Wang, C. Peng, Y. Tang, Synthesis and adsorption properties for metal ions of crosslinked chitosan acetate crown ethers, *J. Appl. Polym. Sci.*, 71 (1999) 2069-2074.
- [117] S. Keleşoğlu, Comparative adsorption studies of heavy metal ions on chitin and chitosan biopolymers [master's thesis]. Izmir Institute of Technology, 2007. 153 p.
- [118] Y. Qiu, Study on treatment technologies for perfluorochemicals in wastewater [dissertation]. Kyoto University, Kyoto University, 2007. 148 p.
- [119] A.R. Shetty, Metal anion removal from wastewater using chitosan in a polymer enhanced diafiltration system [master's thesis]. Worcester Polytechnic Institute, 2006. 86 p.
- [120] P. Sivakumar, P.N. Palanisamy, Packed bed column studies for the removal of acid blue 92 and basic red 29 using non-conventional adsorbent, *Indian J. Chem. Technol.*, 16 (2009) 301-307.
- [121] W. Cheung, J. Ng, G. McKay, Kinetic analysis of the sorption of copper(II) ions on chitosan, *J. Chem. Technol. Biotechnol.*, 78 (2003) 562-571.
- [122] G.P. Kumar, P.A. Kumar, S. Chakraborty, M. Ray, Uptake and desorption of copper ion using functionalized polymer coated silica gel in aqueous environment, *Sep. Purif. Technol.*, 57 (2007) 47-56.
- [123] S.H. Huang, D.H. Chen, Rapid removal of heavy metal cations and anions from aqueous solutions by an amino-functionalized magnetic nano-adsorbent, *J. Hazard. Mater.*, 163 (2009) 174-179.
- [124] D. Chen, W. Li, Y. Wu, Q. Zhu, Z. Lu, G. Du, Preparation and characterization of chitosan/montmorillonite magnetic microspheres and its application for the removal of Cr (VI), *Chem. Eng. J. (Lausanne)*, 221 (2013) 8-15.
- [125] W.S.W. Ngah, S. Fatinathan, Adsorption of Cu(II) ions in aqueous solution using chitosan beads, chitosan-GLA beads and chitosan-alginate beads, *Chem. Eng. J. (Lausanne)*, 143 (2008) 62-72.
- [126] B. Volesky, Detoxification of metal-bearing effluents: Biosorption for the next century, *Hydrometallurgy*, 59 (2001) 203-216.

- [127] S.S. Mark, T.C. Crusberg, C.M. Dacunha, A.A. Di Iorio, A heavy metal biotrap for wastewater remediation using poly-gamma-glutamic acid, *Biotechnol. Prog.*, 22 (2006) 523-531.
- [128] A. Günay, E. Arslankaya, İ. Tosun, Lead removal from aqueous solution by natural and pretreated clinoptilolite: Adsorption equilibrium and kinetics, *J. Hazard. Mater.*, 146 (2007) 362-371.
- [129] A.B. Pérez-Marín, V.M. Zapata, J.F. Ortuño, M. Aguilar, J. Sáez, M. Lloréns, Removal of cadmium from aqueous solutions by adsorption onto orange waste, *J. Hazard. Mater.*, 139 (2007) 122-131.
- [130] H. Yuh-Shan, Citation review of Lagergren kinetic rate equation on adsorption reactions, *Scientometrics*, 59 (2004) 171-177.
- [131] R. Rattanaoudom, Membrane hybrid system for removal of PFOS and PFOA in industrial wastewater: Application of conventional adsorbents and nanoparticles, [dissertation]. Asian Institute of Technology, 2011. 130 p.
- [132] C. Gerente, G. , Y. McKay, P. Andres, L. Cloirec, Interactions of natural aminated polymers with different species of arsenic at low concentrations: Application in water treatment, *Adsorption*, 11 (2005) 859–863.
- [133] F.C. Wu, R.L. Tseng, R.S. Juang, Comparative adsorption of metal and dye on flake- and bead-types of chitosans prepared from fishery wastes, *J. Hazard. Mater.*, 73 (2000) 63-75.
- [134] W.S.W. Ngah, K.H. Liang, Adsorption of gold(III) ions onto chitosan and N-Carboxymethyl chitosan: Equilibrium studies, *Ind. Eng. Chem. Res.*, 38 (1999) 1411-1414.
- [135] Y. Sağ, Y. Aktay, Kinetic Studies on Sorption of Cr(VI) and Cu(II) Ions by Chitin, Chitosan and *Rhizopus Arrhizus*, *Biochem. Eng. J.*, 12 (2002) 143-153.
- [136] G. McKay, Y.S. Ho, J.C.Y. Ng, Biosorption of copper from waste waters: A review, *Sep. Purif. Methods*, 28 (1999) 87-125.
- [137] J. Febrianto, A.N. Kosasih, J. Sunarso, Y.H. Ju, N. Indraswati, S. Ismadji, Equilibrium and kinetic studies in adsorption of heavy metals using biosorbent: A summary of recent studies, *J. Hazard. Mater.*, 162 (2009) 616-645.
- [138] Y.S. Ho, A.E. Ofomaja, Pseudo-second-order model for lead ion sorption from aqueous solutions onto palm kernel fiber, *J. Hazard. Mater.*, 129 (2006) 137-142.

- [139] N. Sankararamakrishnan, A. Dixit, L. Iyengar, R. Sanghi, Removal of hexavalent chromium using a novel cross linked xanthated chitosan, *Bioresour. Technol.*, 97 (2006) 2377-2382.
- [140] M.W. Wan, C.C. Kan, B.D. Rogel, M.L.P. Dalida, Adsorption of copper (II) and lead (II) ions from aqueous solution on chitosan-coated sand, *Carbohydr. Polym.*, 80 (2010) 891-899.
- [141] M.S. Sivakami, T. Gomathi, J. Venkatesan, H.S. Jeong, S.K. Kim, P.N. Sudha, Preparation and characterization of nano chitosan for treatment wastewaters, *Int. J. Biol. Macromol.*, 57 (2013) 204-212.
- [142] F.C. Wu, R.L. Tseng, R.S. Juang, Characteristics of Elovich equation used for the analysis of adsorption kinetics in dye-chitosan systems, *Chem. Eng. J. (Lausanne)*, 150 (2009) 366-373.
- [143] C. Gerente, V.K.C. Lee, P. Le Cloirec, G. McKay, Application of chitosan for the removal of metals from wastewaters by adsorption - Mechanisms and models review, *Crit. Rev. Env. Sci. Tec.*, 37 (2007) 41-127.
- [144] G. Zhu, C. Liu, G. Xu, J. Li, Simultaneous biohydrogen production and wastewater treatment in continuous stirred tank reactor (CSTR) using beet sugar wastewater, *International Conference on Energy and Environment Technology*, (2009) 737-740.
- [145] H. T. Liao, C. Y. Shiau, Analytical solution to an axial dispersion model for the fixed-bed adsorber, *Am. Inst. Chem. Eng. J.*, 46 (2000) 1168-1176.
- [146] Z. Yaneva, B. Koumanova, V. Meshko, Dynamic studies of nitrophenols adsorption on perfl in a fixed-bed column: Application of single and two resistance model, *Water Sci. Technol.*, 62 (2010) 883-891.
- [147] Vahid Sabourian, Ali Ebrahimi, Farzad Naseri, M. Irani, A. Rahimie, Fabrication of chitosan/silica nanofibrous adsorbent functionalized with amine groups for the removal of Ni(II), Cu(II) and Pb(II) from aqueous solutions: Batch and column studies, *RSC Advances*, 6 (2016) 40354-40365.
- [148] S. Sugashini, S. B. K. M. Meera, Column adsorption studies for the removal of Cr(VI) ions by ethylamine modified chitosan carbonized rice husk composite beads with modelling and optimization, *J. Chem.*, 2013 (2013) 1-11.

- [149] C.M. Futralan, C.C. Kan, M.L. Dalida, C. Pascua, M.W. Wan, Fixed-bed column studies on the removal of copper using chitosan immobilized on bentonite, *Carbohydr. Polym.*, 83 (2011) 697-704.
- [150] Z. Xu, J.G. Cai, B.C. Pan, Mathematically modeling fixed-bed adsorption in aqueous systems, *J Zhejiang Univ. Sci. A*, 14 (2013) 155-176.
- [151] S. Sugashini, K.M.M.S. Begum, Performance of Fe-loaded chitosan carbonized rice husk beads (Fe-CCRB) for continuous adsorption of metal ions from industrial effluents, *Environ. Prog. Sustainable Energy*, 33 (2014) 1125-1138.
- [152] C.J. Geankoplis, *Transport Processes and Unit Operations*, New Delhi : Prentice-Hall of India, India, 2002 3rd ed.
- [153] V.V. Goud, K. Mohanty, M.S. Rao, N.S. Jayakumar, Prediction of mass transfer coefficients in packed bed using tamarind nut shell activated carbon to remove phenol, *Chem. Eng. Technol.*, 28 (2005) 991-997.
- [154] P.K. Roy, *Nanofiltration as a Tertiary Treatment for Phosphate Removal from Wastewater [master's thesis]*. Asian Institute of Technology, 1995. 49 p.
- [156] T. Asano, *Wastewater reclamation and reuse*, CRC Press; 1998. 1528 p.
- [157] C. Wang, F. Yang, F. Meng, H. Zhang, Y. Xue, G. Fu, High flux and antifouling filtration membrane based on non-woven fabric with chitosan coating for membrane bioreactors, *Bioresour. Technol.*, 101 (2010) 5469-5474.
- [158] S. Boributh, A. Chanachai, R. Jiratananon, Modification of PVDF membrane by chitosan solution for reducing protein fouling, *J. Membr. Sci.*, 342 (2009) 97-104.
- [159] S.R. Holman, K.N. Ohlinger, An evaluation of fouling potential and methods to control fouling in microfiltration membranes for secondary wastewater effluent, *Proceedings of the Water Environment Federation (WEFTEC 2007)*, (2007) 6417-6444.
- [160] J. Wagner, *Membrane filtration handbook practical tips and hints*, Osmonics, Inc; 2001. 98 p.
- [161] X. Ding, Y. Fan, N. Xu, A new route for the fabrication of TiO₂ ultrafiltration membranes with suspension derived from a wet chemical synthesis, *J. Membr. Sci.*, 270 (2006) 179-186.

- [162] S. Jana, A. Saikia, M. K. Purkait, K. Mohanty, Chitosan based ceramic ultrafiltration membrane: Preparation, characterization and application to remove Hg(II) and As(III) using polymer enhanced ultrafiltration, *Chem. Eng. J. (Lausanne)*, 170 (2011) 209-219.
- [163] G.C. Steenkamp, H.W.J.P. Neomagus, H.M. Krieg, K. Keizer, Centrifugal casting of ceramic membrane tubes and the coating with chitosan, *Sep. Purif. Technol.*, 25 (2001) 407-413.
- [164] V. Zaspalis, A. Pagana, S. Sklari, Arsenic removal from contaminated water by iron oxide sorbents and porous ceramic membranes, *Desalination*, 217 (2007) 167-180.
- [165] T. Lopez Leon, E.L. Carvalho, B. Seijo, J.L. Ortega Vinuesa, D. Bastos Gonzalez, Physicochemical characterization of chitosan nanoparticles: Electrokinetic and stability behavior, *J. Colloid Interface Sci.*, 283 (2005) 344-351.
- [166] Y. Wu, W. Yang, C. Wang, J. Hu, S. Fu, Chitosan nanoparticles as a novel delivery system for ammonium glycyrrhizinate, *Int. J. Pharm.*, 295 (2005) 235-245.
- [167] L.M. Zhao, L.E. Shi, Z.L. Zhang, J.M. Chen, D.D. Shi, J. Yang, Z.X. Tang, Preparation and application of chitosan nanoparticles and nanofibers, *Braz. J. Chem. Eng.*, 28 (2011) 353-362.
- [168] A.A. Babaluo, M. Kokabi, M. Manteghian, R. Sarraf Mamoory, A modified model for alumina membranes formed by gel-casting followed by dip-coating, *J. Eur. Ceram. Soc.*, 24 (2004) 3779-3787.
- [169] E. Malkoc, Y. Nuhoglu, M. Dundar, Adsorption of chromium(VI) on pomace-An olive oil industry waste: Batch and column studies, *J. Hazard. Mater.*, 138 (2006) 142-151.
- [170] Y.S. Ho, G. McKay, The kinetics of sorption of divalent metal ions onto sphagnum moss peat, *Water Res.*, 34 (2000) 735-742.
- [171] S. Sen Gupta, K.G. Bhattacharyya, Kinetics of adsorption of metal ions on inorganic materials: A review, *Adv. Colloid Interface Sci.*, 162 (2011) 39-58.
- [172] A. Tor, N. Danaoglu, G. Arslan, Y. Cengeloglu, Removal of fluoride from water by using granular red mud: Batch and column studies, *J. Hazard. Mater.*, 164 (2009) 271-278.

- [173] E.I. Unuabonah, M.I. El-Khaiary, B.I. Olu-Owolabi, K.O. Adebowale, Predicting the dynamics and performance of a polymer-clay based composite in a fixed bed system for the removal of lead (II) ion, *Chem. Eng. Res. Des.*, 90 (2012) 1105-1115.
- [174] J.T. Nwabanne, P.K. Igbokwe, Kinetic modeling of heavy metals adsorption on fixed bed column, *Int. J. Environ. Res.*, 6 (2012) 945-952.
- [175] Y. Zhu, S. Xia, G. Liu, W. Jin, Preparation of ceramic-supported poly(vinyl alcohol)-chitosan composite membranes and their applications in pervaporation dehydration of organic/water mixtures, *J. Membr. Sci.*, 349 (2010) 341-348.
- [176] L.C. Craig, W. Konigsberg, Dialysis studies. III. modification of pore size and shape in cellophane membranes, *J. Phys. Chem.*, 65 (1961) 166-172.
- [177] M.S. Baei, M.J. Hosseinzadeh, H. Younesi, Whey processing with nano chitosan, *World Appl Sci J.*, 19 (2012) 530-537.
- [178] H. Liu, C. Gao, Preparation and properties of ionically cross-linked chitosan nanoparticles, *Polym. Adv. Technol.*, 20 (2009) 613-619.
- [179] Q. Gan, T. Wang, C. Cochrane, P. McCarron, Modulation of surface charge, particle size and morphological properties of chitosan- TPP nanoparticles intended for gene delivery, *Colloids Surf., B.*, 44 (2005) 65-73.
- [180] P.E. Muhammed Rafeeq, V. Junise, R. Saraswathi, P.N. krishnan, Dilip.C, Development and characterization of chitosan nanoparticles loaded with isoniazid for the treatment of tuberculosis, *Res. J. Pharm. Biol. Chem. Sci.*, 1 (2010) 383-390.
- [181] B. Hu, C. Pan, Y. Sun, Z. Hou, H. Ye, X. Zeng, Optimization of fabrication parameters to produce chitosan-tripolyphosphate nanoparticles for delivery of tea catechins, *J. Agric. Food Chem.*, 56 (2008) 7451-7458.
- [182] A. Nasti, N.M. Zaki, P. de Leonardis, S. Ungphaiboon, P. Sansongsak, M. G. Rimoli, N. Tirelli, Chitosan/ TPP and chitosan/ TPP- hyaluronic acid nanoparticles: systematic optimisation of the preparative process and preliminary biological evaluation, *Pharm. Res.*, 26 (2009) 1918-1930.
- [183] J.P. Chen, M. Lin, Surface charge and metal ion adsorption on an H-type activated carbon: experimental observation and modeling simulation by the surface complex formation approach, *Carbon*, 39 (2001) 1491-1504.

- [184] H.A. Tsai, H.C. Chen, K.R. Lee, J.Y. Lai, Study of the separation properties of chitosan/ polysulfone composite hollow- fiber membranes, *Desalination*, 193 (2006) 129-136.
- [185] A.E. Pagana, S.D. Sklari, E.S. Kikkinides, V.T. Zaspalis, Microporous ceramic membrane technology for the removal of arsenic and chromium ions from contaminated water, *Microporous Mesoporous Mater.*, 110 (2008) 150-156.
- [186] P. Hristov, A. Yoleva, S. Djambazov, I. Chukovska, D. Dimitrov, Preparation and characterization of porous ceramic membranes for micro- filtration from natural zeolite, *J. Univ. Chem. Technol. Metall.*, 47 (2012) 476-480.
- [187] A. Chanachai, K. Meksup, R. Jiratananon, Coating of hydrophobic hollow fiber PVDF membrane with chitosan for protection against wetting and flavor loss in osmotic distillation process, *Sep. Purif. Technol.*, 72 (2010) 217-224.
- [188] C.J.M. Nova, D. Paolucci-Jeanjean, M.-P. Belleville, M. Barboiu, M. Rivallin, G. Rios, Elaboration, characterization and study of a new hybrid chitosan/ceramic membrane for affinity membrane chromatography, *J. Membr. Sci.*, 321 (2008) 81-89.
- [189] N. Bhattarai, H.R. Ramay, J. Gunn, F.A. Matsen, M. Zhang, PEG-grafted chitosan as an injectable thermosensitive hydrogel for sustained protein release, *J. Controlled Release*, 103 (2005) 609-624.
- [190] S. Hou, L.K. McCauley, P.X. Ma, Synthesis and erosion properties of PEG-containing polyanhydrides, *Macromol. Biosci.*, 7 (2007) 620–628.
- [191] M.M. Beppu, R.S. Vieira, C.G. Aimoli, C.C. Santana, Crosslinking of chitosan membranes using glutaraldehyde: Effect on ion permeability and water absorption, *J. Membr. Sci.*, 301 (2007) 126-130.
- [192] J. Kotaś, Z. Stasicka, Chromium occurrence in the environment and methods of its speciation, *Environ. Pollut.*, 107 (2000) 263-283.
- [193] K. Dermentzis, A. Christoforidis, E. Valsamidou, A. Lazaridou, N. Kokkinos, Removal of hexavalent chromium from electroplating wastewater by electrocoagulation with iron electrodes, *Global NEST J.*, 13 (2011) 412-418.
- [194] C. Araneda, C. Fonseca, J. Sapag, C. Basualto, M. Yazdani-Pedram, K. Kondo, E. Kamio, F. Valenzuela, Removal of metal ions from aqueous solutions by

- sorption onto microcapsules prepared by copolymerization of ethylene glycol dimethacrylate with styrene, *Sep. Purif. Technol.*, 63 (2008) 517-523.
- [195] N. Zhao, N. Wei, J. Li, Z. Qiao, J. Cui, F. He, Surface properties of chemically modified activated carbons for adsorption rate of Cr (VI), *Chem. Eng. J. (Lausanne)*, 115 (2005) 133-138.
- [196] S.X. Liu, X. Chen, X.Y. Chen, Z.F. Liu, H.L. Wang, Activated carbon with excellent chromium(VI) adsorption performance prepared by acid-base surface modification, *J. Hazard. Mater.*, 141 (2007) 315-319.
- [197] N. Tewari, P. Vasudevan, B.K. Guha, Study on biosorption of Cr(VI) by *Mucor hiemalis*, *Biochem. Eng. J.*, 23 (2005) 185-192.
- [198] J.W. Wang, Y.M. Kuo, Preparation and adsorption properties of chitosan-poly(acrylic acid) nanoparticles for the removal of nickel ions, *J. Appl. Polym. Sci.*, 107 (2008) 2333-2342.
- [199] S. Ayoob, A. Gupta, P. Bhakat, Analysis of breakthrough developments and modeling of fixed bed adsorption system for As(V) removal from water by modified calcined bauxite (MCB), *Sep. Purif. Technol.*, 52 (2007) 430-438.
- [200] M. T. Uddin, M. Rukanuzzaman, M.M.R. Khan, M. A. Islam, Adsorption of methylene blue from aqueous solution by jackfruit (*Artocarpus heterophyllus*) leaf powder: A fixed-bed column study, *J. Environ. Manage.*, 90 (2009) 3443-3450.
- [201] N. Chen, Z. Zhang, C. Feng, M. Li, R. Chen, N. Sugiura, Investigations on the batch and fixed-bed column performance of fluoride adsorption by Kanuma mud, *Desalination*, 268 (2011) 76-82.
- [202] Z.Z. Chowdhury, S.M. Zain, A.K. Rashid, R.F. Rafique, K. Khalid, Breakthrough curve analysis for column dynamics sorption of Mn(II) ions from wastewater by using mangostana garcinia peel-based granular-activated carbon, *J. Chem.*, 2013 (2013) 1-8.
- [203] D.C.K. Ko, J.F. Porter, G. McKay, Optimised correlations for the fixed-bed adsorption of metal ions on bone char, *Chem. Eng. Sci.*, 55 (2000) 5819-5829.
- [204] M. M. Sekhula, J. O. Okonkwo, C.M. Zvinowanda, Fixed bed column adsorption of Cu (II) onto maize tassel-PVA beads, *J. Chem. Eng. Process. Tech.*, 3 (2012) 1-5.

- [205] B. Ramavandi, S. Farjadfard, M. Ardjmand, Mitigation of orange II dye from simulated and actual wastewater using bimetallic chitosan particles: Continuous flow fixed-bed reactor, *J. Environ. Chem. Eng.*, 2 (2014) 1776-1784.
- [206] E. Bilgin Simsek, U. Beker, B. F. Senkal, Predicting the dynamics and performance of selective polymeric resins in a fixed bed system for boron removal, *Desalination*, 349 (2014) 39-50.
- [207] Z. Aksu, F. Gönen, Biosorption of phenol by immobilized activated sludge in a continuous packed bed: Prediction of breakthrough curves, *Process Biochem.* (Amsterdam, Neth.), 39 (2004) 599-613.
- [208] A.M. El Kamash, Evaluation of zeolite A for the sorptive removal of Cs^+ and Sr^{2+} ions from aqueous solutions using batch and fixed bed column operations, *J. Hazard. Mater.*, 151 (2008) 432-445.
- [209] S. Qian, G. Huang, J. Jiang, F. He, Y. Wang, Studies of adsorption behavior of crosslinked chitosan for Cr(VI), Se(VI), *J. Appl. Polym. Sci.*, 77 (2000) 3216-3219.
- [210] T. Tianwei, H. Xiaojing, D. Weixia, Adsorption behaviour of metal ions on imprinted chitosan resin, *J. Chem. Technol. Biotechnol.*, 76 (2001) 191-195.
- [211] M. Y. Lee, K. J. Hong, Y. Shin Ya, T. Kajiuchi, Adsorption of hexavalent chromium by chitosan-based polymeric surfactants, *J. Appl. Polym. Sci.*, 96 (2005) 44-50.
- [212] B.K. Nandi, R. Uppaluri, M.K. Purkait, Effects of dip coating parameters on the morphology and transport properties of cellulose acetate–ceramic composite membranes, *J. Membr. Sci.*, 330 (2009) 246-258.
- [213] W. Yoshida, Y. Cohen, Ceramic-supported polymer membranes for pervaporation of binary organic/organic mixtures, *J. Membr. Sci.*, 213 (2003) 145-157.
- [214] K.M. Song, W.H. Hong, Dehydration of ethanol and isopropanol using tubular type cellulose acetate membrane with ceramic support in pervaporation process, *J. Membr. Sci.*, 123 (1997) 27-33.
- [215] X. Cao, T. Zhang, Q.T. Nguyen, Y. Zhang, Z. Ping, A novel hydrophilic polymer-ceramic composite membrane: Acrylic acid grafting membrane, *J. Membr. Sci.*, 312 (2008) 15-22.

- [216] H. Yanagisita, D. Kitamoto, K. Haraya, T. Nakane, T. Tsuchiya, N. Koura, Preparation and pervaporation performance of polyimide composite membrane by vapor deposition and polymerization (VDP), *J. Membr. Sci.*, 136 (1997) 121-126.
- [217] A. Zach-Maor, R. Semiat, H. Shemer, Fixed bed phosphate adsorption by immobilized nano-magnetite matrix: experimental and a new modeling approach, *Adsorption*, 17 (2011) 929-936.
- [218] Z. Zhao, J. Zheng, M. Wang, H. Zhang, C. C. Han, High performance ultrafiltration membrane based on modified chitosan coating and electrospun nanofibrous PVDF scaffolds, *J. Membr. Sci.*, 394-395 (2012) 209-217.
- [219] R.S. Vieira, M.M. Beppu, Mercury ion recovery using natural and crosslinked chitosan membranes, *Adsorption*, 11 (2005) 731-736.
- [220] N.S. Behbahani, K. Rostamizadeh, M.R. Yaftian, A. Zamani, H. Ahmadi, Covalently modified magnetite nanoparticles with PEG: preparation and characterization as nano-adsorbent for removal of lead from wastewater, *J. Environ. Health Sci. Eng.*, 12 (2014) 1-11.
- [221] M.J. Zohuriaan-Mehr, Advances in chitin and chitosan modification through graft copolymerization: A comprehensive review, *Iran. Polym. J.*, 14 (2005) 235-265.
- [222] E.W. Wambu, G.K. Muthakia, P.M. Shiundu, K.J.w. Thiongo, Kinetics of copper desorption from regenerated spent bleaching earth, *Am-Euras. J. Sci. Res.*, 4 (2009) 317-323.
- [223] K. Vijayaraghavan, J. Jegan, K. Palanivelu, M. Velan, Removal of nickel(II) ions from aqueous solution using crab shell particles in a packed bed up-flow column, *J. Hazard. Mater.*, 113 (2004) 223-230.
- [224] R. Han, L. Zou, X. Zhao, Y. Xu, F. Xu, Y. Li, Y. Wang, Characterization and properties of iron oxide-coated zeolite as adsorbent for removal of copper(II) from solution in fixed bed column, *Chem. Eng. J. (Lausanne)*, 149 (2009) 123-131.

Appendix

Adsorption isotherms and kinetic of adsorptions

Appendix A: Cr(VI) removal using nanochitosan coated on bituminous activated carbon

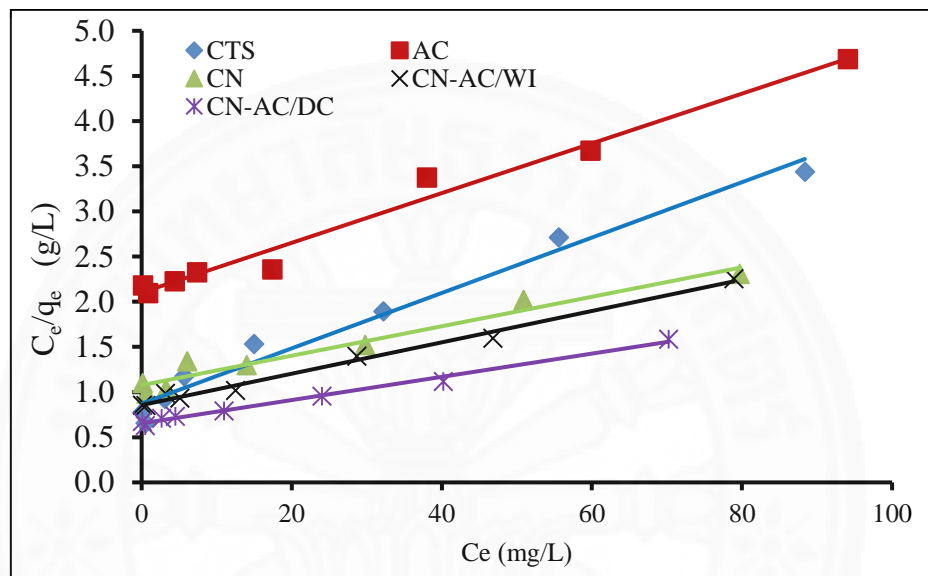


Figure A1 Determination of Langmuir isotherms of Cr (VI) for various adsorbents

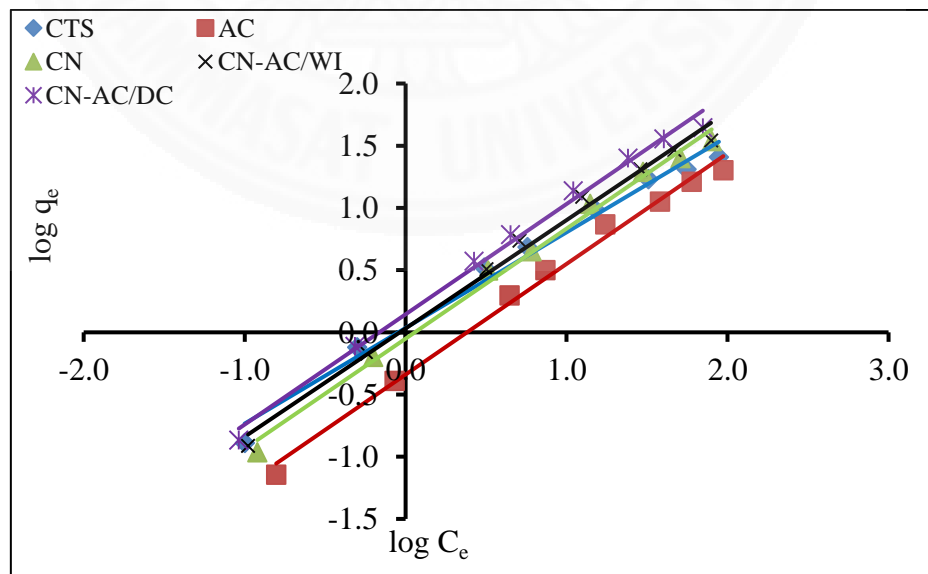


Figure A2 Determination of Freundlich isotherms of Cr (VI) for various adsorbents

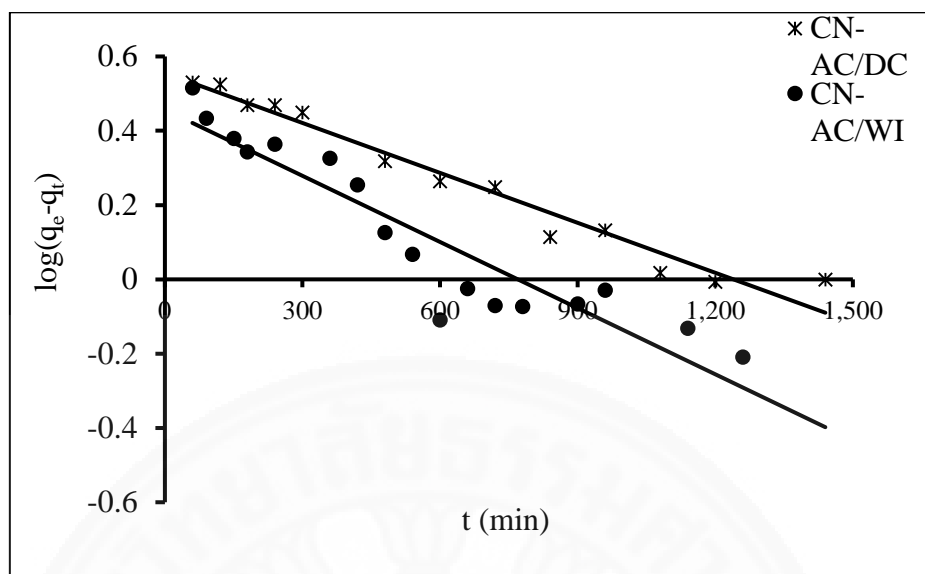


Figure A3 A pseudo-first-order kinetic model of Cr (VI) by nanochitosan-coated bituminous activated carbon using dip coating and wet impregnation methods

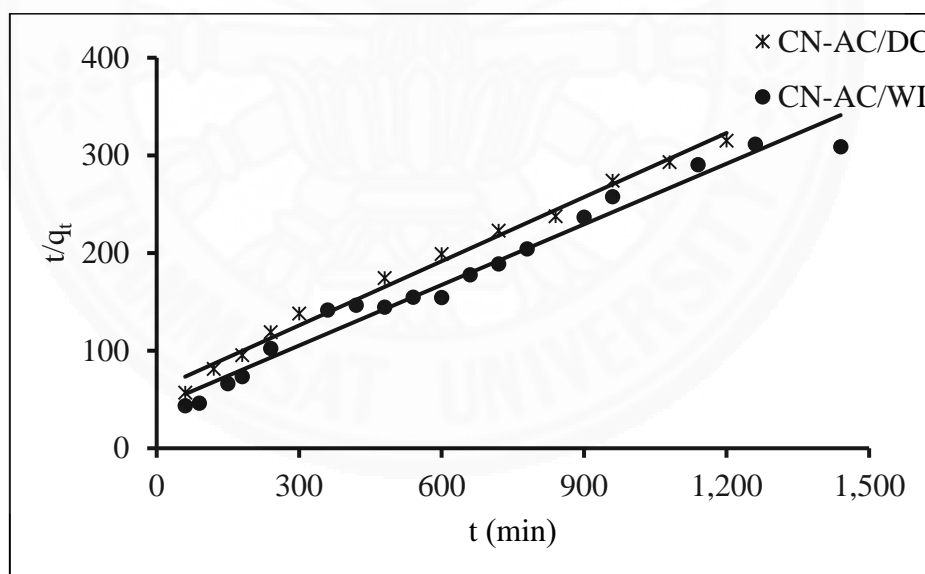


Figure A4 A pseudo-second-order kinetic model of Cr (VI) by nanochitosan-coated bituminous activated carbon using dip coating and wet impregnation methods

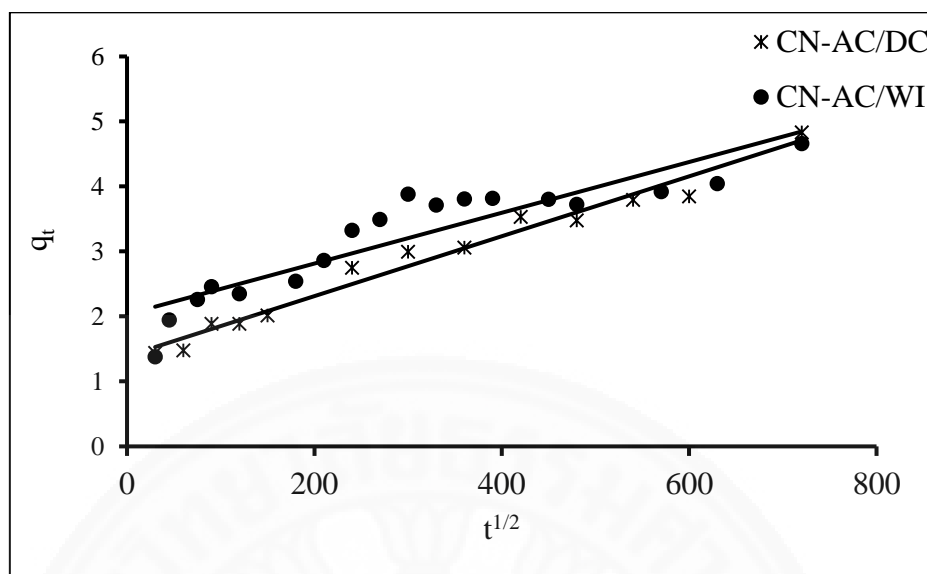


Figure A5 An intraparticle diffusion model of Cr (VI) ion by nanochitosan-coated bituminous activated carbon using dip coating and wet impregnation methods

Appendix B: Cr(VI) removal using nanochitosan coated on alumina ceramic balls

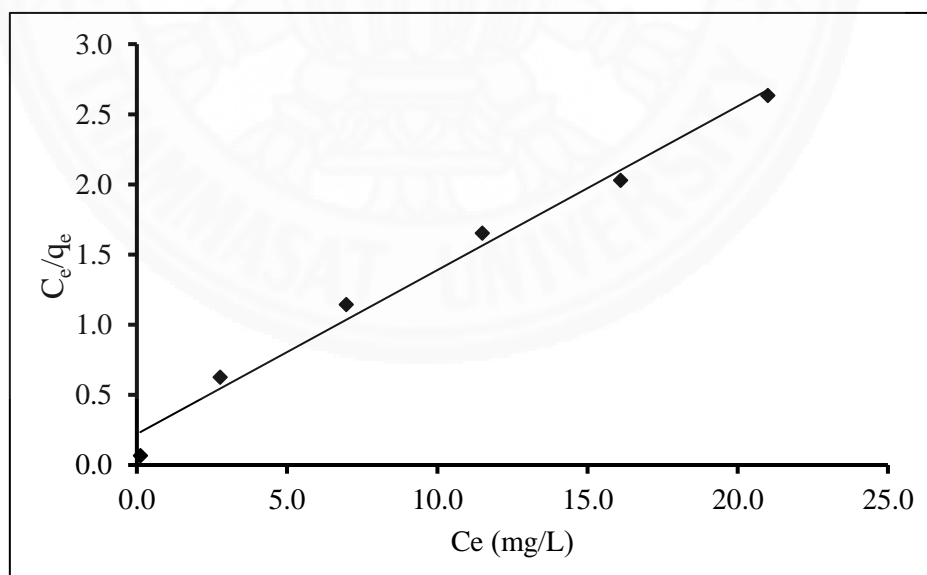


Figure B1 Determination of Langmuir isotherms of Cr (VI) removal by CN-CB

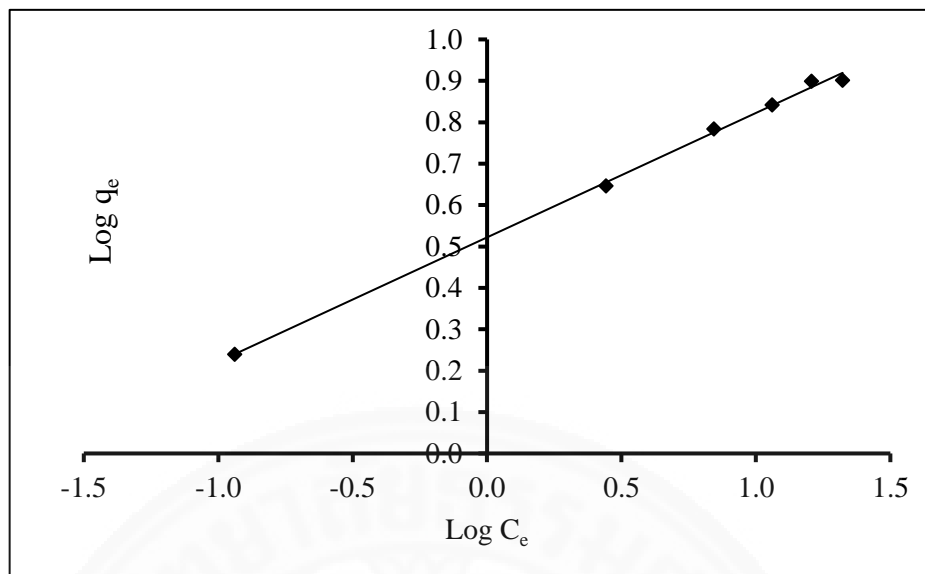


Figure B2 Determination of Freundlich isotherms of Cr (VI) for various adsorbents

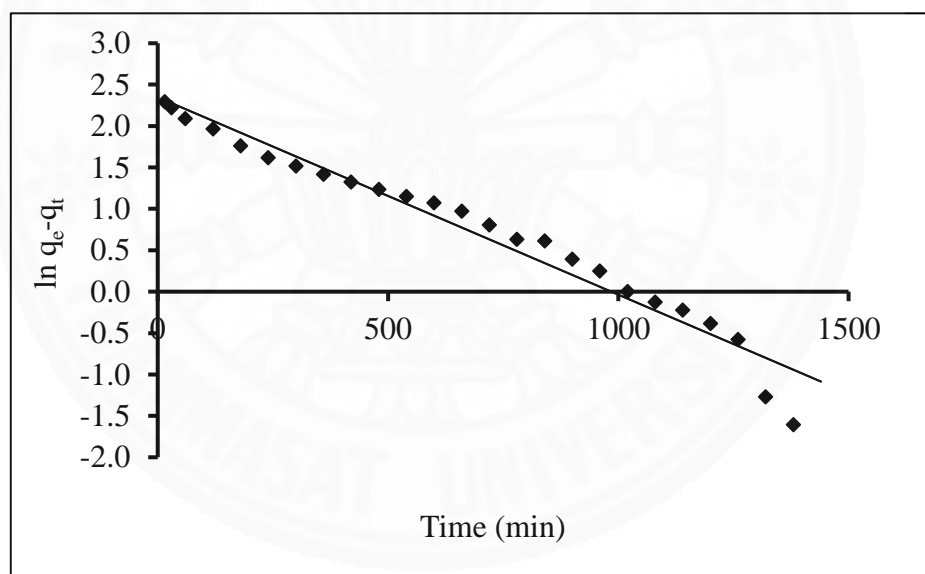


Figure B3 A Pseudo-first-order kinetic model of Cr (VI) by CN-CB

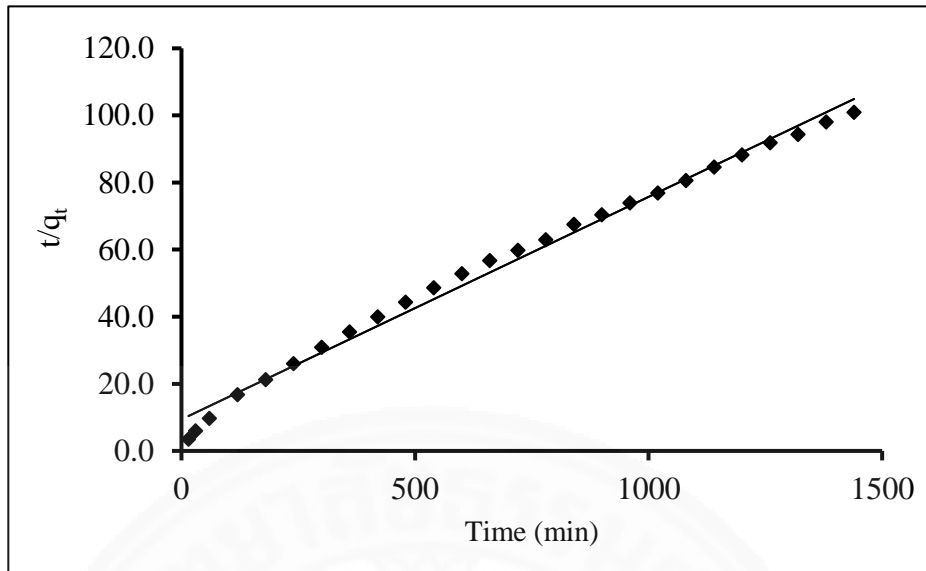


Figure B4 A Pseudo-second-order kinetic model of Cr (VI) by CN-CB

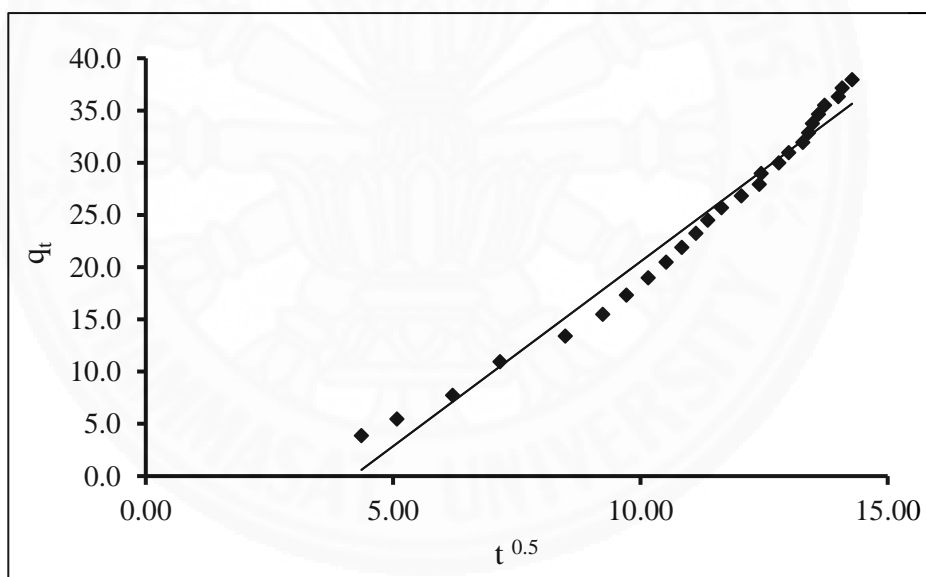


Figure B5 An Intraparticle diffusion model of Cr (VI) by CN-CB

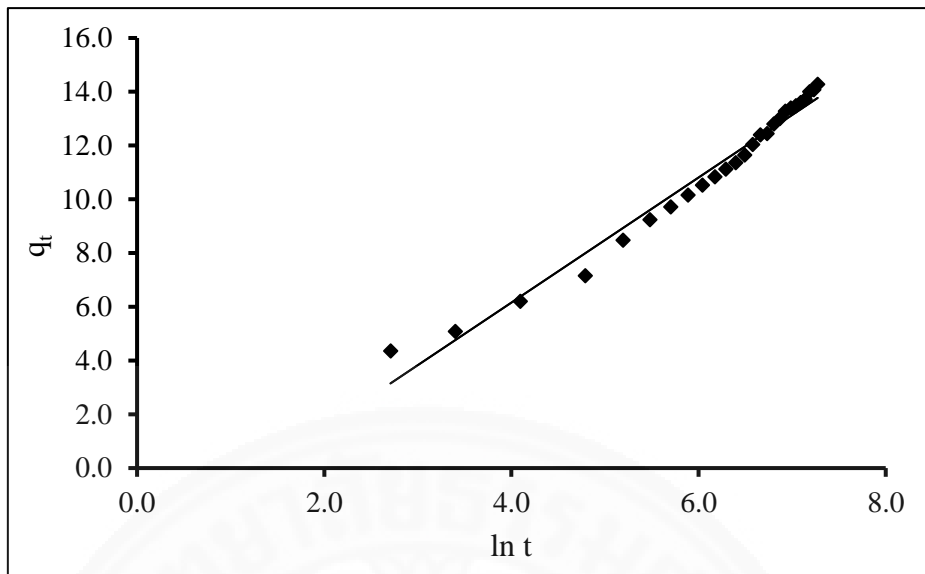


Figure B6 An Elovich kinetic model of Cr (VI) by CN-CB